

RADIATIVE EMISSIVITY OF METALS AND OXIDIZED METALS AT HIGH
TEMPERATURE

Except where reference is made to the work of others, the work described in this dissertation is my own or was done in collaboration with my advisory committee.
This dissertation does not include proprietary or classified information.

George Teodorescu

Certificate of Approval:

Ruel A. Overfelt
Professor
Materials Engineering

Peter D. Jones, Chair
Associate Professor
Mechanical Engineering

Jeffrey Fergus
Associate Professor
Materials Engineering

Bertram Zinner
Associate Professor
Mathematics and Statistics

Joe F. Pittman
Interim Dean
Graduate School

RADIATIVE EMISSIVITY OF METALS AND OXIDIZED METALS AT HIGH
TEMPERATURE

George Teodorescu

A Dissertation
Submitted to
the Graduate Faculty of
Auburn University
in Partial Fulfillment of the
Requirements for the
Degree of
Doctor of Philosophy

Auburn, Alabama
August 4, 2007

RADIATIVE EMISSIVITY OF METALS AND OXIDIZED METALS AT HIGH
TEMPERATURE

George Teodorescu

Permission is granted to Auburn University to make copies of this dissertation at its
discretion, upon request of individuals or institutions and at their expense.

The author reserves all publication rights.

Signature of Author

Date of Graduation

VITA

George Teodorescu, son of Dumitru Gavrilă Teodorescu and Constantina Teodorescu, was born on June 24, 1971, in Craiova, Romania. He graduated from Chemical Engineering High School of Craiova in 1989. He studied at Ploiesti University for five years and graduated with a Bachelor of Science degree in Chemical Engineering in July, 1995. He entered Auburn University in January 2001 to pursue Ph.D. degree in Materials Engineering. In May 2006 he received a Master degree in Probability & Statistics from Auburn University, Alabama.

DISSERTATION ABSTRACT
RADIATIVE EMISSIVITY OF METALS AND OXIDIZED METALS AT HIGH
TEMPERATURE

George Teodorescu

Doctor of Philosophy, August 4, 2007
(M. Probability & Statistics, Auburn University, 2006)
(B.S. Chemical Engineering, Ploiesti University, Romania, 1995)

176 Typed Pages

Directed by Peter D. Jones

Radiative emissivities of metals at high temperatures influence the energy balance and remote sensing in a wide range of manufacturing processes as well as research and development activities and thereby determine performance and even economic viability. Accurate and comprehensive measurements of metals thermal emissivity have always been a challenge due to numerous influential factors such as: spectral range, temperature, sample topology, oxidation, contamination, composition, etc. Therefore, the influence of optically thick and thin metal oxides on normal spectral and directional, as well as on the complex index of refraction, was studied. An experimental setup for emittance measurements in air at high temperature was developed during the course of study, and includes a Fourier Transformed Infrared spectrometer (FTIR) and a special design sample holder which allows full directional measurements.

The optical system can operate over a very wide wavelength range from 1 to 20 μm , with sample temperatures between 673 K and 973 K. Directional measurements were performed from normal to the sample surface to a 72° polar angle. X-ray diffraction (XRD), scanning electron microscopy (SEM), and Auger spectroscopy (AES) were employed to characterize the samples. Experimental data were used in conjunction with electro-magnetic theory to determine the complex index of refraction. The reported data show good agreement with Fresnel's relation; uncertainty in the emissivity measurements was found to be less than 3.5%.

In addition, the normal emissivity of high purity metals such nickel, titanium, and zirconium was studied in ultra high vacuum conditions. Their normal emissivities and determined index of refraction exhibit both free and bound electron effects. A second experimental device was constructed for this study by coupling the FTIR with an electromagnetic levitator (EML) where the sample is electromagnetically heated, leading to reduced chances of sample contamination and/or sample-holder interaction. The optical system operates over a broad spectral range from 1 to 16 μm , with sample temperatures between 1273 K and 1650 K. The uncertainty in emissivity was found to be less than 4 %.

ACKNOWLEDGMENTS

The author would like to sincerely thank Dr. Peter D. Jones and Dr. Ruel A. Overfelt for providing the opportunity to undertake this research project and for their advice, mentorship and guidance during the entire course of this research. Special appreciation is also expressed to Dr. Ruel A. Overfelt and Dr. Peter D. Jones for their important suggestions and constant support on both technical and documentary aspects of the project.

The author would also like to thank Dr. Jeffrey Fergus for his academic support and assistance during the period of study.

The author is grateful to Dr. Bertram Zinner for his personal support and academic guidance during the period of study at Auburn University.

Deepest appreciation is expressed to his wife Carmen Aurora Teodorescu, his daughter Roberta Andreea Teodorescu for their most important encouragement and loving support.

Style manual or journal used: Journal of Materials Science

Computer Software used: Microsoft Word 2000, Kaleidagraph, Microsoft Excel 2002

TABLE OF CONTENTS

LIST OF FIGURES	xi
LIST OF TABLES	xv
LIST OF NOMENCLATURE	xvi
1 INTRODUCTION	1
2 BASIC LITERATURE REVIEW	7
2.1 Emissivity Overview	7
2.2 Theory Overview	9
2.2.1 Maxwell's equations	9
2.2.2 Fresnel's equation	10
2.2.3 Lorentz model	11
2.2.4 Drude model	12
2.2.5 Hagen-Rubens relation	14
2.2.6 Drude-Roberts model	15
2.3 Emissivity Measurement Methods	16
2.4 Emissivity Availability	19
3 OBJECTIVES	22
4 EXPERIMENTAL PROCEDURES	25
4.1 Experimental Procedure for Oxidized Metals with Pyroelectric Detector	25
4.2 Experimental Procedure for Oxidized Metals with FTIR Spectrometer	28
4.3 Experimental Procedure for Metals in High Vacuum	30
4.4 Discussion of Different Experimental Setups	34
5 RESULTS AND DISCUSSION	37
5.1 Oxidized Copper	37
5.1.1 Specific Literature Review	38
5.1.2 Cupric Oxide Spectral Directional Emissance Measurement	39
5.1.3 Experimental Results & Discussion	43

5.2 Oxidized Aluminum.....	55
5.2.1 Specific Literature Review	55
5.2.2 Oxidized Aluminum Spectral Directional Emittance Measurement.....	56
5.2.3 Experimental Results & Discussion.....	60
5.3 Oxidized Nickel.....	68
5.3.1 Specific Literature Review	68
5.3.2 Oxidized Nickel Spectral Directional Emittance Measurement	69
5.3.3 Experimental Results & Discussion.....	71
5.4 Nickel.....	78
5.4.1 Specific Literature Review	78
5.4.2 Normal Spectral Emissivity of Nickel Measurement.....	79
5.4.3 Experimental Results & Discussion.....	81
5.5 Zirconium.....	89
5.5.1 Specific Literature Review	89
5.5.2 Normal Spectral Emissivity of Zirconium Measurement.....	90
5.5.3 Experimental Results & Discussion.....	91
5.6 Titanium.....	98
5.6.1 Specific Literature Review	98
5.6.2 Normal Spectral Emissivity of Titanium Measurement.....	99
5.6.3 Experimental Results & Discussion.....	100
6 GENERAL DISCUSSION OF RESULTS.....	106
7 SUMMARY	131
8 CONCLUSIONS	136
9 FUTURE WORK	138
REFERENCES.....	140
APPENDICES.....	148
Appendix A - Cupric Oxide.....	149
Appendix B - Oxidized Aluminum	151
Appendix C - Oxidized Nickel.....	153
Appendix D - Nickel.....	155
Appendix E - Zirconium.....	156
Appendix F - Titanium	157

LIST OF FIGURES

Figure 1 Directional Emissivity	8
Figure 2 Experimental setup with pyroelectric detector.....	27
Figure 3 Schematic of experimental setup with FTIR spectrometer.....	29
Figure 4 Schematic of experimental setup with high vacuum chamber.....	32
Figure 5 Schematic of electromagnetic induction coil.	33
Figure 6 Micrograph of copper oxide removed from copper substrate.....	40
Figure 7 CuO X-ray diffraction pattern.....	40
Figure 8 Optical thickness of CuO	46
Figure 9 Spectral-directional emittance of CuO at 973 K.	47
Figure 10 Spectral real part of the refractive index at considered temperatures.....	48
Figure 11 Spectral imaginary part of the refractive index at considered temperatures.....	49
Figure 12 Spectral normal emittance of CuO as a function of wavelength.	51
Figure 13 Spectral-directional emittance of CuO at 973 K from present work and oxidized copper at 970 K from [51].....	53
Figure 14 Spectral-directional emittance of CuO from present work and from electromagnetic theory for 3.5 and 7.5 μm	54
Figure 15 AES spectrum after 65 min of Ar ⁺ sputtering	57
Figure 16 AES depth profile through the Al film. The Ar ⁺ sputter rate was 35 $\text{\AA}/\text{min}$ measured on a standard thin film of SiO ₂	57

Figure 17 Comparison of spectral-normal emittance of alumina (99.5%)	59
Figure 18 Spectral refractive index at of oxidized aluminum 673, 773, and 873 K	61
Figure 19 Spectral extinction coefficient of oxidized aluminum at 673, 773, and 873 K.	61
Figure 20 Spectral normal emittance of oxidized aluminum comparison	63
Figure 21 Spectral normal emittance comparison	65
Figure 22 Directional emittance of oxidized aluminum at 3 μm as a function of temperature	67
Figure 23 Directional emittance of oxidized aluminum at 673 K at 9, 10, and 11 μm	67
Figure 24 X-ray diffraction pattern of oxidized nickel.....	70
Figure 25 SEM microstructure of nickel sample. a) as received 2000X, b) oxidized sample 2000X, c) as received 4000X, d) oxidized sample 4000X.	72
Figure 26 Normal spectral-directional emittance of oxidized nickel	73
Figure 27 Spectral-directional emittance of oxidized 99.99% Ni at 873K.....	75
Figure 28 Spectral-normal emittance of oxidized nickel comparison.....	75
Figure 29 Spectral-hemispherical emittance of oxidized nickel as a function of wavelength at 673, 773 and 873K.....	77
Figure 30 X-ray diffraction pattern of nickel sample	80
Figure 31 Spectral-normal emissivity of high purity nickel	82
Figure 32 Spectral-normal emissivity of nickel comparison (a).....	82
Figure 33 Spectral-normal emissivity of nickel comparison (b).....	84
Figure 34 Normal emissivity of nickel prediction and present work	84
Figure 35 K_{∞} versus temperature for nickel.....	87
Figure 36 λ_2 versus temperature for nickel.....	87

Figure 37 Refractive index of nickel	88
Figure 38 Extinction coefficient of nickel	88
Figure 39 X-ray diffraction pattern of zirconium sample.....	91
Figure 40 Normal spectral emissivity of zirconium	92
Figure 41 Normal spectral emissivity of zirconium comparison	92
Figure 42 Normal emissivity of zirconium predictions and present work	93
Figure 43 K_{∞} parameter versus temperature for zirconium	94
Figure 44 λ_2 parameter versus temperature for zirconium	94
Figure 45 Refractive index of zirconium.....	97
Figure 46 Extinction coefficient of zirconium	97
Figure 47 X-ray diffraction pattern of titanium sample.....	100
Figure 48 Normal spectral emissivity of titanium.....	101
Figure 49 Spectral-normal emissivity of titanium comparison.....	102
Figure 50 Normal emissivity of titanium prediction and present work.....	102
Figure 51 K_{∞} parameter versus temperature for titanium	104
Figure 52 λ_2 parameter versus temperature for titanium	104
Figure 53 Refractive index of titanium.....	105
Figure 54 Extinction coefficient of titanium.....	105
Figure 55 Nickel emissivity from Drude and present work.....	110
Figure 56 Normal emissivity of nickel from Hagen-Rubens and present work	112
Figure 57 Normal emissivity of nickel present work and Drude-Roberts [11]	113
Figure 58 Directional emissivity of a metal [14]	116
Figure 59 Directional emittance of oxidized aluminum at 673 K.....	117

Figure 60 Directional emittance of oxidized nickel at 673 K.....	117
Figure 61 Total hemispherical emissivity of titanium.....	119
Figure 62 Total hemispherical emissivity of zirconium.....	119
Figure 63 Directional emittance of oxidized aluminum.....	121
Figure 64 Normal emittance of aluminum oxide.....	124
Figure 65 Normal emittance of SiC [129].....	125
Figure 66 Directional emittance of a dielectric.....	127
Figure 67 Normal emittance of cupric oxide.....	128
Figure 68 Directional emittance of CuO.....	129

LIST OF TABLES

Table 1 Measured Spectral Directional Emittance of CuO at 673 K (1st row), 773 K (2nd row), 873 (3rd row), and 973 K (4th row)	149
Table 2 Spectral-hemispherical emittance and complex refractive index of CuO.....	150
Table 3 Uncertainty estimates of oxidized aluminum	151
Table 4 Measured Spectral-Directional Emittance of Thermally Oxidized Aluminum at 673 K (1st row), 773 K (2nd row), and 873 K (3rd row)	152
Table 5 Uncertainty Estimates of Oxidized Nickel Emittance Measurement	153
Table 6 Measured spectral-directional emittance of at 673 K (1st row), 773 K (2nd row), 873 K (3 rd row).....	154
Table 7 Uncertainty Estimates of Nickel Emissivity Measurement.....	155
Table 8 Uncertainty Estimates of Zirconium Emissivity Measurement.....	156
Table 9 Uncertainty Estimates of Titanium Emissivity Measurement.....	157

LIST OF NOMENCLATURE

α	thermal diffusivity [m^2/s]
a	side dimension of sample [m]
c	speed of light in vacuum [$2.998 \cdot 10^8 \text{ m/s}$]
c_2	second radiation constant [$14388 \text{ } \mu\text{m K}$]
C	calibration factor
γ	damping parameter
$\delta\lambda$	spectral bandwidth [μm]
ε'_λ	spectral directional emissivity
$\varepsilon_{h\lambda}$	spectral hemispherical emissivity
ε	total hemispherical emissivity
ε_0	permittivity of empty space [$8.854 \cdot 10^{-12} \text{ F/m}$]
ε	complex dielectric constant
ε_1	polarization
ε_2	absorption
e	electron charge [$1.602 \cdot 10^{-19} \text{ C}$]
E	electric field strength
E_0	maximum value of the electric field strength
E_λ	spectral emissive power [$\text{W/m}^2 \mu\text{m sr}$]

g	acceleration of gravity [m/s^2]
h	Planck's constant [$6.626 \cdot 10^{-34} \text{ J s}$]
I_λ	spectral intensity [$\text{W/m}^2 \mu\text{m sr}$]
μ	permeability of empty space [H/m]
k	extinction coefficient
k_{Cu}	thermal conductivity of copper [W/m K]
k_{oxide}	thermal conductivity of copper oxide [W/m K]
K	spring constant
K_∞	contribution of bound electrons at wavelength larger than their relaxation wavelength
λ	wavelength [μm]
λ_0	relaxation wavelength of the Drude single electron theory [m]
λ_i	relaxation wavelength of different types of carrier charges [m]
m	electron mass [$9.11 \cdot 10^{-31} \text{ kg}$]
M	magnetic field strength [H]
n	real index of refraction
N	complex index of refraction
N_f	number of free electron per cubic centimeter
Nu	Nusselt number
ρ	reflectivity
r_e	electrical resistivity [ohm cm]
R	radiometer reading [W]
R_c	blackbody radiometer reading [W]

σ	optical conductivity
σ_0	d.c. conductivity [1/ohm cm]
σ_B	Stefan-Boltzmann constant [$5.67 \cdot 10^{-8} \text{ W/m}^2 \text{ K}^4$]
σ_∞	parameter to account for deviations due to material imperfections
σ_i	conductivity components due to different types of carrier charges
t	thickness [m]
T	temperature [K]
T_{th}	temperature measured by the thermocouple [K]
u_e	uncertainty in emissivity
u_{Tc}	uncertainty in blackbody temperature
u_{Ts}	uncertainty in sample surface temperature
ν	frequency [Hz]
ν	kinematic viscosity [m^2/s]
x	displacement [m]
z	penetration distance [m]
ω	angular frequency [s^{-1}]
Ω	solid angle [sr]

SUBSCRIPTS

a	air
b	blackbody
c	calibration
s	sample
∞	surrounding

1 INTRODUCTION

Knowledge of thermal radiative emissivity of various metallic surfaces is at high demand for both engineers and researchers, and difficult to quantify because of the many influential physical parameters. Emissivity of metal surfaces at high temperatures is of importance to design and monitoring of numerous manufacturing processes, thermal performance of systems operating in space, as well as to a wide range of research and development activities including but not limited to: electron beam processing; laser welding; and metal refining. Emissivity is also the most influential parameter in temperature measurement by remote sensing devices widely used in fabrication processes. Furthermore, emissivity is a key parameter required in high temperature thermophysical properties measurements for metals, such as specific heat. Emissivity uncertainty has proved to have the greatest contribution to the total uncertainty of specific heat measurement [1, 2].

Thermal radiative emissivity is a surface property which strongly depends on material temperature, wavelength, direction, surface morphology, contamination, aging, and oxidation. Temperature is one of the parameters that influence thermal emissivity. The Hagen-Rubens relation predicts that spectral normal emissivity of metals at long enough wavelengths is proportional to the square root of absolute temperature. This variation causes an emissivity variation of 3-4 fold or more for metals, for a temperature rise from room temperature to just below the melting point. The same trend should also

hold for total hemispherical emissivity. Different variation with temperature is observed before and after the crossover point (wavelength) for many metals [3]. Emissivity of such metals does not depend on temperature at crossover point. Thermal radiative emissivity varies greatly over the electromagnetic radiation spectrum, and a variation in magnitude from near IR to mid IR over 3-4 fold or higher is usually seen [4, 5].

Direction of emission is an important parameter which affects the thermal emissivity and for an optically smooth surface is given by Fresnel's relation. For a high purity metallic surface according to Fresnel's relation, emissivity slightly increases with increasing polar angle and reaches a maximum at grazing angles [3].

The treatment of emissivity is often based on the assumption that the material surface is optically smooth. For an optically smooth surface, the surface roughness scale length is much less than the electromagnetic wave wavelength. For example, a material surface that is optically smooth in mid IR may be rough at short wavelengths; hence the electromagnetic wave theory does not accurately predict emissivity at short wavelengths.

Surface roughness is another parameter which greatly influences the radiative emissivity. Surface roughness, generally quantified as root mean square roughness, affects spectral emissivity as well as directional emissivity and generally an increase in emissivity is observed. The roughness character might be significantly different for different surfaces depending on material type, surface preparation, manufacturing method, etc [4].

Surface damages especially for an optically smooth surface can greatly influence the thermal radiative emissivity. Machining processes can damage or distort the crystal lattice near/on the surface, altering the thermal emissivity.

Another parameter that can significantly influence the emissivity is the thin coating which may be developed due to chemical reactions, adsorptions, or electrostatics. A thin oxide layer can coat a metallic surface even at room temperature, thus altering the radiative emissivity.

In summary, the limited thermal radiative emissivity available data should be taken with caution. Firstly, without elaborate descriptions of surface purity, topology, treatment, preparation, etc., available emissivity data may suggest little more than an order of magnitude estimate. Secondly, it is important to mention that surface properties can readily change due to oxidation and/or contamination during a process or even overnight. Thus, the thermal radiative emissivity of metals is hard to know due to the influence of too many parameters, which leads to lack of available data.

Radiative emissivity studies at elevated temperatures require more cautions regarding the sample's surface conditions, leading to complex experimental setups. The high temperature radiative emissivities of numerous metals in both atmospheric and vacuum conditions have been previously compiled [5-7]. Both oxidized and unoxidized metals studies were generally performed over a limited spectral range and typically only on normal direction.

Metals at high temperatures react easily with oxygen from the surroundings and form metal oxides. The metal oxide's emissivity differs from that of the base metal, and the oxidized metal emissivity is either more like the oxide or more like the metal, depending on the optical thickness of the oxide. In most prior studies, insufficient attention has been paid to surface condition, which can greatly affect the thermal

emissivity [4]. In a few instances [8, 9] where surfaces have been better characterized and controlled, the emissivity measurements were carried out over a narrow spectral range.

Now we need to differentiate between the high temperature radiative emissivity studies on high purity metals in air and in high vacuum conditions. High temperature radiative experiments on metals in vacuum are much rarer and have been performed most often in inadequate vacuum conditions, thus allowing oxide formation [5]. Surface contamination estimation based on the reported system pressures often indicates a high probability of inadequately controlled atmosphere, which can lead to significant departures from metal behavior [5].

High temperature metals emissivity studies in air (allowing oxidization) are generally limited to the normal direction, and made over a narrow/limited spectral range; hence, analysis on the influence of the metal oxide grown on the metallic surface cannot be adequately studied for further understanding of radiative properties. The metallic oxide has a great influence on the directional properties as well as on the complex refractive index. The complex index of refraction, which is difficult to find in the literature for materials at high temperatures, provides a comprehensive insight to radiative behavior, and can be reduced from a fully directional emissivity data.

The scarce reported work in this area leads to a very low confidence in the results due to large scatter of data between different reports. The reported results from various studies very rarely agree within their stated uncertainty limits, and these limits easily reach 10-15% [5, 6].

Thus, it is important to develop measurement techniques at high temperature to overcome the drawbacks of measurements over limited spectral range, directional range, and accuracy.

Electromagnetic wave theory is used as a foundation to develop theories on thermal radiative properties of metals. Classical theories such as Drude, Hagen-Rubens [10], and later Drude-Roberts [11], were used to explain the optical constants of optically smooth metallic surfaces; optical properties are strongly related to radiative properties. However, for most real metals the classical theory provides only a qualitative description of the variation of the radiative properties with wavelength and temperature. Later theories (Drude-Roberts) prove to be more suitable in describing the radiative properties of metals.

It is important to note here that radiative emissivity studies involve building complex apparatus which differ substantially for measurements performed in air and in high vacuum conditions. Usually these types of apparatus are very expensive and require costly maintenance. This leads to a limitation on radiative emissivity studies unless specific funding is provided. Therefore, it is important to use the theory to estimate radiative emissivity in order to reduce the number of necessary experiments.

Taking all the above into account, more accurate, easily reproducible, and comprehensive thermal radiative emissivity of both oxidized metals and high purity metals is needed. Moreover, scientists [12, 13] emphasized the need for additional emissivity experimental data for a better scientific understanding of physical properties. The present research studies oxidation effects on spectral, normal, as well as directional emissivity of metals, and brings insight into high temperature complex indices of

refraction. Moreover, this research studies the normal emissivity of metals over a wide spectral range and in special high vacuum conditions.

This is achieved for oxidized metals in air by using an experimental method which allows fully directional measurements to be performed, rather than only normal, and a very broad infrared spectrum through the use of a FTIR spectrometer. High accuracy in emissivity data is achieved using this experimental setup. The sample surfaces used in these experiments are examined using known characterization techniques. The resulting normal and fully directional emissivity data for oxidized metals is used in conjunction with the Fresnel's relation to derive the high temperature complex index of refraction; a property practically unavailable in the literature.

Research on high purity metals is achieved through the use of an experimental setup where the sample is heated using a non-contact method which avoids measurement contaminations and/or interaction with the sample, and provides high accuracy in emissivity measurement. Furthermore, adequate vacuum conditions are maintained to ensure that there is no surface oxidization, and surfacing techniques are employed to assure the sample surface integrity. The resulting normal emissivity data for metals at high temperature covers a wide infrared region from near IR well into mid IR, and is used to approximate the total hemispherical emissivity.

2 BASIC LITERATURE REVIEW

2.1 Emissivity Overview

Real surfaces have non-ideal properties which depend on numerous factors. Whereas blackbodies exhibit the maximum possible thermal emission, real surfaces display only a fraction of this emission. Emissivity is generally defined as the ratio of the radiation emitted by a surface to the radiation emitted by a blackbody radiator, both being at the same temperature. Spectral directional emissivity, (ϵ'_λ), of a surface at the temperature (T) is defined as the ratio of the intensity of the radiation emitted at the wavelength (λ) and in the direction (θ) -surface polar angle and (ϕ) - surface azimuthal angle to the intensity of the radiation emitted by a blackbody (which is independent of direction, or diffuse) at the same values of temperature and wavelength:

$$\epsilon'_\lambda = \frac{I_{\lambda,e}(\lambda, \theta, \phi, T)}{I_{\lambda,b}(\lambda, T)} \quad (1)$$

A reasonable assumption for most surfaces is that (ϵ'_λ) is independent of (ϕ). Therefore, Eqn. (1) becomes:

$$\epsilon'_\lambda = \frac{I_{\lambda,e}(\lambda, \theta, T)}{I_{\lambda,b}(\lambda, T)} \quad (2)$$

In general the directional distribution as shown in Fig. 1, may be other than the blackbody diffuse one.

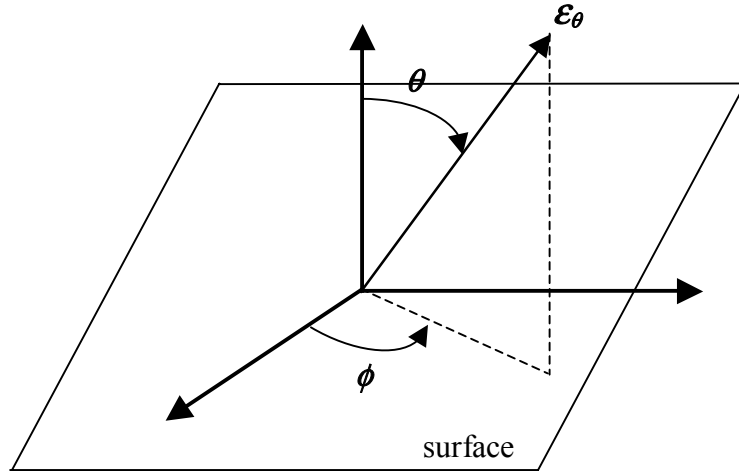


Figure 1 Directional Emissivity

Spectral hemispherical emissivity, ($\epsilon_{h\lambda}$), compares the emission into all directions above the surface (spectral emissive power) with the spectral emissive power of a black emitting surface:

$$\epsilon_{h\lambda}(T, \lambda) = \frac{E_{\lambda}(T, \lambda)}{E_{b\lambda}(T, \lambda)} \quad (3)$$

Eqn. 3 may be written as:

$$\epsilon_{h\lambda}(T, \lambda) = \frac{\int_0^{2\pi} \int_0^{\pi/2} I_{\lambda}(T, \theta, \lambda) \sin \theta \cos \theta d\theta d\phi}{\pi I_{b\lambda}(T, \lambda)} \quad (4)$$

Eqn. 4 can be further simplified to relate spectral hemispherical emissivity to spectral directional emissivity, (ϵ'_{λ}):

$$\epsilon_{h\lambda}(T, \lambda) = \frac{1}{\pi} \int_0^{2\pi} \int_0^{\pi/2} \epsilon'_{\lambda}(T, \theta, \lambda) \sin \theta \cos \theta d\theta d\phi \quad (5)$$

Finally, the total hemispherical emissivity, which is used in radiative heat transfer calculations, (ε), is a spectral average having as its weighting factor the spectral emissive power:

$$\varepsilon = \frac{\int_0^{\infty} \int_0^{2\pi} \int_0^{\pi/2} I_{\lambda}(T, \theta, \lambda) \sin \theta \cos \theta d\theta d\phi d\lambda}{\pi I_{b\lambda}(T, \lambda)} \quad (6)$$

2.2 Theory Overview

The propagation of electromagnetic waves in a medium in terms of its macroscopic electrical and magnetic properties is described by classical electromagnetic theory. Classical electromagnetic theory predicts the absorption and velocity of these waves, together with their reflection and refraction at an interface between two media. This theory provides the basis for methods used in determining the radiative properties of opaque surfaces in terms of their optical constants.

2.2.1 Maxwell's equations

The set of Maxwell's equations is the basis of electromagnetic theory. The equations for a homogeneous, isotropic medium can be written:

$$\begin{aligned} \nabla \cdot \vec{E} &= 0 & \nabla \times \vec{E} &= -\frac{\mu}{c} \frac{\partial \vec{H}}{\partial t} \\ \nabla \cdot \vec{H} &= 0 & \nabla \times \vec{H} &= \frac{\epsilon}{c} \frac{\partial \vec{E}}{\partial t} + \frac{4\pi\sigma}{c} \vec{E} \end{aligned} \quad (7)$$

where, H and E are the magnetic and the electric field vectors, while μ , ϵ and σ are the permeability, the real dielectric constant and the conductivity of the medium.

From the Maxwell's equations a wave equation involving the electric field vector E may be obtained:

$$c^2 \nabla^2 \vec{E} = \epsilon \frac{\partial^2 \vec{E}}{\partial t^2} + 4\pi\sigma \frac{\partial \vec{E}}{\partial t} \quad (8)$$

The typical solution for Eqn. 8 is a periodic plane wave solution:

$$E = E_0 \exp\left[i\omega\left(t - \frac{zN}{c}\right)\right] \quad (9)$$

where E_0 is the maximal value of the electric field strength, $\omega = 2\pi\nu$ is the angular frequency, z is the penetration distance into the metal, and N is the complex index of refraction defined as:

$$N = \left[\epsilon_1 - \frac{4\pi\sigma}{\omega} i \right]^{1/2} = n - ik \quad (10)$$

Here, n is the real index of refraction and k is the extinction coefficient which represents a measure of the damping of the electromagnetic wave as it penetrates the metal. The complex index of refraction is related to the complex dielectric constant through:

$$\hat{N}^2 = n^2 - k^2 - 2nki \equiv \hat{\epsilon} = \epsilon_1 - i\epsilon_2 \quad (11)$$

2.2.2 Fresnel's equation

The Fresnel's equation [14] can be used in conjunction with Kirkhoff's law to determine spectral directional emissivity of an opaque medium in vacuum. The Fresnel's equation described in Eqn. 12, assumes that the vacuum to material interface is sharp and the optical properties n and k are constant with depth into the material. The equation also assumes an isotropic material with no dependence on the azimuthal angle.

$$\varepsilon'_\lambda = 1 - \frac{1}{2} \left(\frac{(n_\lambda \beta - \cos \theta)^2 + (n_\lambda^2 + k_\lambda^2) \alpha - n_\lambda^2 \beta^2}{(n_\lambda \beta + \cos \theta)^2 + (n_\lambda^2 + k_\lambda^2) \alpha - n_\lambda^2 \beta^2} + \frac{(n_\lambda \gamma - \alpha / \cos \theta)^2 + (n_\lambda^2 + k_\lambda^2) \alpha - n_\lambda^2 \gamma^2}{(n_\lambda \gamma + \alpha / \cos \theta)^2 + (n_\lambda^2 + k_\lambda^2) \alpha - n_\lambda^2 \gamma^2} \right) \quad (12)$$

where,

$$\alpha^2 = \left(1 + \frac{\sin^2 \theta}{n_\lambda^2 + k_\lambda^2} \right)^2 - \frac{4n_\lambda^2}{n_\lambda^2 + k_\lambda^2} \left(\frac{\sin^2 \theta}{n_\lambda^2 + k_\lambda^2} \right), \quad (13)$$

$$\beta^2 = \frac{n_\lambda^2 + k_\lambda^2}{2n_\lambda^2} \left(\frac{n_\lambda^2 - k_\lambda^2}{n_\lambda^2 + k_\lambda^2} - \frac{\sin^2 \theta}{n_\lambda^2 + k_\lambda^2} + \alpha \right), \quad (14)$$

$$\gamma = \frac{n_\lambda^2 - k_\lambda^2}{n_\lambda^2 + k_\lambda^2} \beta + \frac{2n_\lambda k_\lambda}{n_\lambda^2 + k_\lambda^2} \left(\frac{n_\lambda^2 + k_\lambda^2}{n_\lambda^2} \alpha - \beta^2 \right)^{\frac{1}{2}}, \quad (15)$$

2.2.3 Lorentz model

Lorentz explained radiative absorption in dielectric materials by treating the electrons as simple harmonic oscillators. He postulated that electrons are bound to their respective nuclei. Electromagnetic fields such thermal radiation and light are the driving forces for the oscillators. The Lorentz model postulates that matter is a collection of harmonic oscillators which are independent, identical and isotropic. A linear restoring force Kx acts upon each oscillator, where K is a spring constant and x is the displacement from equilibrium. Each oscillator has a mass m and charge e and the damping force on the oscillator is $\gamma \dot{x}$ where γ is the damping constant.

$$m \frac{d^2 x}{dt^2} + \gamma \frac{dx}{dt} + Kx = eE_0 \exp(i\omega t) \quad (16)$$

The interaction between the oscillator and the electromagnetic radiation is driven by a time harmonic with ω the frequency of the radiation. The solution is:

$$x = \frac{e/mE}{\omega_{res}^2 - \omega^2 - i\gamma\omega} \quad (17)$$

where $\omega_{res} = K/m$. The complex index of refraction and the dielectric constant are then:

$$n^2 - k^2 = \epsilon_1 = 1 + \frac{\omega_{pl}^2(\omega_{res}^2 - \omega^2)}{(\omega_{res}^2 - \omega^2)^2 + \omega^2\gamma^2} \quad (18)$$

$$2nk = \epsilon_2 = \frac{\omega_{pl}^2\omega\gamma}{(\omega_{res}^2 - \omega^2)^2 + \omega^2\gamma^2} \quad (19)$$

The bound electron effects described by Lorentz, correspond to the interband transitions described by quantum mechanics [10]. The variation of optical constants of silicon nitride [15] was studied and the general features of the ideal oscillator were found apparent. The Lorentz model was used in understanding optical properties of some insulators in some degree although more complex oscillator models provide better agreement with experiments.

2.2.4 Drude model

Drude proposed a model which treats the free (unbound) charges within conducting materials by allowing the restoring force of the Lorentz model to go to zero.

The oscillator equation of motion then becomes:

$$m \frac{d^2x}{dt^2} + \gamma \frac{dx}{dt} = eE_0 \exp(i\omega t) \quad (20)$$

The damping constant is considered to be a function of N_f , the number of free electrons per cubic centimeter; e is the electron charge, and σ_0 is the d.c. conductivity:

$$\gamma = \frac{N_f e^2}{\sigma_0} \quad (21)$$

The solution of Eqn. 20 is:

$$x = \frac{E}{\frac{N_f e \omega}{\sigma_0} i - \frac{m \omega^2}{e}} \quad (22)$$

The optical constants can be written as [16]:

$$n^2 - k^2 = \epsilon_1 = 1 - \frac{N_f e^2 \tau^2}{m \epsilon_0 \omega (1 + \omega^2 \tau^2)} \quad (23)$$

$$2nk = \epsilon_2 = \frac{N_f e^2 \tau}{m \epsilon_0 \omega (1 + \omega^2 \tau^2)} \quad (24)$$

Considering the damping constant, $\gamma = 2\pi c/\lambda_0$, angular frequency, $\omega = 2\pi c/\lambda$,

and $\sigma_0 = \frac{N_f e^2}{2\pi c} \lambda_0$, the complex dielectric constant of a metal can also be written as:

$$\epsilon = 1 - \frac{\lambda^2}{2\pi c \epsilon_0} \left(\frac{\sigma_0}{\lambda_0 - i\lambda} \right) \quad (25)$$

Separating the real and the imaginary parts, and by the use of Eqn. 11, gives the result

[11, 17]:

$$n^2 - k^2 = 1 - \frac{\lambda^2}{2\pi c \epsilon_0} \left(\frac{\sigma_0 \lambda_0}{\lambda_0^2 + \lambda^2} \right) \quad (26)$$

$$2nk = \frac{\lambda^3}{2\pi c \epsilon_0} \left(\frac{\sigma_0}{\lambda_0^2 + \lambda^2} \right) \quad (27)$$

where λ_0 is the relaxation wavelength of the Drude single electron theory, ϵ_0 is the permittivity of empty space, and c is the speed of light in a vacuum.

The Drude model provides only a quantitative insight to the variation of the complex index of refraction with wavelength for most real metals, especially for monovalent metals. Although the Drude model gives a good agreement with experimental data on optical constants for most liquid metals at room temperature for optical constants, no correlation between theory and the experiments was found for multivalent metals.

2.2.5 Hagen-Ruben relation

For wavelengths larger than 30 microns the Drude model can be used to obtain the Hagen-Ruben approximation. For low frequencies, inertial forces on the free electrons in metals become negligible [18] and the equation of motion can be simplified to:

$$\gamma \frac{dx}{dt} = eE_0 \exp(i\omega t) \quad (28)$$

In this spectral region the index of refraction n and the extinction coefficient k become similar:

$$n = k = \sqrt{\frac{0.003\lambda}{r_e}} \quad (29)$$

The normal spectral emissivity can then be calculated from the electrical resistivity as:

$$\varepsilon_n(\lambda_0) = 0.365 \sqrt{\frac{r_e}{\lambda}} - 0.0667 \frac{r_e}{\lambda} \quad (30)$$

Here, λ is given in μm and r_e in ohm-cm [19]. For metals, this equation sometimes exhibits qualitative agreement with experiments at wavelengths as short as $5\mu\text{m}$, but this should be regarded as fortunate. At shorter wavelengths the Hagen-Rubens relation

underestimates the emissivity for highly smooth, pure surfaces. The majority of real surfaces exhibit higher emissivity in this region due to effects generally appearing during sample preparation [20]. Among those effects are: roughening, oxidation due to air exposure, heat treatments and contaminations/interactions.

The Hagen-Rubens relation can also predict the variation of the optical constants and the normal spectral emissivity with temperature through the electrical resistivity temperature dependence.

2.2.6 Drude-Roberts model

Roberts [11] attempted to improve one of the models suggested by Drude and later abandoned. The model claimed that at least two free charge carriers are free to move in metals and contribute to their optical properties. Roberts suggested that the dielectric constant of materials can be expressed by:

$$\epsilon = K_{\infty} - i \frac{\sigma_{\infty} \lambda}{2\pi c \epsilon_0} - \frac{\lambda^2}{2\pi c \epsilon_0} \left(\frac{\sigma_1}{\lambda_1 - i\lambda} + \frac{\sigma_2}{\lambda_2 - i\lambda} \right) \quad (31)$$

where, σ_1 and σ_2 are the conductivity components due to the two types of charge carrier and λ_1 and λ_2 are the corresponding relaxation wavelengths. The constant K_{∞} is used to account for the contribution of the bound electrons at wavelengths λ which are large relative to the resonance wavelengths. Roberts included in this model the conductivity term σ_{∞} to account for deviations due to material imperfections, but no theoretical grounds were given. Roberts treated λ_2 , σ_2 , σ_{∞} , K_{∞} , σ_1/λ_1 as being insensitive to temperature and λ_1 , σ_1 as temperature dependent. The d.c. conductivity is related to the conductivity components through:

$$\sigma_0 = \lim_{\lambda \rightarrow \infty} \left(\frac{i2\pi c \epsilon_0 \epsilon}{\lambda} \right) = \sigma_1 + \sigma_2 + \sigma_\infty \quad (32)$$

Furthermore, the complex index of refraction obtained from Roberts's model is:

$$n^2 - k^2 = K_\infty - \frac{\lambda^2}{2\pi c \epsilon_0} \left(\frac{\sigma_1 \lambda_1}{\lambda_1^2 + \lambda^2} + \frac{\sigma_2}{\lambda_2^2 + \lambda^2} \right) \quad (33)$$

$$2nk = \frac{\sigma_\infty \lambda}{2\pi c \epsilon_0} + \frac{\lambda^3}{2\pi c \epsilon_0} \left(\frac{\sigma_1}{\lambda_1^2 + \lambda^2} + \frac{\sigma_2}{\lambda_2^2 + \lambda^2} \right) \quad (34)$$

Drude-Roberts model brought an improvement in the description of the optical properties of some metals such as nickel, platinum, iridium, and tungsten by fitting the reported experimental data at room temperature, on a generalized Drude model. This model was able to predict the X-point seen in some metals. At X-point the emissivity does not depend on temperature.

2.3 Emissivity Measurement Methods

Various experimental techniques have been developed for measuring the radiative properties of opaque materials. These techniques may be separated into three different categories: calorimetric emission measurements, reflection measurements, and radiometric emission measurements.

The total-hemispherical emittance of a sample can be determined using calorimetric emission measurements [21-26] by measuring the net radiative heat loss or gain of an isolated specimen. A typical experimental setup has the sample suspended inside an evacuated chamber with walls coated with a near black material. The chamber walls are cooled while the sample is electrically heated and both the temperature of the sample and the chamber are monitored.

A major source of uncertainty is the uncertainty in the measured sample temperature because the thermocouple used to measure sample temperature, can pick up a potential due to current flowing in the sample. However, calorimetry is usually free of large systematic errors and therefore is suitable for engineering heat transfer applications that need total hemispherical emissivity.

Radiometric reflection measurements are used indirectly to determine emissivity, through of Kirchoff's law. The different types of experiments can be divided into four categories: heated cavity reflectometers, integrating sphere reflectometers, integrating mirror reflectometers, and bi-directional reflectometers [27-34]. In order to evaluate emissivity by measuring reflectivity, all the reflected flux must be collected and measured, which is practically impossible because the solid angles of the incident and reflected beams are mutually exclusive.

Spectral measurements generally become more difficult at long wavelengths in the infrared due to the low emissive power from the sample as well as from the available sources required for reflection measurements. Especially for metals at long wavelengths, when reflectance tends to unity, reflectance must be measured precisely in order to infer accurate values of the spectral emissivity, $\epsilon_\lambda = 1 - \rho_\lambda$.

Radiometric emission measurement techniques are used to determine the spectral and directional surface emissivities of a sample at high temperature. The most widely used methods compare the sample emission to the emission from a separate blackbody or an integral blackbody cavity under exactly the same conditions.

In radiometric emission measurement, the energy emitted from a sample is compared to the energy emitted from a blackbody reference cavity at the same

wavelength and the same temperature. Using a specific experimental setup, which allows sample surface to be directionally viewed, the energy emitted by the sample, can be detected in a specific direction. If the same detection system or equivalent detection systems are used for both measurements, then the spectral-directional emittance can be determined by simply taking the ratio of the two signals.

One type of radiometric experiment uses an integrated blackbody [35-39], where the sample is incorporated into the design of the blackbody. The setup can be realized by heating the sample at the bottom of a deep, cylindrical, isothermal cavity. In this case the radiation emitted by the sample will correspond to that of a blackbody. By replacing the hot wall with a cold one the radiation leaving the sample will be due to emission alone. The effect of hot side walls can be suppressed if the sample is mounted on a movable rod which can be moved toward the exit of a furnace during the emission measurement, or by fixing the sample at the base of the furnace and dropping a cold tube into the cavity when emission measurements are taken. The integral blackbody technique is usually preferred at very high temperatures and for normal emissivity measurements.

Measurements are usually performed in air, although a few very expensive experimental setups capable of performing measurements in a vacuum are reported [40, 41]. A major drawback of the integral blackbody method is that it is limited to measurements in the direction of the sample surface normal. Another disadvantage of the integral blackbody method for vacuum measurements is that the low signal-to-noise ratio reported at shorter wavelengths generates large scatter in the data or values that exceed unity.

Another type of experiment can be realized with a separate blackbody [42-49], which is heated to the same temperature as the sample. In order to monitor the sample and blackbody emissions using the same optical path, two identical optical paths can be used, or the sample and the blackbody can alternatively be placed into identical optical path. An experimental setup which uses two identical paths is realized by using moving optical components. An important advantage arises here because the sample can be viewed easily from different directions, which allows directional measurements rather than only the normal direction [50-55].

Radiometric emission measurements provide reliable emissivity data on a spectral basis which is generally limited by the detector limits. Reported uncertainty in emissivity is usually around 10-15%. A broad spectral range emissivity can be conveniently used to determine total hemispherical emissivity according to [56]. Measurements can be performed in air or in a vacuum, depending on specific applications.

2.4 Emissivity Availability

A significant volume of thermal radiative properties for metals are included in available data compilations [5-7]. However, researchers and engineers involved in thermal radiation analysis problems frequently encounter difficulties in their search for emissivity data. Significant variations between the results reported by different investigators on the same material are typically found. Scatter in the reported data can often be traced to the sample surface condition upon which experimental investigation was performed. For example, the presence of oxide layers can strongly influence the emissivity of metals. In addition, the sample surface topology together with composition, contamination, and ageing significantly affects the emissivity of metals [5]. These effects

easily lead to significant differences among the same material on both spectral as well as directional bases.

The majority of the spectral emissivity data available, even for the most common metals, is taken at room temperature and is generally derived from reflectivity. This is sufficient for those few metals which show no temperature dependence of emissivity over a broad spectral range. However, there is a significant number of metals (e.g. transition metals) for which emissivity depends strongly on temperature, and an even larger number of metals for which the temperature dependence is unknown. This is further complicated by the fact that the influence of temperature is wavelength dependent. Thus, even if data is available for the total hemispherical emissivity as a function of temperature, there is often no information about the temperature dependence of the spectral emissivity at any given wavelength.

For high purity metals, high temperature spectral emissivity studies have been generally performed at a single wavelength [57-62], or a narrow spectral region [63-68], mostly limited to the visible part of the spectrum.

Studies of spectral emissivity performed on the same metal lead to contradictory results. Serious differences in magnitude and spectral emissivity profile, and different temperature dependence [69-71] were obtained. This means that the processing and measurement conditions, as well as uncertainty in measurement influence the emissivity to a great extent.

Total hemispherical emissivity of metals at high temperatures is required for engineers dealing with radiative heat transfer in different manufacturing processes such as casting, forming, extrusion, laser welding, metal refining, electron beam processing,

vacuum arc remelting, etc., as well as remote sensing devices. Studies from different authors performed on the same metal lead to large scatter in data, generating differences as high as 50% with a standard deviation of 20% or higher [72-77].

Studies were performed to find out the X-point of metals. The X-point represents a specific wavelength at which the spectral emissivity does not depend on temperature which might be explained by an optical homogeneity. Generally, there is no agreement within the reported work, studies performed on the same metal resulting in different X-points [59, 71, 78-83].

Spectral dependence of emissivity for high purity metals has always been a challenge due to difficulties and challenges associated with the experimental setup, measurement conditions, and due to the high reactivity of metals at high temperature. If measurements were performed in improper vacuum conditions, departure from a metallic behavior is evident [84-86].

Spectral emissivity studies on oxidized metals are scarcer than studies performed on high purity metals, and directional studies are practically non-existent. The variability in the reported data is much more significant than that reported on high purity metals studies. The influence on metal emissivity, of the grown metal oxide is on both a spectral as well as a directional basis. Practically, the limited reported data on oxidized metals varies on spectral basis from a low asymptotic behavior in near IR around 0.1 and reaches easily to values of 0.8 or higher [5]. Thus, based on the available data, obtaining emissivity behavior with reasonable uncertainty is a challenge for researchers and engineers.

3 OBJECTIVES

High temperature emissivity of metals is a key parameter required for numerous manufacturing processes, thermophysical properties and remote sensing devices. The emissivity, reflectivity and absorptivity are the main optical properties of a solid opaque metallic surface.

The optical properties of a metal can be obtained from theoretical predictions or through experimental methods. Optical properties derived from theoretical predictions have only limited applicability since the theory is derived for pure and optically smooth surfaces. Such obtained data is considered useful only in identifying expected trends. Thus, the most reliable method in obtaining accurate optical properties is through experimental methods. The reported literature emissivity data, found mostly in compilations [5-7], are generally limited, display a significant degree of scatter, and have high uncertainty. These limitations are referred to spectral and temperature ranges, direction of emission, surface conditions, etc.

In order to address the entire challenging problem of finding emissivity, for a specific metal surface, previously reported data, theoretical prediction, experimental methods or a combination of these must be taken into account. High temperature emissivity of metals is greatly influenced by the oxidization on both spectral and directional matter. Therefore, the investigation of emissivity behavior of metals and oxidized metals at high temperature represents the objective of the current study.

Specifically, the first objective of this research is to study the normal emissivity of pure metals for a wide infrared spectral range. The research will contribute to the understanding the emission in metals, and will help quantify the total hemispherical emissivity required not only by the radiative heat transfer applications and also by the thermophysical properties measurements. In addition, this will provide correlation with available theories, and complex index of refraction.

This objective will be achieved by investigating pure, smooth metallic surfaces and by the use of an experimental setup where the sample is heated by a non contact method capable of performing accurate, normal spectral measurements. Such an experimental setup minimizes tremendously the likelihood of sample contamination and oxidization due to sample-holder interaction, which can easily alter the data. This experimental setup can be successfully used for further investigations even on levitated metals. Particularly, nickel, titanium and zirconium are studied. In this research we will determine how normal emissivity varies over a very broad infrared spectral range. This will provide a significant useful reference for future research and thus, make it possible to tailor the radiative properties of these materials for advanced applications.

The second objective is to study how the metal oxide artificially grown on metal surface and processing conditions influences the normal spectral, as well as directional emissivity. It is known that metal oxide influence on substrate emissivity depends on its optical thickness. This objective will be achieved through investigating both an optically thick and thin surfaces.

Specifically, an optically thick surface of oxidized copper artificially grown by heating in air high purity copper will be investigated. The experimental setup used for

optically thick metal oxide layer incorporates a pyroelectric detector and a sample holder which allows fully directional measurements. In addition, optically thin surfaces obtained by heating in air aluminum and nickel will be studied. The experimental setup used for optically thin surfaces replaces the detection system from the above mentioned setup with an FTIR spectrometer. The FTIR spectrometer is capable of performing rapid and accurate measurements over a broad spectral range.

4 EXPERIMENTAL PROCEDURES

A radiometric emission measurement technique was used to develop distinct experimental setups for high temperature emissivity measurement. This experimental setup is intended for oxides and oxidized metals in air and in high vacuum conditions for metals. The first experimental setup used in this study had a very good uncertainty in emissivity but the spectral range was limited and measurements were performed slowly, at one wavelength at a time. The second experimental setup eliminated the drawbacks of the first experimental setup by measuring all wavelengths at a time for an extended spectral range. The third experimental setup is designed for high temperature emissivity measurements in high vacuum for metallic samples both below and above the melting point.

4.1 Experimental Procedure for Oxidized Metals with Pyroelectric Detector

The experiment setup developed by Jones et al. [51] can be used to measure the spectral and directional emissivity of oxides and oxidized metals in air and uses a pyroelectric detector in conjunction with an optical discrimination system to determine emissivity of oxidized metals and artificially grown oxides in air as a function of temperature, wavelength and direction. The spectral measurements can be performed for a spectral range from 2 to 8 μm for one wavelength at a time. The calculated uncertainty was found to be within 3.5% in emissivity value.

Radiative flux was measured within a finite solid angle (Fig. 2) of 0.02 sr (maximum polar variation of 9°). Radiation leaving the sample (2) is reflected from an off-axis parabolic gold-coated mirror (4) into a collimated beam. The collimated beam is then trimmed by a beam trimming plate (5), which has an aperture of 19 mm diameter. The 19 mm beam is chopped (6) in order to help distinguish the intensity signal from background noise. The modulated beam is passed through a set of optical filters (7) to attenuate over and undertones and is refocused by a second off-axis parabolic mirror (8) into a grating monochromator (9) in order to achieve spectral discrimination. The output of the monochromator, which represents the radiative flux within a certain bandwidth, is focused onto a pyroelectric detector head (10). The signal of the pyroelectric detector is amplified and read by a radiometer.

The radiometer reading is calibrated using a blackbody (massive radiating cavity) controlled to the same temperature as the sample. The first mirror used in the optical path can be rotated using a rotation mechanism (11) and the sample and heater block assembly can be set in different positions on its rack (1). This allows the surface of the sample to be viewed from different angles between normal and 84° .

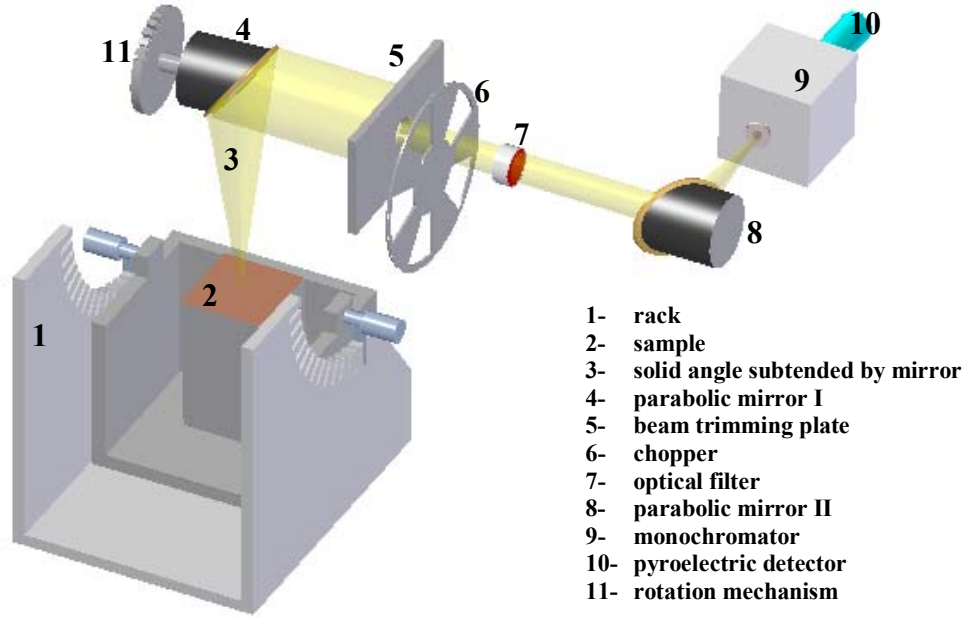


Figure 2 Experimental setup with pyroelectric detector

4.2 Experimental Procedure for Oxidized Metals with FTIR Spectrometer

The experiment setup developed for oxidized metals in air replaces the pyroelectric detector and the optical discrimination system with an FTIR spectrometer, and can measure the emissivity of oxidized metals and artificially grown oxides in air as a function of temperature, wavelength, and direction. The spectral measurements can be performed for an extended spectral range from 1 to 20 μm simultaneously. Such a broad spectral range can be used for hemispherical emissivity approximation. The maximum calculated uncertainty was found to be within 3.5% in emissivity value (Appendix C).

The heater block (Fig. 3) and the sample are heavily insulated up to the plane of the sample surface. The heater block, sample and insulation are contained in a slotted arc rack casing (1). The sample surface temperature is monitored and controlled by a thermocouple that is embedded through the heater into the sample up to a point just beneath the sample's radiating surface. An FTIR spectrometer (Spectrum GX) was incorporated into the previous apparatus described in Chapter 4.2, to replace the optical discrimination system and the pyroelectric detector. Radiative flux is measured within a finite solid angle of 0.0049 sr using a 12 mm aperture. The radiation that leaves the sample (2) is reflected from an off-axis parabolic mirror gold-coated (4) into a collimated beam (6). The collimated beam is then directed into an FTIR spectrometer (7) using the external FTIR viewport. The optical path is calibrated using a blackbody cavity, which is positioned at 90° from the sample and can be viewed by rotating the parabolic mirror.

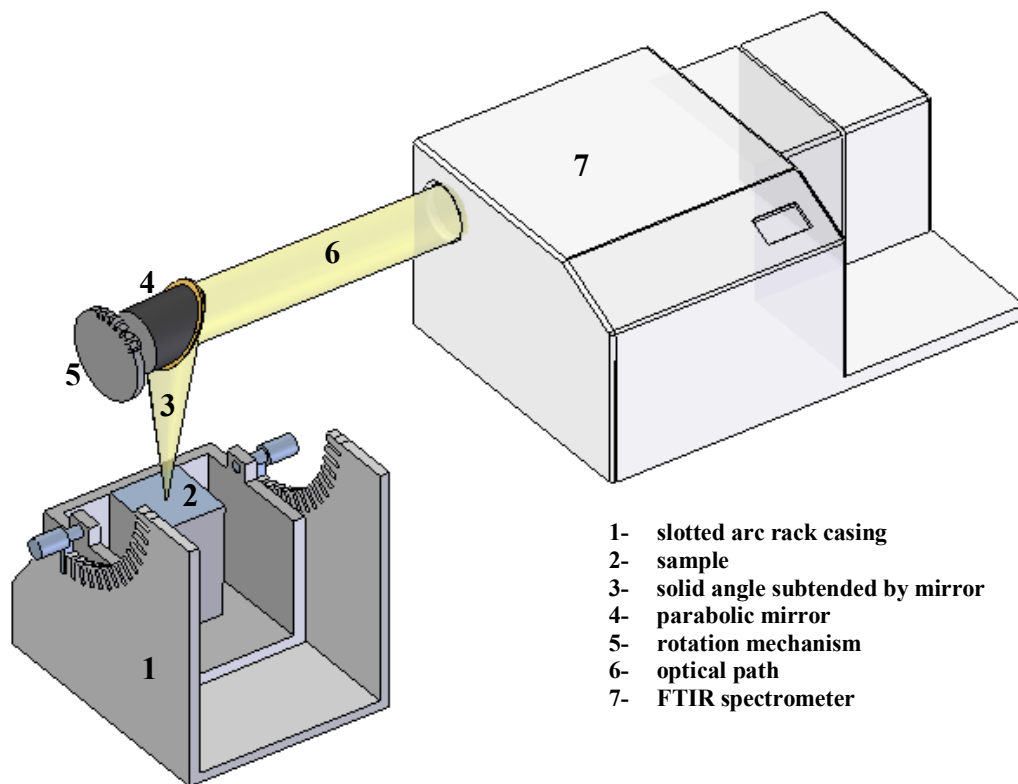


Figure 3 Schematic of experimental setup with FTIR spectrometer

The blackbody-radiating cavity was machined into 152 mm diameter copper, insulated by a 76 mm thick ceramic wool blanket and its wall temperature is kept at the same temperature as the sample surface using a PID temperature controller. By rotating the parabolic off-axis mirror (4) using a rotation mechanism (5), and moving the sample position to a corresponding position on the slotted arc rack, measurements at different angles to the surface normal are achieved.

4.3 Experimental Procedure for Metals in High Vacuum

The second experiment setup was built by coupling an electromagnetic levitator developed at Auburn University with a high temperature blackbody and the FTIR spectrometer in order to measure normal emissivity of metals in high vacuum conditions. The spectral measurements can be performed for an extended spectral range from 1 to 16 μm and for high temperatures below the melting point. A high vacuum condition is used in order to avoid sample oxidation. The calculated uncertainty is found to be less than 4% in emissivity value. A schematic diagram of the experimental apparatus used to measure normal spectral emissivity of electromagnetically heated nickel is illustrated in Fig. 4. The sample surface temperature is monitored by a Mikron two-color pyrometer. The radiation heat flux, which leaves the sample inside the vacuum chamber (1), is collected by a plano-convex zinc selenide lens (2), which has a focal length of 254 mm. The custom made zinc selenide lens has a proprietary coating which ensures a transmissivity of more than 95% for the spectral range considered. The collected radiation is then collimated into the optical path (3) and directed toward a gold-coated plane mirror (4). The radiation reflected by the gold-coated plane mirror is directed toward the FTIR spectrometer external viewport. At the end of the optical path another plano-convex zinc

selenide lens (5) with a focal length of 127 mm is used to refocus the beam into the FTIR spectrometer (6). The radiation flux leaving the blackbody cavity is collected by another plano-convex zinc selenide lens (8) and collimated into the optical path. The blackbody cavity radiation flux can be directed toward the FTIR spectrometer (6) by adjusting the position of the gold-coated plane mirror (4).

Collected data were averaged over ten scans using 16 cm^{-1} resolution. The blackbody-radiating cavity used in the experiment was a high purity alumina furnace provided by Mellen Inc., highly insulated, with a maximum operating temperature of 1873K. Its wall temperature was kept at the same temperature as the sample surface using a PID temperature controller.

The electromagnetic levitator (EML) system developed at Auburn University uses one set of coils operated at a single frequency to levitate and heat the sample. Figure 5 shows a schematic diagram of the RF coils system and the geometric configuration for the coils set. A key part of the EML is the induction coil housed in a vacuum chamber capable of lower than 10^{-7} torr obtained using a turbomolecular pump. A commercial 1 kW RF power supply is used to provide a high frequency alternating current of approximately 175 amps and 280 kHz to the induction coil. The induction coil is configured to impose a quadrupole positioning field to keep the sample approximately in the middle of the coil. One of the advantages of the quadrupole design is that the system is very simple and easy to build, and has high degree of symmetry.

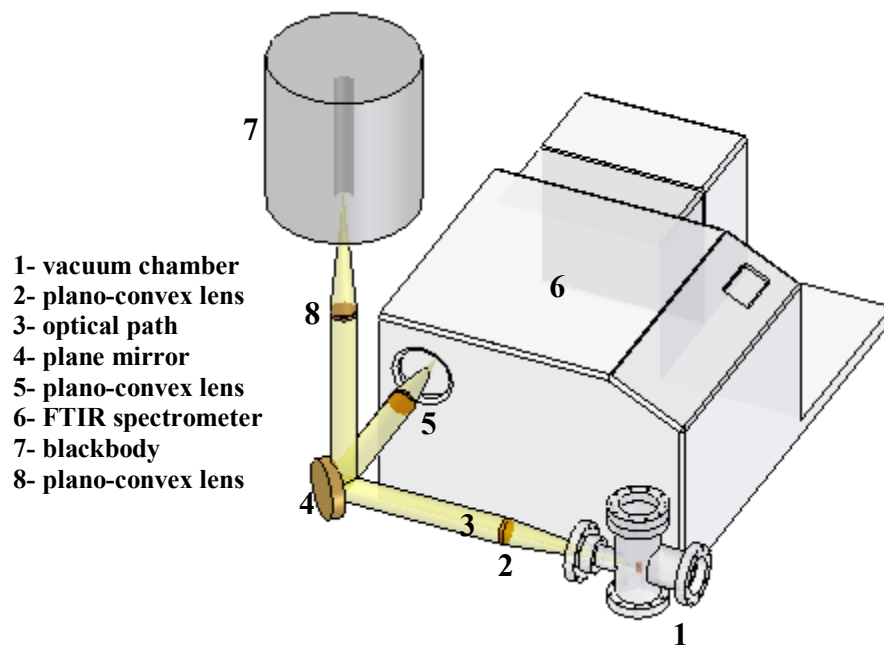


Figure 4 Schematic of experimental setup with high vacuum chamber

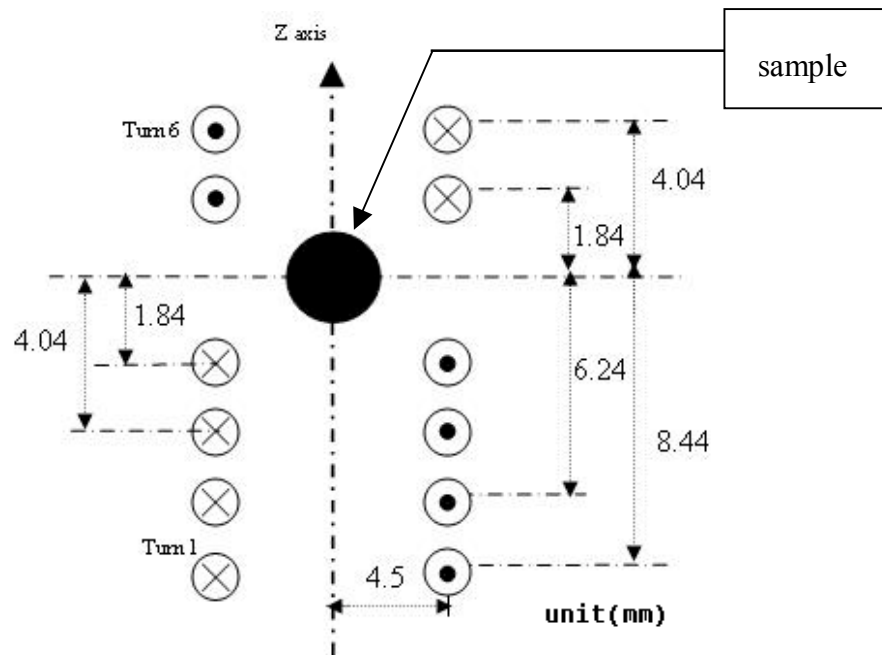


Figure 5 Schematic of electromagnetic induction coil.

4.4 Discussion of Different Experimental Setups

The radiometric experimental setup with a pyroelectric detector used to study the normal, spectral and directional emittance of cupric oxide exhibits a series of advantages and disadvantages. The low total and maintenance costs, and more important the availability of setup [51] represent the main advantages. One of the important disadvantages of the experimental setup with a pyroelectric detector is the limitation of the spectral range (1 to 8 μm), which is not broad enough for a total hemispherical emittance approximation. A set of optical filters coupled with gratings and a monochromator were used to perform measurements at each specific wavelength. Therefore, another disadvantage is the discontinuity in the resulting spectrum. Due to the fact that that investigations were performed at one wavelength at a time and adjustments in the optical path were needed at each wavelength, the experiment is very time consuming, which is one of the most important drawbacks.

The next step in this investigation was to eliminate the above drawbacks for further studies. The experimental setup built in this study replaces the pyroelectric detector and the optical discrimination system in the previous experimental setup with a FTIR spectrometer.

The FTIR spectrometer provides a rapid and accurate detection and processing of the signal. Fourier transform spectrometers have the capability to modulate their radiation source. The spectrometer's detector is sensitive only to modulated radiation. Considering that there is a unique modulation frequency for each source frequency, the FTIR spectrometer allows simultaneous frequencies detection and eliminates the chopping need. Therefore, the experimental setup built can easily achieve spectral measurements

over a very broad spectral range from 1 to 20 μm simultaneously, which is wide enough for total hemispherical emissivity approximation. Directional measurements can be achieved from normal to the sample surface up to 84° polar angle with a step of 6° . The sample's surface temperature over which measurements can be taken varies from 673 to 973K and maximum uncertainty in emissivity attained in this work was less than 3.5%. The temperature range is dictated by the blackbody cavity used in this experiment.

The next experimental setup built in this study uses the broad spectral range of the FTIR for normal emissivity studies of pure metals. This experimental setup has an important feature: it couples the broad band capability of the FTIR with a non-contact heating method which minimizes the possibility of sample interaction and contamination during the experiment. Such an experimental setup can be used for normal emissivity studies of metals at temperature between 1273 and 1673K. The limitation of the temperature range is established by the two wavelength pyrometer used to monitor the sample surface temperature, and the maximum operating temperature of the blackbody cavity. Investigations on spectral range can be performed from 1 to 16 μm rather than the broader FTIR capability. The limitation is dictated by the plano-convex lenses and viewport window transmissivities.

The high vacuum environment is attained before heating began by a roughing and a turbomolecular vacuum pump, and levels of 10^{-7} - 10^{-8} Torr proved to be sufficient in preventing sample surface oxidization. The measurements performed on pure metals were preceded by heating the samples near the melting point. Heating titanium and zirconium samples near the melting point in high vacuum levels (around 10^{-8} Torr) was performed in order to remove the adsorbed gasses [72, 87] other impurities, and to

prevent oxidization. Moreover, a polished sample surface is achieved through heating near the melting point.

5 RESULTS AND DISCUSSION

This chapter will reveal the experiments and the results of emissivity behavior of specific metals and oxidized metals studied during this work. Copper, aluminum and nickel are the oxidized metals studied in air. The experimental setup used for oxidized copper in air incorporates a pyroelectric detector for emission detection, which was later replaced with an FTIR spectrometer for oxidized aluminum and nickel studies. Fully directional measurements are performed rather than normal only to the surface, at temperatures between 676 K and 973 K. Nickel, titanium and zirconium are the pure metals investigated in a vacuum. The experimental setup used for measurements in vacuum uses a FTIR spectrometer for emission detection and performs sample heating using a non-contact method. The spectral normal emissivity of metals will be studied for a wide spectral range and at high temperatures above 1300 K. The resulting data is compared with available literature data and is also used to determine the complex index of refraction.

5.1 Oxidized Copper

The asymptotic composition of copper oxide, when oxygen-annealed in atmospheric pressure and at less than 1373 K, is cupric oxide, CuO. Cupric oxide grown on high purity copper will be studied for the purpose of gaining knowledge of thermal emittance behavior of an optically thick film. No prior studies have been reported about

high temperature emittance of CuO on a spectral and directional basis, and no results on the complex index of refraction are available at high temperature in infrared.

5.1.1 Specific Literature Review

A considerable amount of experimental data has been compiled on optical properties of oxidized copper [88-93], although most of it encompasses only total-hemispherical and total-normal properties rather than a complete spectral directional description, and none of them relate the radiative properties with cupric oxide CuO. The radiative properties of CuO have been addressed in a number of works [12, 94, 95]. Features considered in these earlier studies that impact thermal management are: the temperature of the oxide, the thickness and composition of the oxide, and the wavelength range over which radiative properties are obtained. Drobny and Pulfrey [94] report on CuO produced by reactive sputtering in an oxygen/argon mixture.

The complex index of refraction was calculated from reflectance and transmittance measurements over the mainly visible range of 0.4-0.8 μm for CuO thickness of 225 \AA at room temperature. Wieder and Czanderna [12] present similar measurements for a film thickness of 880 \AA , grown in air, as do Karlsson et al. [95]. These results are in qualitative agreement, though there is significant quantitative deviation between them. Jones et al. [51] present the spectral-directional emittance of copper oxide from emission measurements at the higher temperatures (672 - 970 K) and wavelengths (1.5-10 μm) that are of interest in radiative heat transfer studies. The real part of refractive index was reduced from emittance. However, X-ray diffraction studies of the samples in Jones et al. [51] indicated the presence of both cupric oxide, CuO and

cuprous oxide, Cu_2O . Some anomalous data were also reported at wavelengths between 6 μm and 7 μm .

5.1.2 Cupric Oxide Spectral Directional Emittance Measurement

Copper forms only two oxides which are thermodynamically stable, CuO – cupric oxide and Cu_2O – cuprous oxide. For oxidation temperatures of about 973 K in an O_2 atmosphere of less than 1 atm pressure, those stable phases are indicated by a pressure-temperature diagram reported by Jian et al. [96]. Due to higher oxygen partial pressure on the surface, the CuO – cupric oxide phase is expected to be the outer layer and Cu_2O – cuprous oxide is expected to be next to the copper substrate. Oxidation of copper at high temperatures was studied by [97-99], and the presence of the two distinct layers was identified in each of these by X-ray diffraction and/or SEM.

A sample of pure copper plate (99.9%), 75 x 75 x 6 mm thick, polished smooth with 2400 grit paper, was used in the experiment. The plate was held at high temperature for an extended period to oxidize, and then emittance was measured. After cooling the sample, it was seen that the copper oxide is comprised of two distinct layers. Figure 6 shows a micrograph of the copper oxide removed from the copper substrate. The presence of the outer CuO layer can be seen on the left side and the Cu_2O on the right side. Also, a porous region is apparent between the copper oxide layers. X-ray diffraction analysis performed on the upper layer (Fig. 7) shows this is cupric oxide (CuO), for which all the peaks were identified. Later SEM analyses of these layers indicate that the outer layer has an O/Cu atomic concentration ratio of approximately $r=1$, whereas the ratio of the second layer was $r=1/2$, and these are associated with CuO and Cu_2O phases, respectively. The CuO grown layer had a nominal surface roughness of 0.832 μm ,

determined with a profilometer. The thicknesses of both oxides were determined from micrograph pictures to be about 106 μm for CuO and 209 μm for Cu_2O .

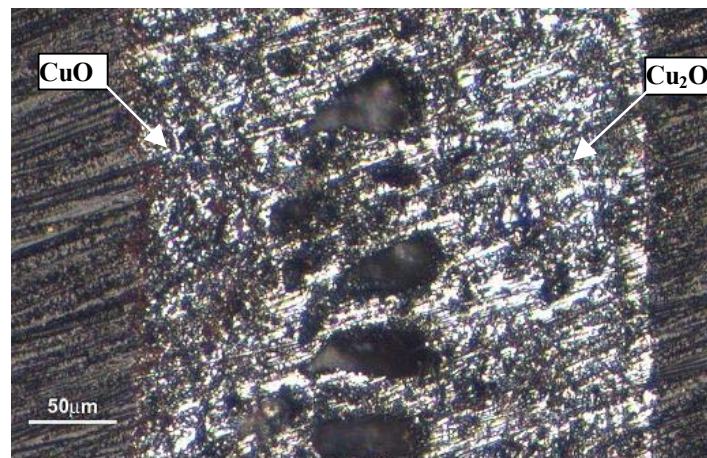


Figure 6 Micrograph of copper oxide removed from copper substrate

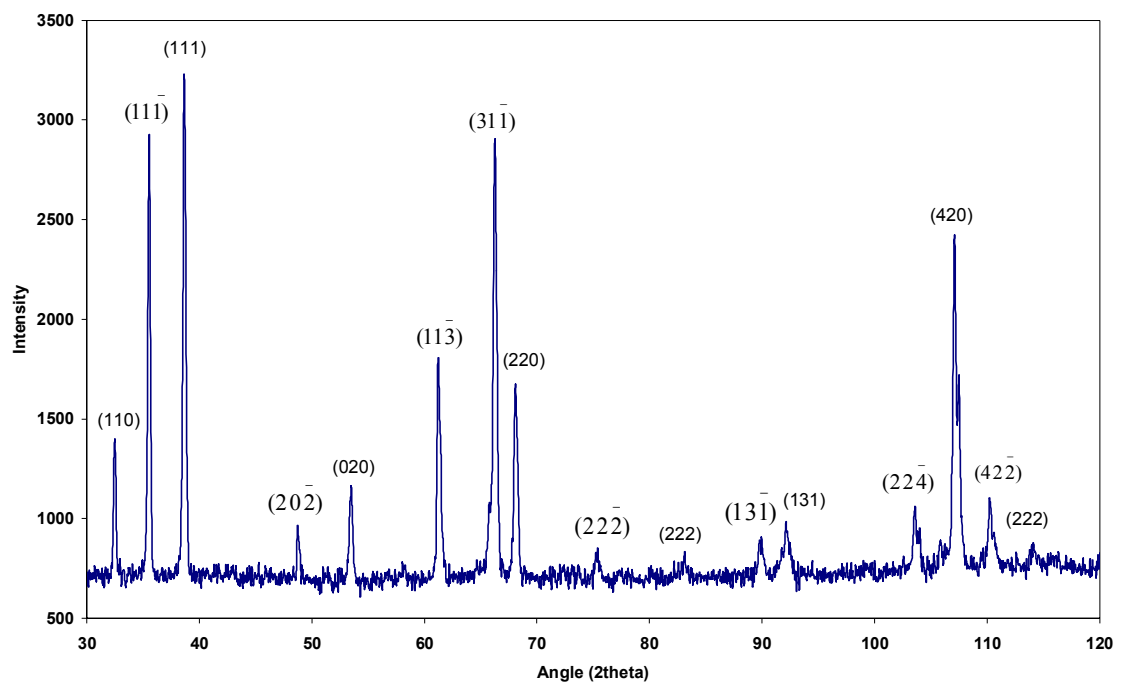


Figure 7 CuO X-ray diffraction pattern

Copper plates were held at 973 K for oxidation. The change in normal emittance was monitored as the oxide grew. Stable normal emittance was achieved after 270 h of continuous heating. The stability in normal emittance was also confirmed after another 48 h of heating. The surface temperature was measured using a thermocouple embedded through the heater block and extended into the copper plate to a point just beneath its radiating surface. A heat flux-based extrapolation from there to the actual surface was performed. Radiation measurement series were taken at 973 K (maximum operating temperature of the setup) and then decreased in 100 K increments to 673 K (minimum operating temperature for emitted flux measurement using the present apparatus). Measurements of surface emittance were performed at different wavelengths by adjusting the grating angles in the monochromator and the exclusion range of the filters. Measurements at different angles to the surface normal were achieved by adjusting both the parabolic collecting mirror and the sample holder position on the slotted arc rack. A radiating cavity blackbody source, kept at the same temperature as the sample surface temperature, is used for online calibration of the intensity measurement system. The blackbody cavity is machined into 152-mm-diameter copper and has a covering aperture plate with a 9.5 mm diameter aperture and a 15° emission cone. The blackbody wall temperature is controlled by a PID temperature controller to the same temperature as the oxidizing plate. The blackbody is insulated with 76 mm thick ceramic wool blanket. Ten complete calibration spectra measurements of intensity performed on the blackbody indicate a standard deviation of less than 1% from the mean for all considered temperatures and wavelengths of interest. Measurements performed on the sample surface were compared with the calibration measurements to determine the sample

surface emittance. A calibration factor C for the intensity measurement system is determined according to:

$$C(\lambda, T_c) = \frac{I}{R_c(\lambda, T_c)} \left[\int_{\lambda-\delta\lambda/2}^{\lambda+\delta\lambda/2} I_{\lambda b}(T_c) d\lambda \right] \delta\Omega, \quad (35)$$

where R_c is the radiometer measurement taken with the blackbody source set at temperature T_c , λ is the wavelength setup, $\delta\lambda$ is the wavelength measurement interval about wavelength λ , $I_{\lambda b}$ is the blackbody intensity, θ is the polar angle relative to the surface normal, and $\delta\Omega$ is the finite measurement solid angle. The spectral-directional emittance ε is determined by:

$$\varepsilon_{\lambda,\theta}(T_s) = \frac{R_s(\lambda, \theta, T_s) * C(\lambda, T_s)}{\left[\int_{\lambda-\delta\lambda/2}^{\lambda+\delta\lambda/2} I_{\lambda b}(T_c) d\lambda \right] \delta\Omega} \quad (36)$$

where R_s is the sample surface radiometer measurement and T_s is the sample surface temperature. The measurement solid angle, $\delta\Omega$, and the wavelength are kept the same between the radiometer measurement using blackbody source R_c and the sample surface R_s . Therefore, the data reduction system is simplified to the ratio of R_s to R_c as long as T_s and T_c are equal. The intensity emitted from the cupric oxide surface at the temperatures considered is assumed to be unpolarized. However, the sample was rotated and no bias was found due to orientation.

The uncertainty of the spectral-directional emittance may be derived as:

$$u_\varepsilon^2 = \left(\frac{\delta\varepsilon}{\delta R_s} * u_{R_s} \right)^2 + \left(\frac{\delta\varepsilon}{\delta R_c} * u_{R_c} \right)^2 + \left(\frac{\delta\varepsilon}{\delta T_c} * u_{T_c} \right)^2 + \left(\frac{\delta\varepsilon}{\delta T_s} * u_{T_s} \right)^2, \quad (37)$$

where the uncertainties are denoted by u and their subscripts, and $\delta\Omega$ and $\delta\lambda$ are considered to be perfectly repeatable. Further, considering that $T_c \approx T_s$, and $I_{\lambda b}(T_c) \approx I_{\lambda b}(T_s)$, the uncertainty may be reduced to :

$$u_{\varepsilon}^2 = (1 + \varepsilon^2) \left[t_{9,95} * \left(\frac{S_{R_c}}{R_c} \right) \right]^2 + \left(\frac{4\varepsilon}{T_s} \right)^2 * (u_{T_c}^2 + u_{T_s}^2), \quad (38)$$

for ten complete calibration spectra and a 95% confidence interval, where S is the sample standard deviation and t is a t-test distribution parameter. For the data presented it may be shown that the uncertainty of the emittance is dominated by the uncertainty of temperature measurement. Other sources of uncertainty are relatively insignificant.

The uncertainty in spectral-directional emittance was found to be approximately 3.4% of the emittance value.

5.1.3 Experimental Results & Discussion

Reduced data for spectral-directional emittance of CuO are shown in Table 1 Appendix A, for surface temperatures of 673, 773, 873 and 973 K. Due to low emissive power, for 673 K and the wavelength of 1.5 μm the measurements could not be performed. Since the sample surface temperature cannot be known until the oxide thickness is accurately known, an identical sample was heated in the same conditions and for the same period of time, and upon cooling the oxide thickness was measured using SEM cross-section. Then the temperature of the sample surface was calculated according to [51]:

$$\frac{T_{th} - T_s}{(t/k)_{Cu} + (t/k)_{oxide}} = Nu \frac{4k_a}{a} (T_s - T_a) + \varepsilon_{CuO} \sigma_B (T_s^4 - T_{\infty}^4), \quad (39)$$

The Nusselt number corresponds to a hot, horizontal square surface facing up [100]:

$$Nu = 0.54 \left[\frac{2ga^3}{(T_s + T_a)\nu_a \alpha_a} (T_s - T_a) \right]^{1/4}, \quad (40)$$

where t , k and their subscripts denote the material thickness(m) and thermal conductivity(W/m-K), T_{th} and T_s are the temperature measured by the near-surface thermocouple and the sample surface temperature, a is the side dimension of the square sample(m), T_a , T_∞ are the temperature of the air over the sample surface(K) and surroundings visible to sample surface, and ν_a , α_a are the kinematic viscosity of air over the sample surface (m^2/s), and the thermal diffusivity of air (m^2/s). All the thermophysical properties above were taken from data [5] and [100], and a , t_{Cu} were measured. T_a , T_∞ were taken to be equal and T_{th} is recorded from each experiment setup. Upon cooling the sample, the oxide flakes off and oxide thickness was measured. In practice, T_s was determined to be 1-3 K lower than T_{th} . This analysis allows the corresponding setup temperature T_{th} (the temperature measured by the thermocouple just beneath the copper surface) to be specified in order to obtain a desired surface temperature.

Using the Fresnel's relations [14], the complex index of refraction was computed using the full data set that includes spectral as well as directional data. A curve fitting algorithm based on the secant iteration method which minimizes the deviation between the Fresnel relations and the present data was used to compute the complex index of refraction according to [51].

The optical thickness of CuO was approximated for all considered temperatures by neglecting the scattering coefficient according to [14], and it is shown in Fig. 8. The optical thickness was found to decrease from 330 to 25, with increasing wavelength from 1.5 μm to 8 μm and a sudden drop was observed in spectral range between 3 μm to 4.5

μm . The influence of temperature on optical thickness is generally not found to be significant excepting the spectral range from $3 \mu\text{m}$ to $5.5 \mu\text{m}$ where decreases with increasing temperature. The $106 \mu\text{m}$ CuO layer was found to be optically thick for all considered wavelengths and temperatures. This means that the emittance of CuO is not affected by the substrate.

Figure 9 shows the emittance data of CuO as a function of direction (polar plot) at various wavelengths between $2\text{-}8 \mu\text{m}$ and at a temperature of 973 K . From the polar plot it may be seen that normal emittance increases with wavelength from 0.697 for $\lambda=2 \mu\text{m}$ to 0.9 for $\lambda=8 \mu\text{m}$. Also, from the same plot, it can be seen the emittance increases with wavelength for all directions and there is a significant drop of emittance beyond 72° .

The real part of the refractive index of CuO, Fig. 10, is seen to decrease with increasing temperature and wavelength and the imaginary part, Fig. 11, is seen to be very low and constant for short wavelengths ($2 \leq \lambda \leq 4.5 \mu\text{m}$), decreases steeply for intermediate wavelengths ($4.5 \leq \lambda \leq 6 \mu\text{m}$), and remain constant (0.001) for long wavelengths ($6 \leq \lambda \leq 8 \mu\text{m}$). The constant values of the extinction coefficient at short and long wavelengths are an artifact of fitting algorithm. For example, the constant value of the extinction coefficient at long wavelengths was determined in order to achieve the smallest error between Fresnel's equation and emittance data.

The ratio of hemispherical to normal emissivity was calculated for all of the temperatures considered, and compared with the ratio of hemispherical to normal emissivity given by Jakob [56]. The mean difference found between Jakob reported correlation factor and the calculated ratio was 5.0% , with a standard deviation of 2.2% .

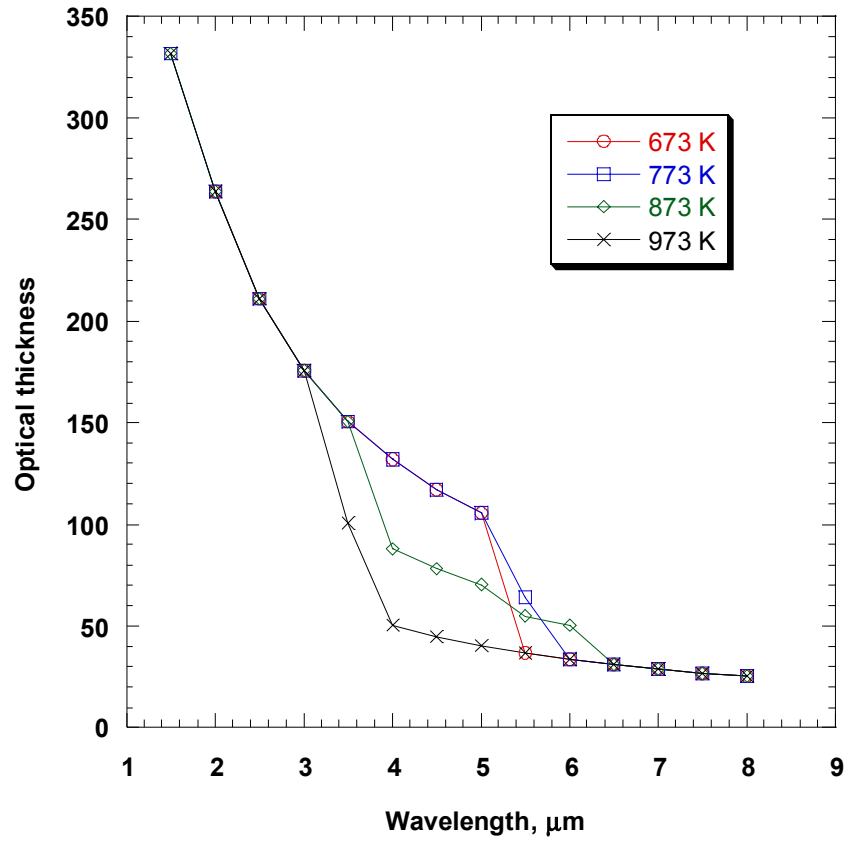


Figure 8 Optical thickness of CuO

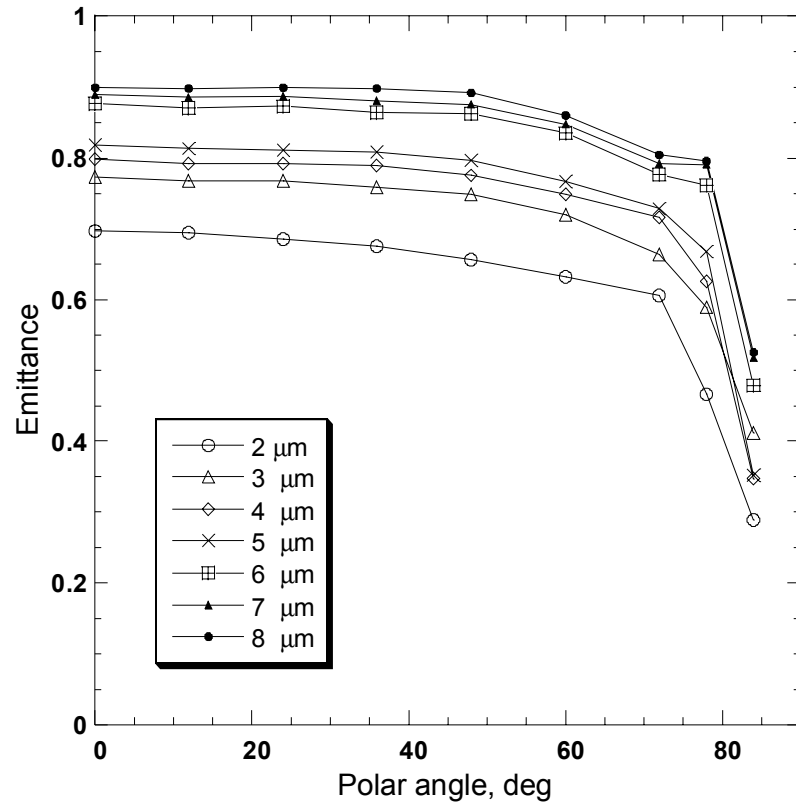


Figure 9 Spectral-directional emittance of CuO at 973 K.

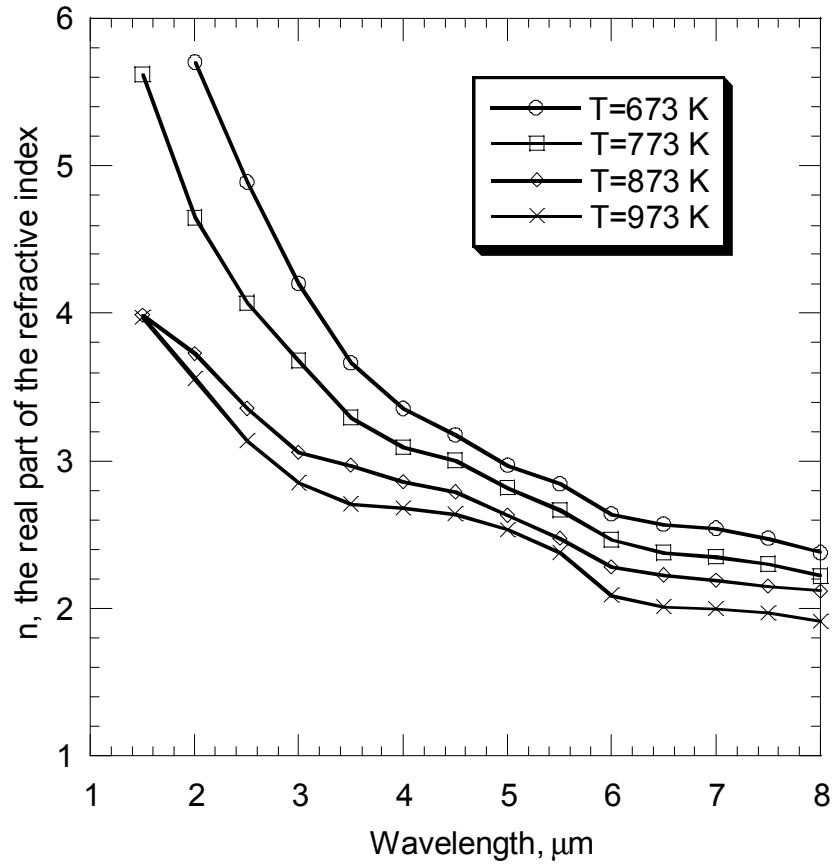


Figure 10 Spectral real part of the refractive index at considered temperatures.

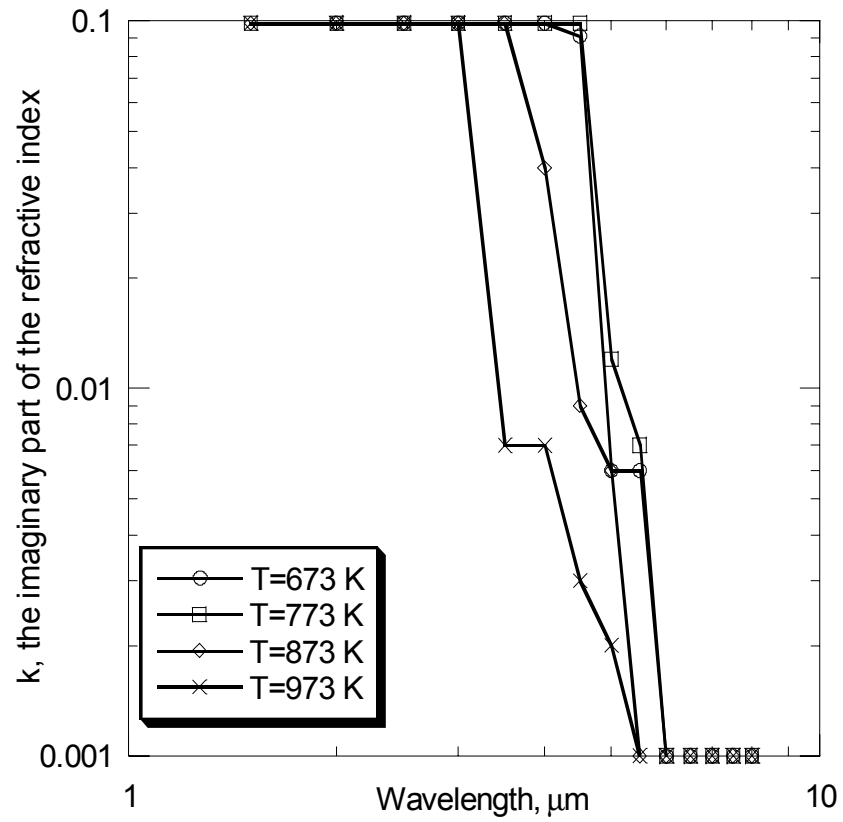


Figure 11 Spectral imaginary part of the refractive index at considered temperatures.

Spectral-normal emittance was computed from the refractive index of CuO reported in [12, 94, 95]. All of the above, together with the spectral-normal emittance reported in [51] and the present work data are shown in Fig. 12.

Even though the data from [12], [94], and [95] are in the same spectral region (visible) there is not a good agreement among them. Further, the spectral-normal emittance from [12] is seen to increase between 0.4 to 0.983 over the same spectral region rather than decrease as seen in [94] and [95]. The measurements reported in [12, 94, 95] were performed at room temperature, the oxide thicknesses were 2.25 μm [12], 0.088 μm [94], and 0.08 μm [95] respectively, and the spectral range was beneath that of the present data. Jones et al. [51] performed spectral-directional emittance measurements of oxidized copper, but failed to ensure that the top layer of oxidized copper was pure CuO. The temperatures considered differ from the present work just by few degrees Celsius and the spectral range is even wider than that of the present work. Generally, the spectral-normal emittance is seen to increase with wavelength and temperature for the spectral range considered in [51] and in present work. The values of spectral-normal emittance from the present work are slightly higher than those of Jones et al. [51] for short wavelengths ($2 \leq \lambda \leq 6 \mu\text{m}$), and very close at long wavelengths. We believe that the difference comes from the composition of copper oxide which in [51] showed the presence of Cu_2O . Furthermore, the anomalous points (decrease of normal emittance) between 6-7 μm which appear in [51] were not seen in the present work.

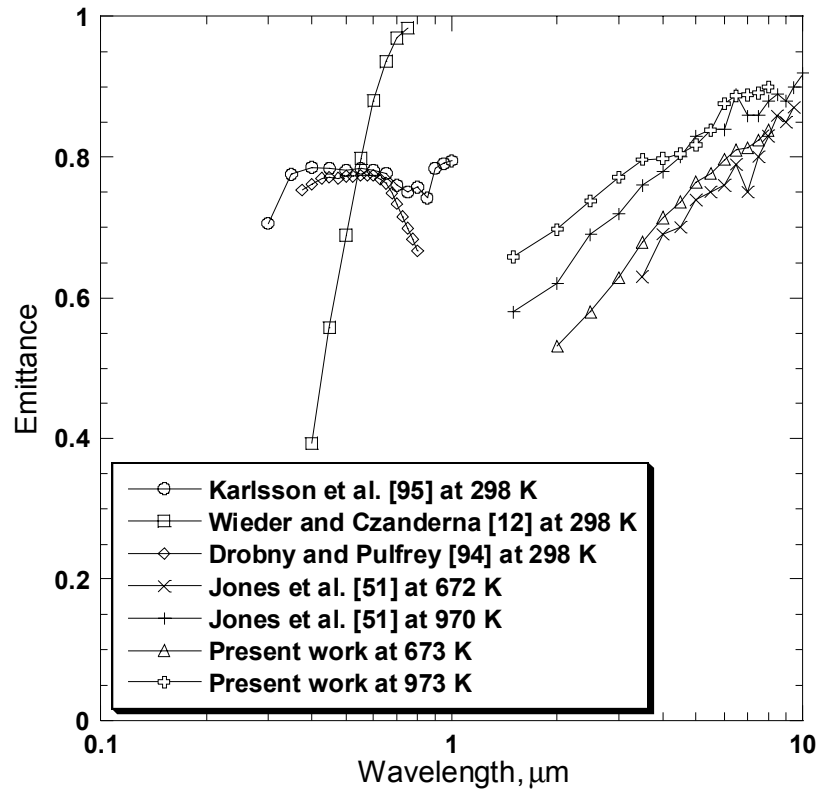


Figure 12 Spectral normal emittance of CuO as a function of wavelength.

Figure 13 shows a comparison between the spectral-directional emittance of CuO from the present work at 973 K and the spectral-directional emittance of oxidized copper comprised mostly of CuO from [51] at 970 K for wavelengths of 3.5 and 7 μm . From Fig. 13 it may be seen that the spectral-directional emittance of CuO from the present work is less directional than that from [51], which suggests that CuO behaves as a dielectric material. In both the present work and in [51], emittance is shown to slowly decrease as the polar angle goes from the surface normal to 65°, and to decrease rapidly from 65° to grazing.

Figure 14 represents spectral-directional emittance of CuO both as measured in the present work and as derived from the general Fresnel relations using the experimentally derived, best-fit complex index of refraction. The error between the Fresnel relations and the experimental data is no greater than 8% for all angles from normal to 72°, and has a variance of 2.5%. Greater errors are obtained for longer wavelengths and angles near grazing, indicating a possible effect of surface roughness.

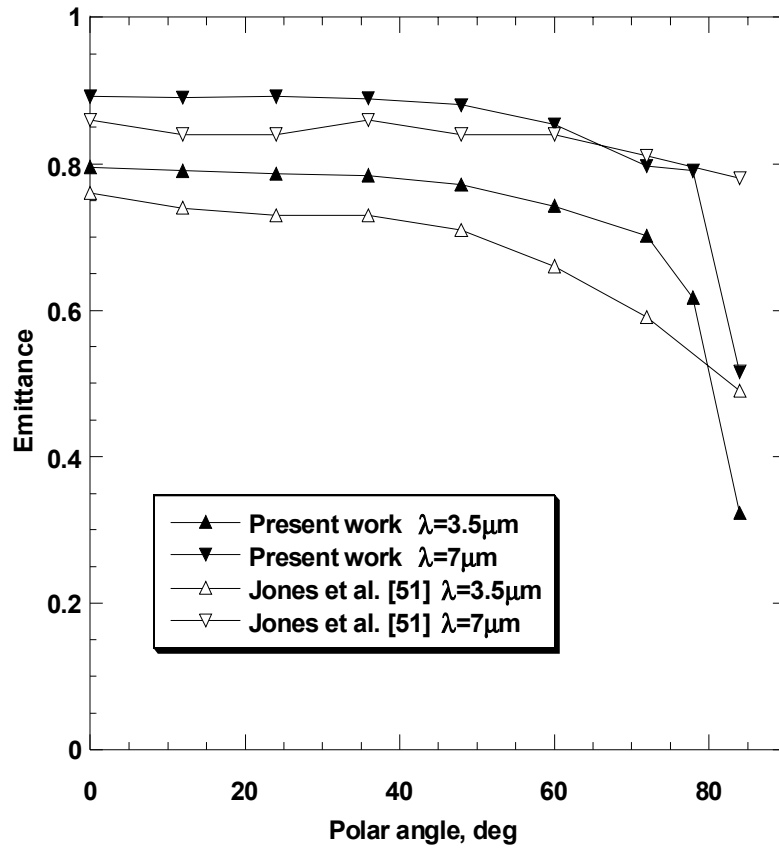


Figure 13 Spectral-directional emittance of CuO at 973 K from present work and oxidized copper at 970 K from [51].

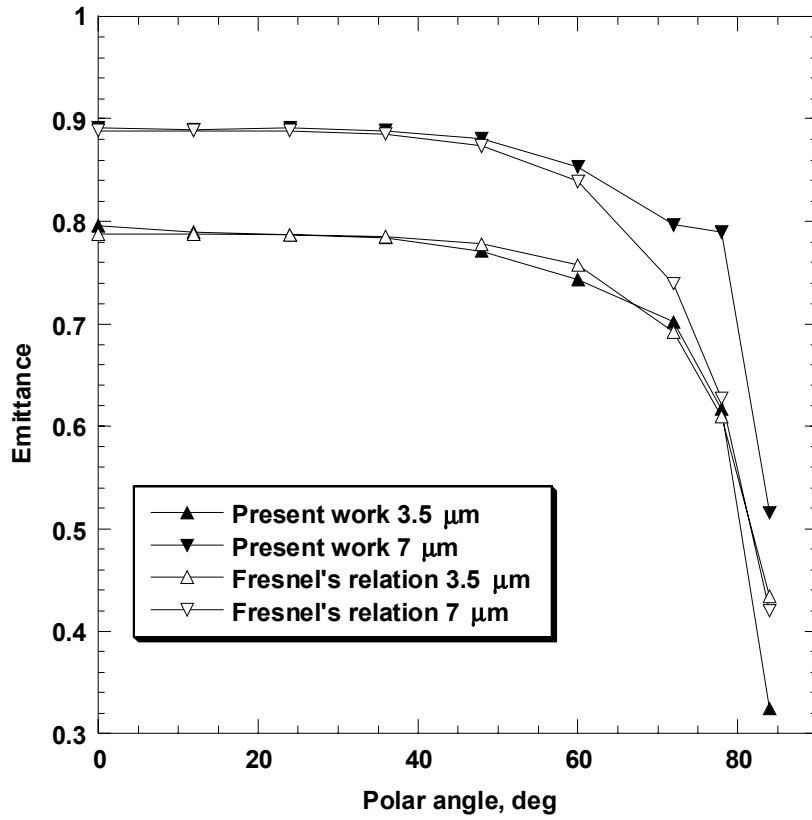


Figure 14 Spectral-directional emittance of CuO from present work and from electromagnetic theory for 3.5 and 7.5 μm .

5.2 Oxidized Aluminum

During the course of study the limitation of spectral range was overcome by incorporating an FTIR spectrometer capable of scanning a broad spectrum. Oxidized aluminum has caught our attention due to very low and varying emittance reported in literature. Moreover, oxidized aluminum and aluminum oxide were also used to prove the accuracy of the FTIR spectral range and its detector sensitivity, and to study the influence of aluminum oxide thin film.

5.2.1 Specific Literature Review

The radiative properties of thermally oxidized aluminum have been reported in a number of studies [28, 42, 44, 89]. Randolph and Overholzer [89] report oxidized aluminum total emissivity measurements at 473, 673, and 873 K. The aluminum samples used in the experiment had a disc shape and were cleaned and polished before mounting. The total emissivity was found to slightly increase with temperature from 0.113 at 473 K to 0.192 at 873 K for an initially polished aluminum sample. Reynolds [42] presents a more careful study of the spectral emissivity of various aluminum surfaces under different heat treatments. The thin-walled cylindrical specimens used were formed from extruded commercial-purity aluminum (99.7%). The measurements were performed at temperatures between 473 and 813 K for a spectral range between 1 to 14 μm . The radiation was collected at 15° from the normal to the sample surface, and the estimated uncertainty was $\pm 20\%$ for polished aluminum and $\pm 10\%$ for roughened and oxidized aluminum over the spectral range from 2 to 10 μm and lower outside. Conroy et al. [44] determined spectral emissivity of 99.99% pure aluminum at 413 and 623 K, chemically treated to produce a 20 \AA aluminum oxide layer. The samples had a square shape, and a

broad band at 980 cm^{-1} ($10.2\text{ }\mu\text{m}$) was observed for emissivity at 623 K due to an amorphous aluminum oxide film. A significant amount of noise was seen in spectral emissivity data for the spectral range between 1900 and 1400 cm^{-1} (5.2 to $7.1\text{ }\mu\text{m}$). Edwards and Catton [28] present the spectral normal emittance of 1100 aluminum sandblasted with different micron-sized particles. The normal emittance was determined from reflectance measurements, and normal reflectivity measurements were performed at 298 K from the sample normal. The sample temperature was about 305.4 K and the spectral normal emissivity varied greatly with surface roughness. Although there is qualitative agreement among reported data, there is a significant deviation among them and none of them report full directional distributions of the emittance of oxidized aluminum and the characterization of the oxide layer grown.

5.2.2 Oxidized Aluminum Spectral Directional Emittance Measurement

A sample of pure aluminum plate (99.99%), $75\text{ mm} \times 75\text{ mm} \times 6\text{ mm}$ thick, polished smooth, with a nominal surface roughness of $0.635\text{ }\mu\text{m}$ was used in the experiment. The plate was maintained at 873 K for an extended period of time (150 h) to allow oxidization, and then radiative emittance measurements were performed. After cooling the sample, the oxide composition was determined by AES. The oxide layer composition consisted of Al_2O_3 and Al, as shown by the binding energy of the Al2p feature at 74.9 eV (Al_2O_3 at 74.7 eV) seen in Fig. 15, by the Al/O peak ratio (which was ~ 1.5), and by the general AES peak shapes, which are similar to the AES signature for stoichiometric Al_2O_3 .

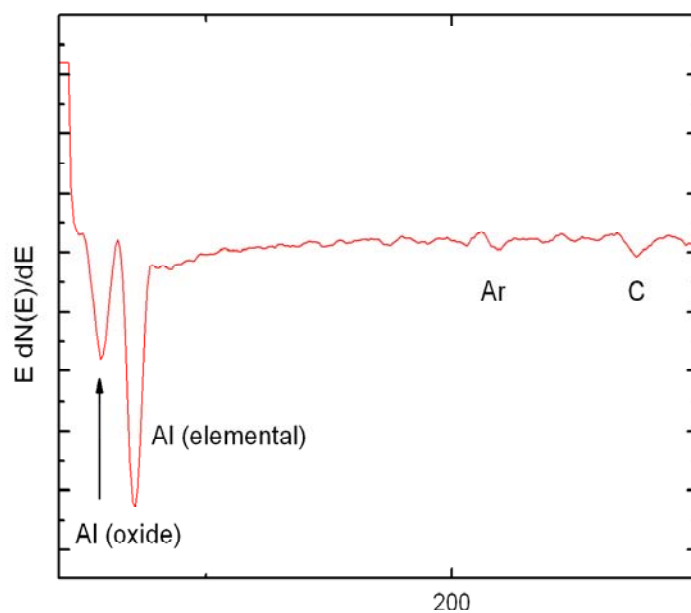


Figure 15 AES spectrum after 65 min of Ar+ sputtering

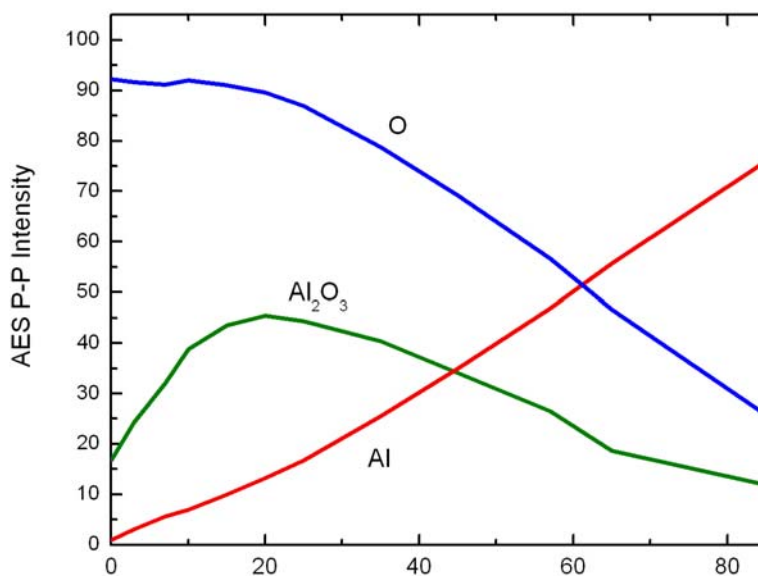


Figure 16 AES depth profile through the Al film. The Ar+ sputter rate was $35 \text{ \AA}/\text{min}$ measured on a standard thin film of SiO_2

An AES depth profile performed on the oxide layer showed an increasing concentration of elemental Al from the surface to the bottom of the oxide layer, and consequently a decrease of oxygen content from the surface to the bottom of the oxide layer. The presence of elemental Al in the oxide, obtained by AES depth profile suggests a variation in sample surface roughness. The thermally grown layer consists of elemental aluminum and aluminum oxide with a thickness of ~ 290 nm, as shown in Fig. 16. The oxidized aluminum emittance magnitude suggests that the radiating aluminum oxide layer is optically thin.

Radiation measurements were performed at surface temperatures of 873, 773, and 673 K. Using a 12 mm aperture, the radiation flux was collected over a solid angle of 0.0049 sr, which is small enough to assume that the spectral intensity I_λ is constant. All spectral data were averaged over ten scans using an 8 cm^{-1} resolution. In order to derive the emittance, the ratio of radiative flux leaving the sample to the radiative flux from the blackbody at the same temperature was determined. Background spectral noise is subtracted from both fluxes. The spectral emittance is calculated from:

$$\varepsilon(\lambda, \theta, T_s) = \frac{I_s(T_s, \lambda, \theta) - I_b(T_r, \lambda)}{I_b(T_b, \lambda) - I_b(T_r, \lambda)} \quad (41)$$

where $I_s(T_s, \lambda, \theta)$ is the intensity emitted by the sample surface at temperature T_s , $I_b(T_b, \lambda)$ is the intensity emitted by the blackbody cavity at temperature T_b (which is equal to the sample surface at temperature T_s), and $I_b(T_r, \lambda)$ is the intensity emitted by the surrounding at room temperature, T_r . The uncertainty in the emittance value $\delta\varepsilon$ is given by [46]:

$$\delta\varepsilon_\lambda = \varepsilon_\lambda \frac{\delta T}{\lambda T_s^2} \frac{c_2}{[\exp(-c_2 / \lambda T_s) - 1]} \quad (42)$$

where λ is the wavelength and $c_2 = h c / k$. According to Eqn. 42, the relative uncertainty is inversely proportional to λT_s^2 , resulting in a maximum uncertainty at lower temperatures and shorter wavelengths.

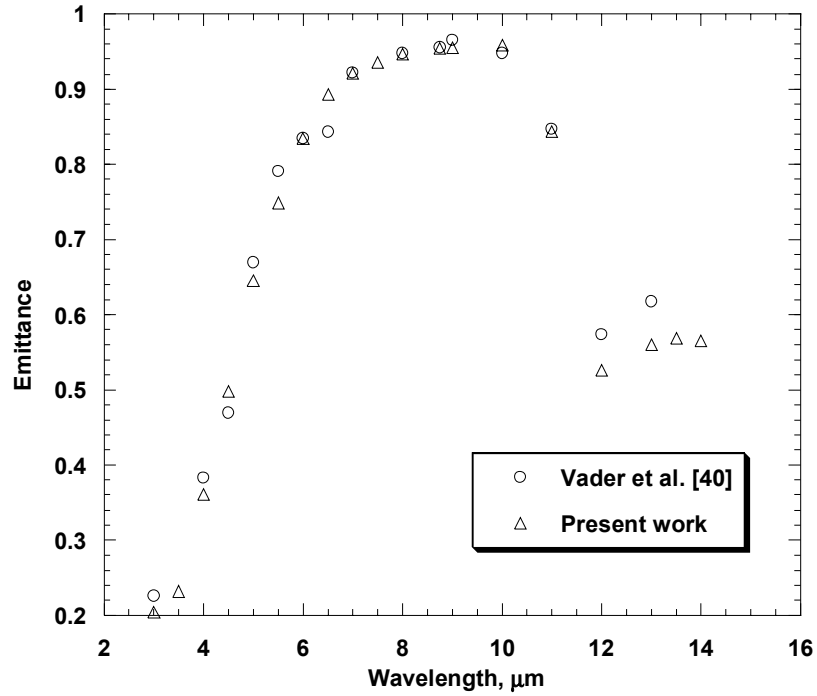


Figure 17 Comparison of spectral-normal emittance of alumina (99.5%)

The temperature uncertainty is comprised of the uncertainty of the blackbody temperature, sample surface temperature and the stability of the temperature control. The uncertainty of thermocouples used in experiment was 0.4% and the uncertainty of the temperature control stability 0.05%, respectively. The uncertainty estimation procedure from [101] was used to determine the total estimated uncertainty as shown in Table 3, Appendix B. The maximum uncertainty in the emittance value was found to be less than 3.5% for the spectral range considered. The experimental setup was tested for

accuracy with pure alumina (99.5% provided by Morgan Advanced Ceramics) at 823 K. The data obtained (Fig. 17) showed good agreement with data published by [40]. The data represent an average of three measurements collected at different times.

5.2.3 Experimental Results & Discussion

Reduced spectral-directional emittance data for thermally oxidized aluminum is shown in Table 4, Appendix B, for surface temperatures of 673, 773, and 873 K. The data at each wavelength were fit with functions of polar angle; some smoothing was necessary to fit the data beyond 8 μm . These curves were compared to Fresnel's equation in order to identify the real and imaginary parts of the spectral complex index of refraction using a secant iteration method. The refractive index n is shown in Fig. 18 to increase with temperature and wavelength. Between 3 and 8 μm the refractive index n increases slightly with temperature and wavelength, and increases more significantly beyond 8 μm . The extinction coefficient k is seen to increase with wavelength and temperature as shown in Fig. 19. The complex index of refraction at the measurement temperatures, determined through Fresnel's equation, does not reflect departure from a metallic behavior ($k > n$) [4].

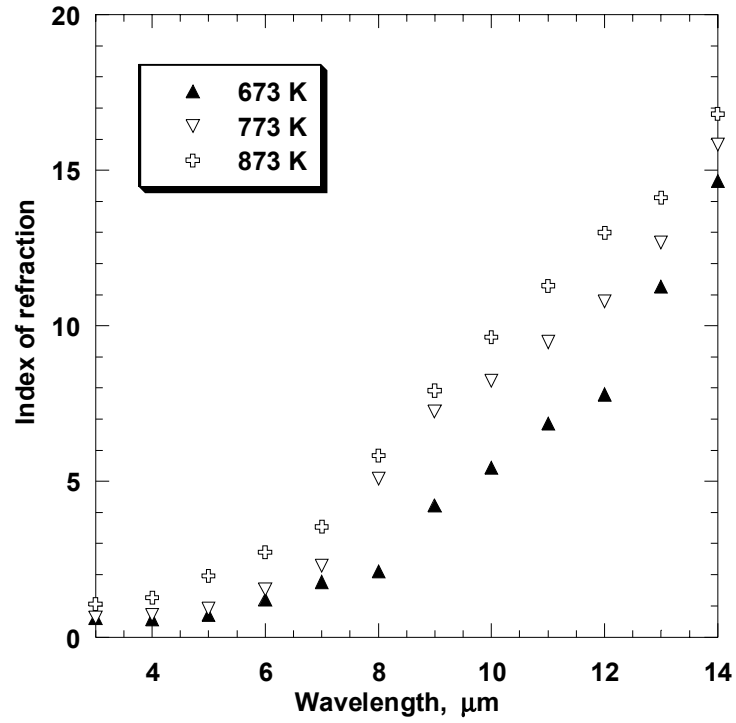


Figure 18 Spectral refractive index at of oxidized aluminum 673, 773, and 873 K

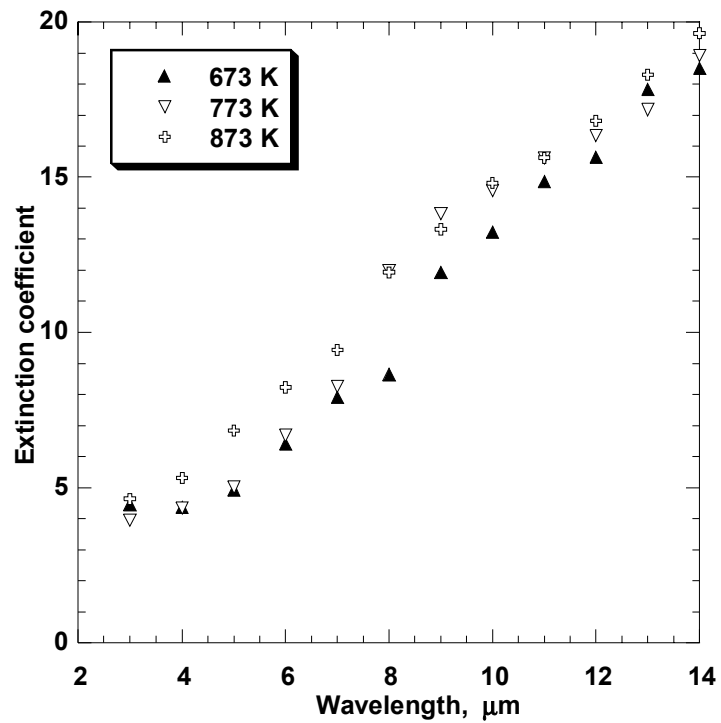


Figure 19 Spectral extinction coefficient of oxidized aluminum at 673, 773, and 873 K

Spectral-normal emittance data from [42, 44], together with the present data, are shown in Fig. 20. Even though the data from [42, 44] are in the same spectral region, the agreement between them is not good. The data from [42] give both the spectral emissivity of 99.7% pure polished aluminum at 697 K and the spectral emissivity of 99.7% pure roughened aluminum at 599 K after various heat treatments. Here the effect of surface roughness clearly dominates the emittance increase over the temperature effect. The measured values of spectral-normal emittance from the present work are higher than values reported in [42] for a polished sample, and this is probably due to higher surface roughness. Similar trends are observed in both data sets.

The data from [44] come from a 99.99% pure aluminum sample measured in air with a surface roughness of 0.762 μm , which was cleaned in a chrome/phosphoric acid solution in order to obtain a 2 nm thickness of consistent, uniform barrier aluminum oxide layer. The measurement was performed at 623 K. In spite of an almost 373 K temperature measurement difference, there is some agreement between data from the roughened sample in [42] and the chemically treated sample in [44]. Comparing the spectral normal emittance from the present work with the data from [44] there is an obvious difference even though the samples used have very close surface roughness – 0.635 μm in the present work and 0.762 μm in [44]. The difference can be explained by taking into account the sample compositions. The aluminum sample used in [44] was chemically treated to produce a uniform barrier oxide. The oxide thickness was only approximated to be about 2 nm although no further evidence was provided.

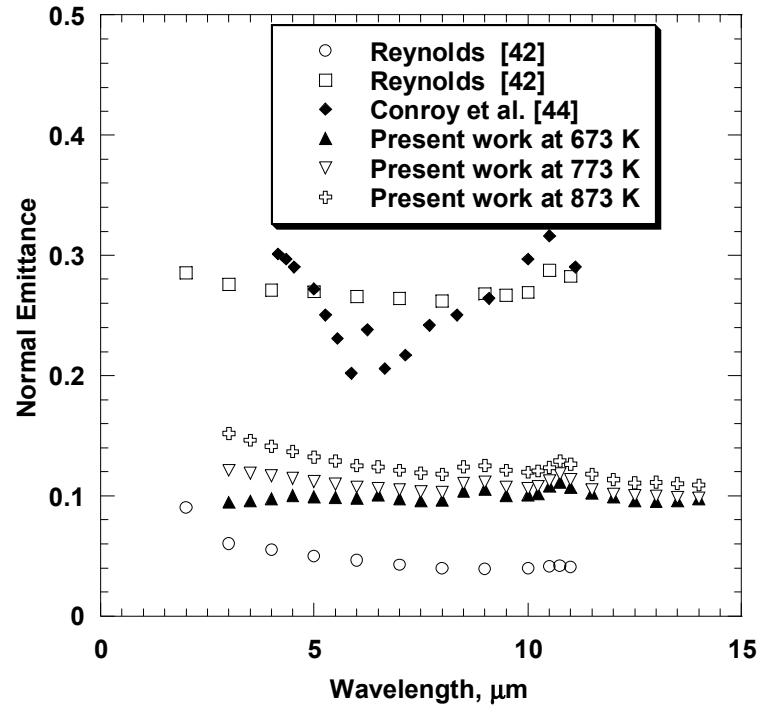


Figure 20 Spectral normal emittance of oxidized aluminum comparison

Auger electron spectroscopy performed on the present samples revealed that the thermal layer grown on the sample surface is comprised of pure aluminum and aluminum oxide and has a thickness of about 290 nm. This explains the higher emittance observed on samples in [44] due to the influence of greater aluminum oxide properties of the consistent and uniform barrier layer. Unfortunately, the oxide layer composition is not addressed in both [42, 44].

The spectral-normal emittance data from the present work is seen to increase slightly with temperature as shown in Fig. 20. The two slight peaks observed at 8.5 and 11 μm may be attributed to aluminum oxide grown on the sample surface.

Figure 21 shows the spectral-normal emittance from the present work together with data from [49]. The sample used in [49] is an Al 5754 alloy (polished) that contains at least 95.7% aluminum. The measurements were performed in a vacuum and a protective gas atmosphere to avoid oxidation. From Fig. 21, it can clearly be observed that the spectral normal emittance from [49] does not exhibit any peak between 8 to 12 μm and that normal emittance decreases smoothly with wavelength for the spectral range considered suggesting a pure metallic behavior. The data from the present work at 673 K agree qualitatively with data from [49], even though the emittance value is higher beyond 5 μm . The difference may be explained by the presence of aluminum oxide that not only slightly increases the emittance, but also develops two slight peaks as mentioned above.

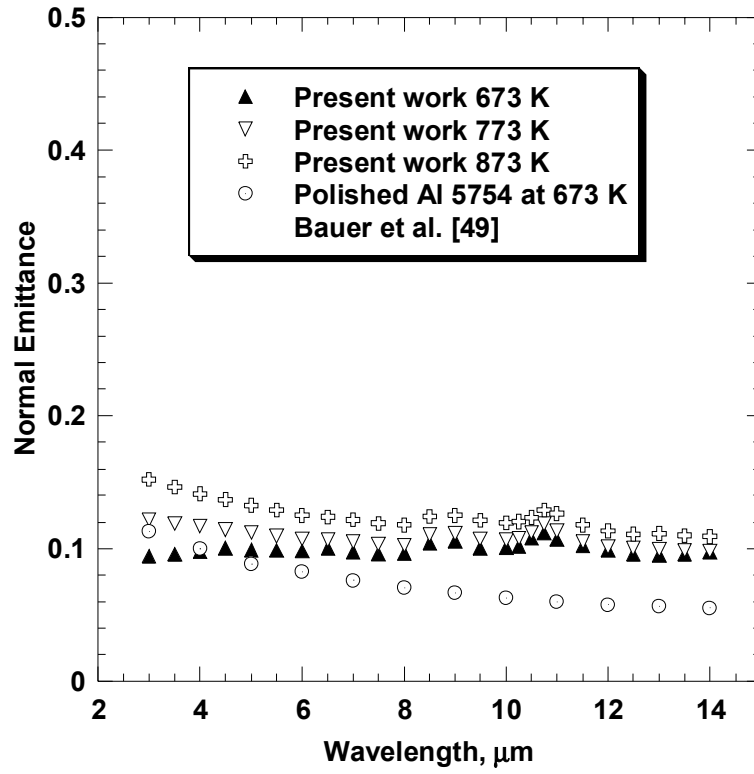


Figure 21 Spectral normal emittance comparison

Moreover, the surface roughness of samples used in the present work is higher than that of the polished sample from [49]. Figure 22 shows the present measurements of the directional emittance of Al oxidized at high temperatures below its melting point at a wavelength of 3 μm . The directional emittance is seen to increase slowly with polar angle up to 36° and more quickly thereafter until grazing, suggesting a metallic behavior. Generally, the directional emittance is seen to increase slightly with temperature.

Figure 23 presents the directional emittance of oxidized aluminum at 673 K at wavelengths of 9, 10, and 11 μm . Here at longer wavelengths the emittance is seen to increase with polar angle from the surface normal to 72°. The behavior at 11 μm should be noted, near around where a maximum of the normal emittance is seen. At a wavelength of 11 μm , the directional emittance increases sharply with polar angles beyond 24° until 72°, as compared with wavelengths of 9 and 10 μm . This behavior can probably be explained by the presence of aluminum oxide in the 290 nm layer grown by heating. Then the appearance of aluminum oxide into elemental aluminum gives not only a couple of slight peaks in normal emittance but also alters the directional behavior around the spectral range where the peaks were developed. This influence is seen to increase with temperature.

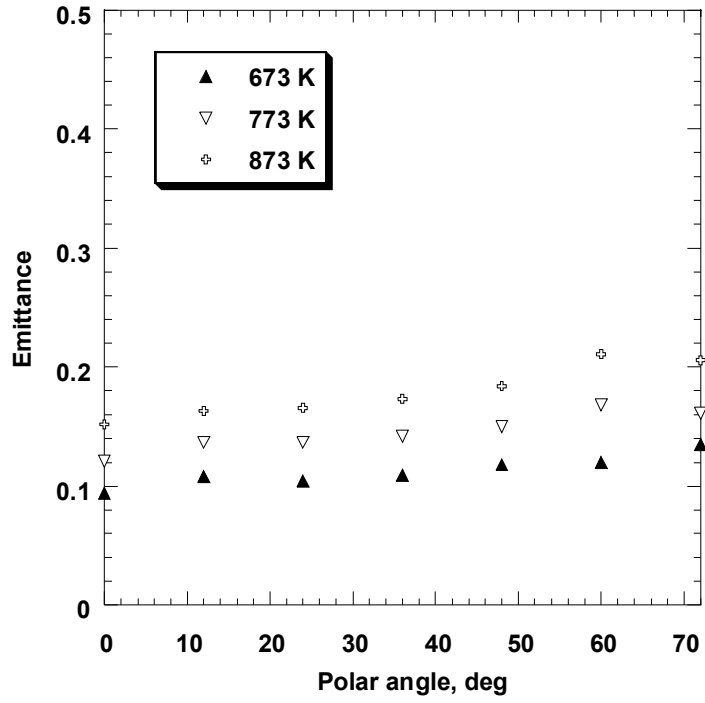


Figure 22 Directional emittance of oxidized aluminum at 3 μm as a function of temperature

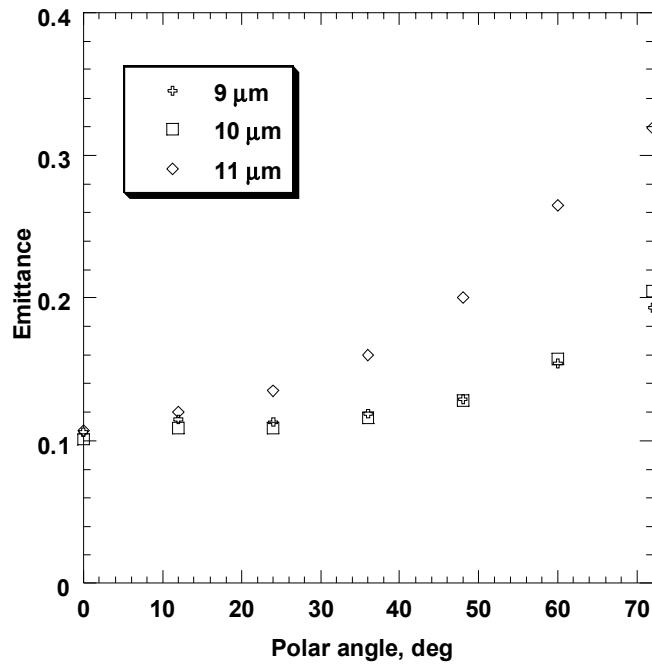


Figure 23 Directional emittance of oxidized aluminum at 673 K at 9, 10, and 11 μm

5.3 Oxidized Nickel

Reports on emittance of oxidized nickel at high temperatures on spectral and directional base are, as nearly as can be determined, practically nonexistent. The study will investigate the radiative emissivity of oxidized nickel in air for an extended infrared spectral region, close to the limit of our experimental setup detector capability.

5.3.1 Specific Literature Review

The total emissivity of oxidized nickel was reported in [89] for a polished nickel surface oxidized at temperatures of 473, 673, and 873 K. Metal disc samples of 19.1 cm diameter and 6 to 13 mm thickness were used. Thermocouples attached to the back of the metal sample were used to measure the sample temperature, not the surface temperature itself. The nickel samples used in this experiment were oxidized at 873 K until the emissivity had become constant prior to taking measurements at the above temperatures. Calibration was performed using a potentiometer, showing the relation between millivolts and energy radiated by a blackbody cavity. The blackbody – a cast iron pipe, had a uniform wall temperature within 3° at 773 K. Data from [89] give no information about spectral or directional emittance of oxidized nickel, or topology of the metal's surface. The surface composition was not quantified.

Clausen et al. [48] report normal spectral emissivity of an oxidized nickel specimen, below 390 K, for a spectral range 2.8 – 5.7 μm . The researchers used a specimen of lightly oxidized nickel with dimensions 20 x 20 x 1 mm. The specimen had a normal emissivity at 773 K of 0.64 at 3.18 μm and 0.57 at 5.06 μm . The authors do not specify the sample preparation, initial composition and surface roughness. The emittance reported in [48] is limited to the normal direction, and the spectral range is narrow.

Bauer et al. [49] determined the normal spectral emissivity of sand blasted pure nickel in a vacuum for a spectral range of 0.6 to 16 μm at 673 K using a radiometric technique with a separate blackbody. The measurement device was comprised of a prism monochromator, three different detectors, and a Lock-in-Amplifier. Although there is some data in the literature [48, 89] on total emittance and spectral normal emittance of oxidized nickel, a correlation cannot be performed because the sample surface preparation is not well quantified, the spectral range is very limited, and no spectral-directional emittance of oxidized nickel was reported.

5.3.2 Oxidized Nickel Spectral Directional Emittance Measurement

Samples of nickel plate (99.99%), 75 x 75 x 6 mm thick, polished smooth, with a nominal surface roughness of 4.1 μm were used in this study. The sample surface was brought from room temperature to 673 K in air and maintained at 673 K for one hour prior to taking emission measurements to allow oxidation. Afterwards, the sample surface temperature was increased by a step increment of 100 K until a maximum temperature of 873 K was attained. The sample was maintained at the measurement temperature 1h prior to emittance measurement.

Subsequently X-ray diffraction analysis performed on the sample indicated the presence of nickel oxide on the surface as shown on X-ray diffraction pattern in Fig. 24. The first three strongest reflections were identified for nickel oxide, which has a cubic structure. The corresponding peaks identified for (111), (200) and (220) planes are seen in Fig. 24. Furthermore, the SEM analysis performed on the sample surface indicated an O/Ni atomic concentration ratio of approximately $r = 1$ which is associated with NiO phase.

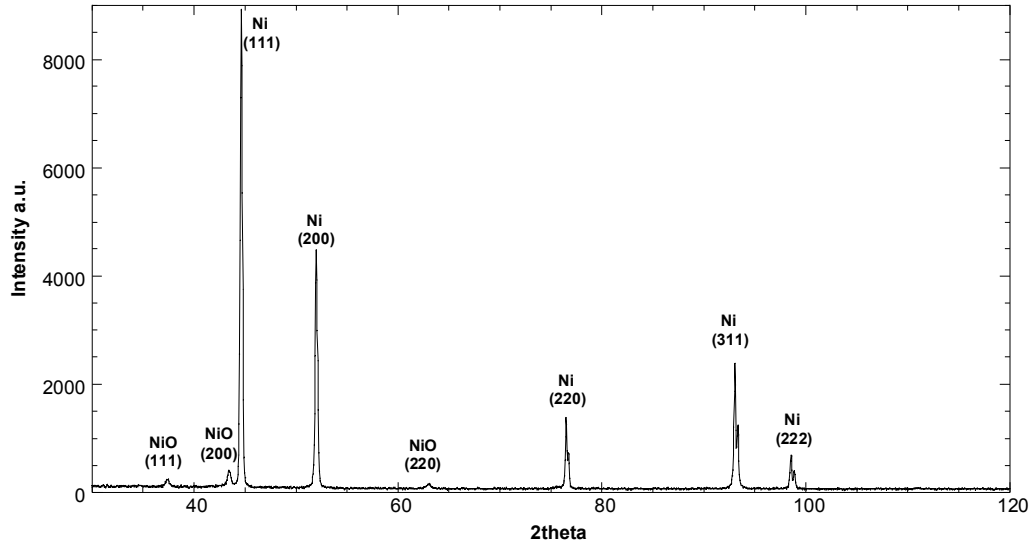


Figure 24 X-ray diffraction pattern of oxidized nickel

The micrograph of the oxidized nickel sample (b, d) shows significant modifications as a result of nickel oxide grains formed on the sample surface (Fig. 25).

The absorption coefficient of nickel oxide used to determine the optical thickness was reported in [102] at 300 K. The absorption coefficient of nickel oxide at this measurement temperature was not available. The thickness of nickel oxide layer was evaluated according to [103] to be about 600 nm and the maximum optical thickness value determined for nickel oxide layer was found to be about $2.4 \cdot 10^{-6}$ (much less than 1) suggesting that the nickel oxide is optically thin.

According to Eqn. 42, the relative uncertainty is inversely proportional to λT_s^2 , resulting in a maximum uncertainty at lower temperatures and shorter wavelengths. The temperature uncertainty is comprised of the uncertainty of the blackbody temperature, the sample surface temperature, and the stability of the temperature control. The uncertainty of type J special thermocouples used in this experiment are reported by their manufacturer (Watlow Controls) as 0.4%, and 0.05% for temperature control stability (Series 965 auto tuning control), respectively. The maximum uncertainty in the emittance value shown in Table 5, Appendix C was found to be less than 3.5% for the spectral range considered.

5.3.3 Experimental Results & Discussion

Figure 26 shows spectral normal emittance data at the three temperatures considered. The spectral-normal emittance is seen to increase very slightly with temperature from 673 to 873 K, as shown in Figure 26. A very important key feature observed here is the apparition of two slight peaks (the plot magnitude is decreased to

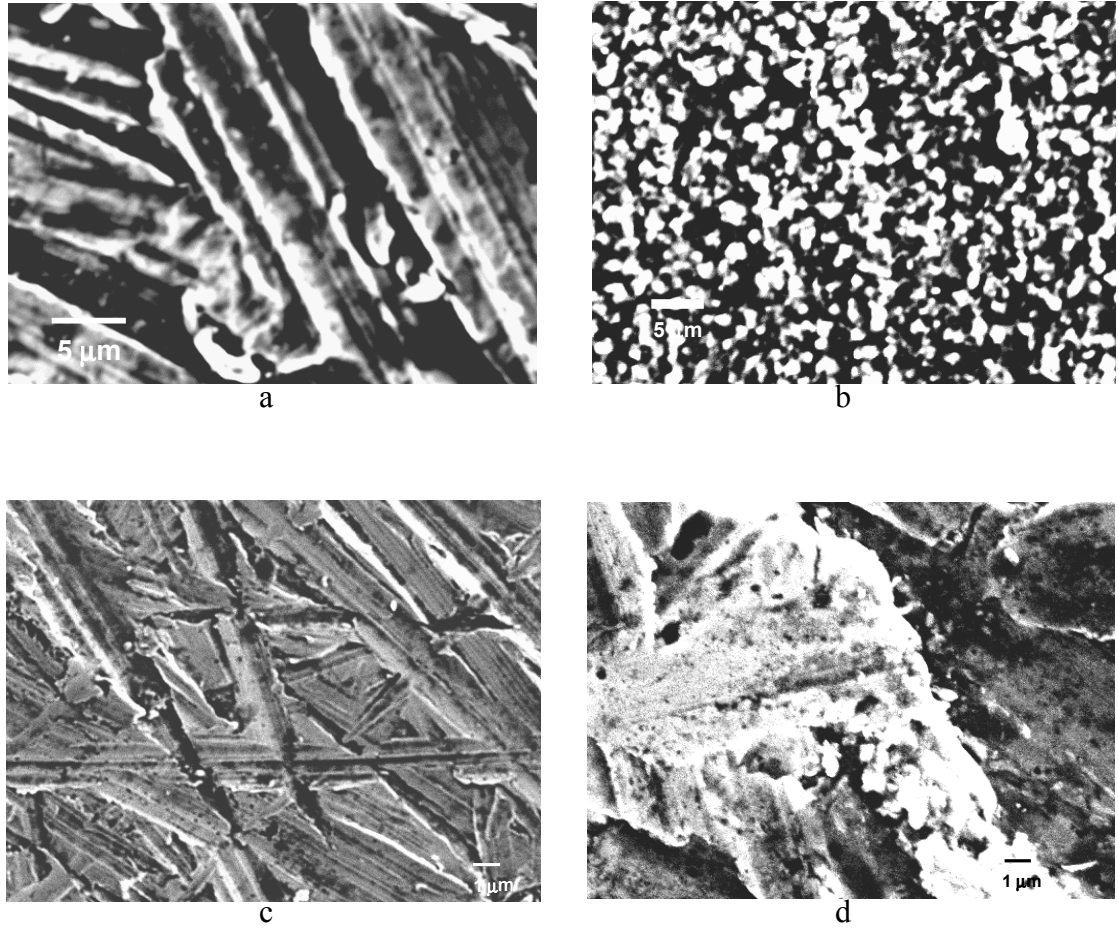


Figure 25 SEM microstructure of nickel sample. a) as received 2000X, b) oxidized sample 2000X, c) as received 4000X, d) oxidized sample 4000X.

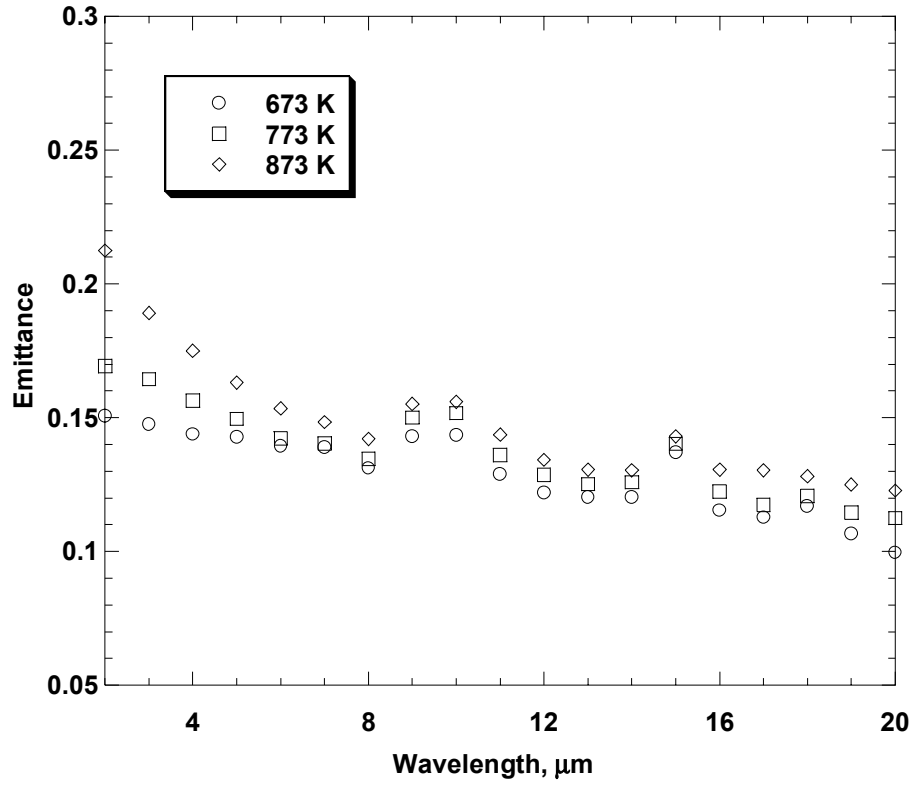


Figure 26 Normal spectral-directional emittance of oxidized nickel at 673,773 and 873 K.

enhance the peaks for better visualization). The peaks are observed at wavelengths of 9.5 and 15 μm , and may be attributed to nickel oxide grown on the sample surface.

Figure 27 shows emittance data as a function of direction at various wavelengths for 99.99% pure nickel oxidized at 873K for 1h. From Fig. 27 it can be distinguished that for the spectral range from 17 to 20 μm , the directional emittance increases slightly with direction and the increase is more pronounced at polar angles higher than 30°. This behavior does not agree with the behavior of pure metals, which is typically that directional emittance is almost constant for polar angles less than 40°, suggesting that radiative properties of pure nickel are slightly altered by the nickel oxide grown on the surface.

Figure 28 shows the normal-spectral emittance of nickel oxidized in air at 673 K for 1h, with a surface roughness of 4.1 μm , from present work and from the spectral-normal emissivity of pure nickel reported in [49] at the same temperature. The measurement in [49] was performed in a vacuum and protective gas atmosphere to avoid oxidation at high temperatures. Comparing these two sets of data it can be observed that the magnitude of the spectral-normal emittance of nickel oxidized in air is higher than that presented in [49] for nickel heated in a vacuum and a controlled gas atmosphere. Clearly this can be influenced by the nickel oxide grown in air on the surface, and by the surface roughness. Unfortunately, the authors [49] did not report the surface roughness in order to make an inference.

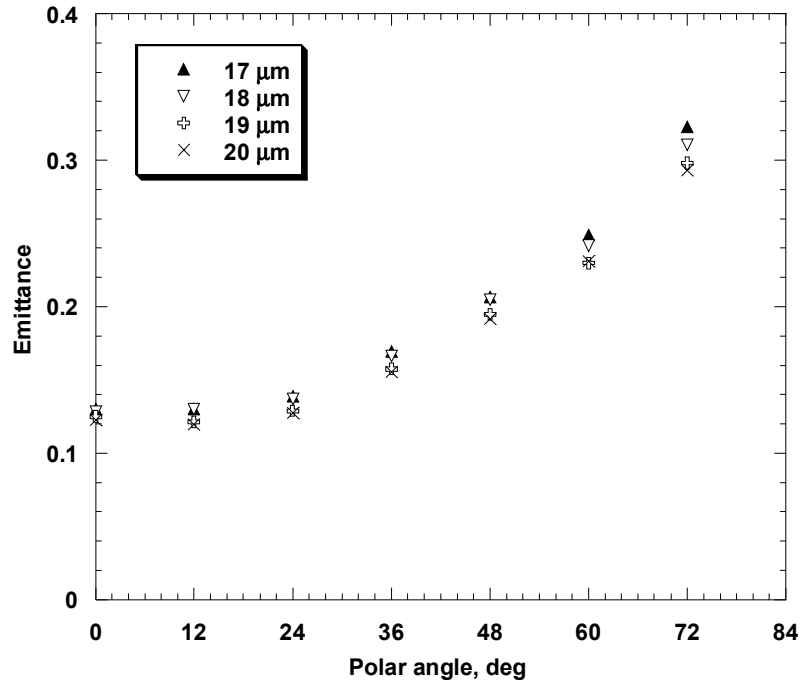


Figure 27 Spectral-directional emittance of oxidized 99.99% Ni at 873K.

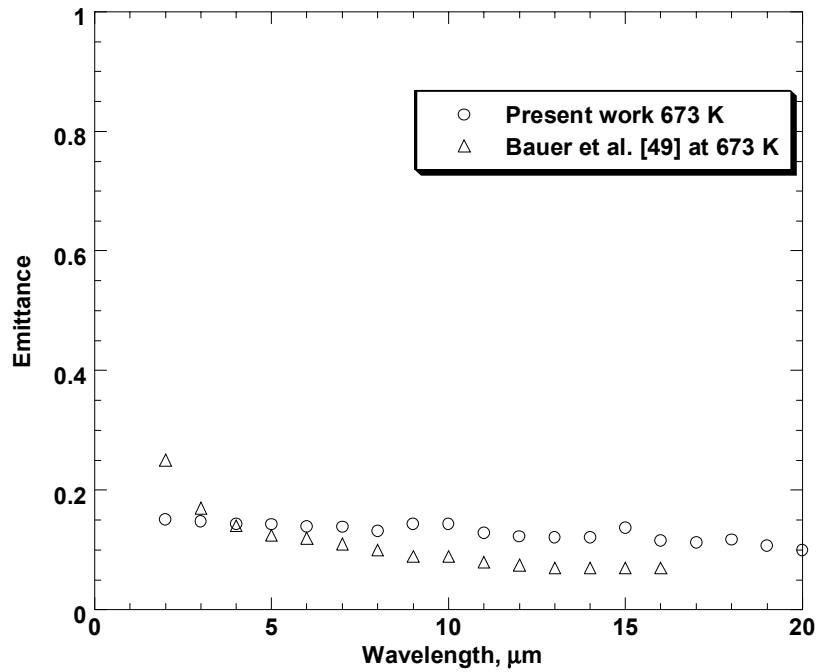


Figure 28 Spectral-normal emittance of oxidized nickel comparison

Furthermore, the two slight peaks observed in the spectral-normal emittance from the present work were not observed in [49] because of the gas protective atmosphere and vacuum environment, which help us attribute them to nickel oxide grown on the surface over a 1h period of heating. The spectral-directional emittance data are presented in Table 6 Appendix C.

The spectral hemispherical emittance was determined by integrating the present data over polar angle. Figure 29 shows spectra for different temperatures suggesting that the spectral hemispherical emittance of oxidized nickel for 1 h at 673 K and 1 h at 773 K does not change significantly. A greater temperature dependence of spectral hemispherical emittance of nickel oxidized is obvious for nickel oxidized for 1 h at 873 K. Other important features evident on Fig. 29 are the peaks around 9.5 and 15 μm , which are more significant here than in spectral-normal emittance.

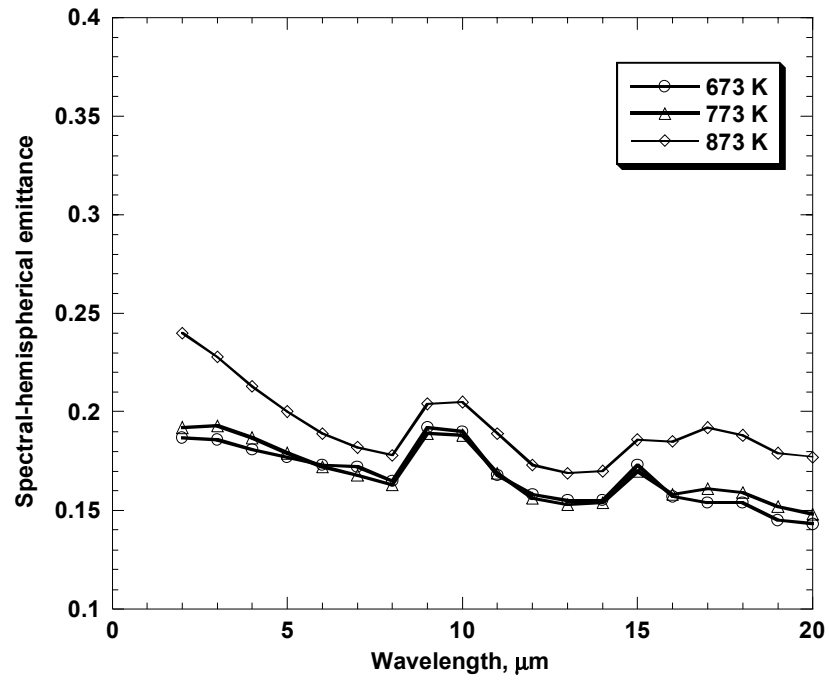


Figure 29 Spectral-hemispherical emittance of oxidized nickel as a function of wavelength at 673, 773 and 873K

5.4 Nickel

Nickel was found to have a crossing point or X-point at a wavelength of about 2 μm by Price [70]. However, its high temperature radiative emissivity is unavailable in the beyond 6.5 μm at temperatures above 1273 K. Its radiative emissivity follows a metallic behavior at lower temperatures as reported by [49], with a monotonic decrease in emissivity with an increase in wavelength. Therefore, besides providing insight on the radiative thermal emissivity of nickel, data from this experiment will be used to verify the accuracy of the experimental setup. The study will extend spectral emissivity knowledge at temperatures above 1273 K in the mid IR spectral range, and will be used together with theoretical models to further reduce the number of required measurements.

5.4.1 Specific Literature Review

Relatively few studies [59, 69, 70, 104-106] have been reported on the normal spectral emissivity of high purity Ni, especially at elevated temperatures where metals are highly reactive and the rate of oxides to form on their surfaces is great. The reported data are scattered and the spectral range is often very narrow. Hurst [69] determined the spectral normal emissivity of a nickel rod (99.5 % nickel content) in vacuum at 1123 K and 1273 K by comparing the radiative heat flux emitted from the sample and a blackbody slit cut in the sample itself. The emissivity was reported over a spectral range from 1 μm to 6.5 μm . Price [70] measured the spectral normal emissivity of high purity nickel (99.97% nickel content) in a vacuum at 1383 K. Based on comparison of radiation heat fluxes from the sample and a blackbody, the emissivity was determined for a spectral range from 0.65 μm to 4 μm . Riethof [104] presented spectral normal emissivity of nickel at 1297 K, 1318 K, 1377 K, and 1396 K for a spectral range from 1 μm to 4 μm .

The spectral normal emissivity data were computed from reflectivity measurements. Worthening [59] determined the spectral hemispherical emissivity of nickel (98.8% nickel content) at 0.665 μm , 0.535 μm and 0.460 μm , at high temperatures and reflectivity at room temperature. High temperature measurements were taken over a temperature range from 1300 K to 1660 K, and no indication of a change with temperature was found. Moreover, the values obtained at high temperatures agreed with the room temperature values obtained from reflectivity. Autio and Scala [105] measured the normal spectral emissivity of high purity nickel (99.95%) at 1238 K. The sample was embedded in the top of a graphite block contained in a SiC furnace. The blackbody cavity was a hole drilled in the graphite block with a depth to diameter ratio of 6.75. The spectral range was limited by a monochromator to several wavelengths between 1.43 μm and 6.57 μm . Ward [106] performed normal spectral emissivity measurements on nickel at high temperatures between 923 K and 1623 K for a narrow spectral range from 1.2 μm to 2.4 μm . The normal spectral emissivity of nickel was found to increase with increasing temperature for all of the wavelengths considered, except at 1.2 μm .

5.4.2 Normal Spectral Emissivity of Nickel Measurement

Nickel samples (99.9% pure) of 6 mm diameter were used in this experiment. The samples were CNC machined from a nickel rod, resulting in a very smooth sample surface. The sample was electromagnetically heated until it reached a steady state at four temperatures: 1440 K, 1488 K, 1551 K, and 1605 K. Prior to taking measurements the sample was heated to higher temperatures in order to remove any impurities and adsorbed gases.

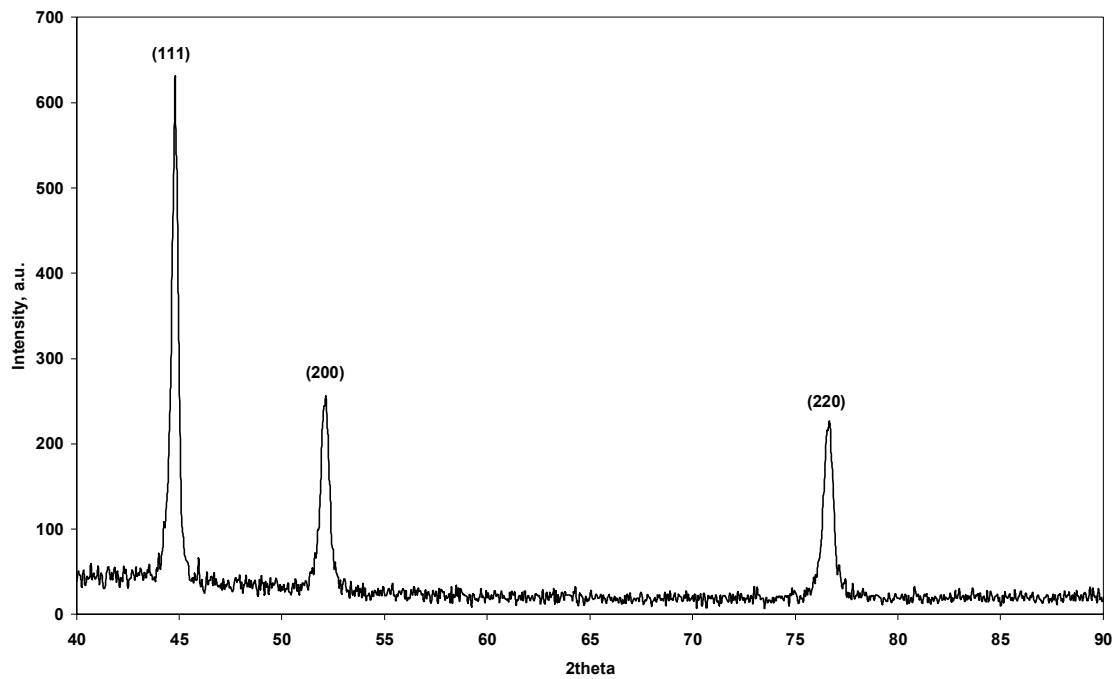


Figure 30 X-ray diffraction pattern of nickel sample

The sample surface was visually inspected after all experiments, and no evidence of surface oxidation was observed. The sample surface was clear mirror like. The X-ray diffraction pattern of the nickel sample in Fig. 30 indicates no sample surface oxidization, within limits of X-ray diffraction and nickel peaks were indexed.

The uncertainty in the spectral normal emissivity value $\delta\epsilon_{n\lambda}$ is defined as in Eqn. 41. The temperature uncertainty is derived from the uncertainty of the blackbody temperature, sample surface temperature, and the stability of the temperature control. According to Eqn. 41 the relative uncertainty is inversely proportional to λT_s^2 , resulting in a maximum uncertainty at lower temperatures and shorter wavelengths. The uncertainty estimation procedure from [101] was used to determine the total estimated uncertainty as shown in Table 7 Appendix D. The maximum uncertainty of emissivity was found to be less than 4% for the spectral and temperature ranges considered. As shown in Table 7 Appendix D, the largest contribution to the uncertainty in emissivity measurements is the uncertainty in sample surface temperature measurement. The sample surface temperature was measured using a Mikron ratio pyrometer which has a $\pm 0.5\%$ uncertainty as specified on the calibration bulletin provided by the manufacturer.

5.4.3 Experimental Results & Discussion

Figure 31 shows the measured spectral-normal emissivity of 99.9% pure nickel. The spectral-normal emissivity is found to increase slightly with increasing temperature from 1440 K to 1605 K, and to decrease with increasing wavelength between 1 μm and 16 μm .

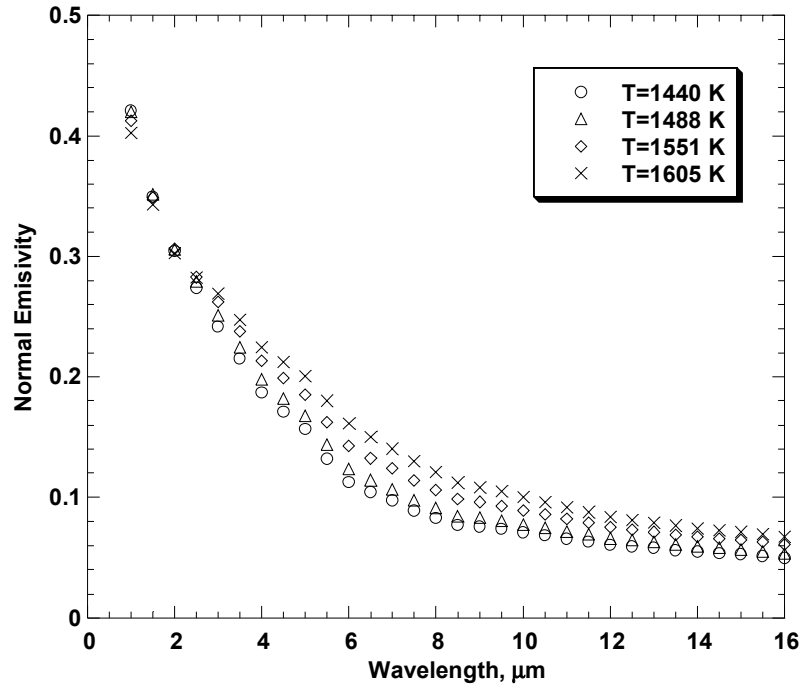


Figure 31 Spectral-normal emissivity of high purity nickel

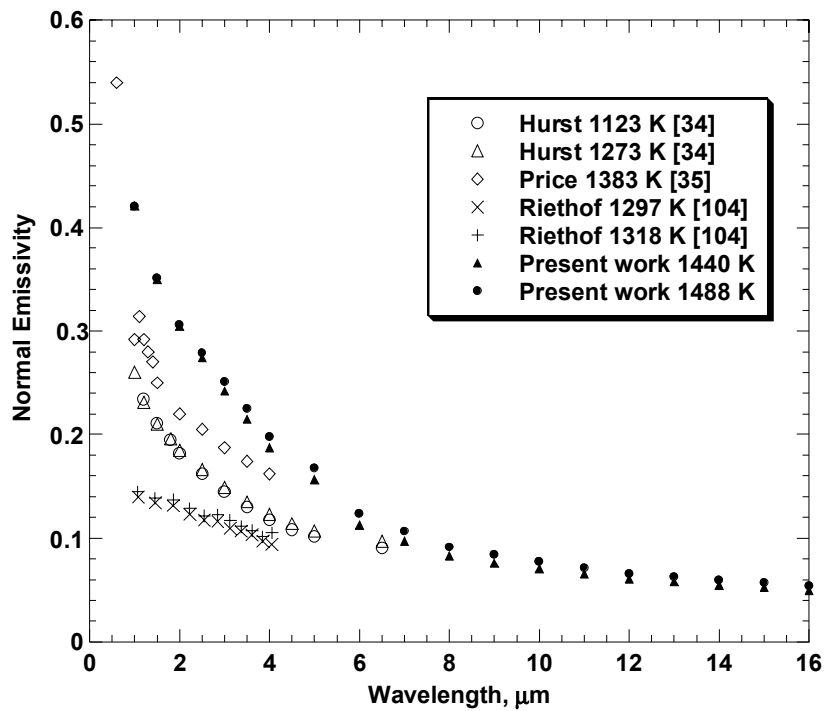


Figure 32 Spectral-normal emissivity of nickel comparison (a)

The measured spectral-normal emissivity shows good agreement with the characteristic metallic behavior reported by [4, 14] and an X-point (crossover) is clearly observed at wavelength of 2 μm .

Spectral-normal emissivity data from [69, 70, 104] are shown together with the present work in Fig. 32. Data reported by Hurst [69] at 1123 K and 1273 K are similar, suggesting that the spectral-normal emissivity of 99.5% pure nickel does not significantly depend on temperature. However, this finding is not supported by either the present work or by data reported in [104]. Riethof [104] observed that the spectral-normal emissivity of nickel increased slightly with increasing temperature between 1297 K and 1318 K, although the nickel purity and surface topography for this experiment were not reported. Similar trends are seen in Refs. [69] and [70], as well as in the present work. The normal emissivity measured in the present work, together with that reported in [105, 106], is plotted as a function of wavelength in Fig. 33. The emissivity from the present work for a spectral range from 1 μm to 5 μm is slightly higher than the published results of [105], where the nickel sample was mechanically polished prior to taking measurements. Data from [105] at 1238 K and 1403 K indicate very similar emissivities at 1.43 μm , 2.13 μm , 2.55 μm and 5.50 μm , different emissivity at 1.63 μm and 5.5 μm , and a very slight increase in emissivity with a 165 degree increase in temperature. This finding does not agree with the present results, where the emissivity at 1440 K in the same spectral range is significantly higher and the increase of emissivity with increasing temperature is more pronounced.

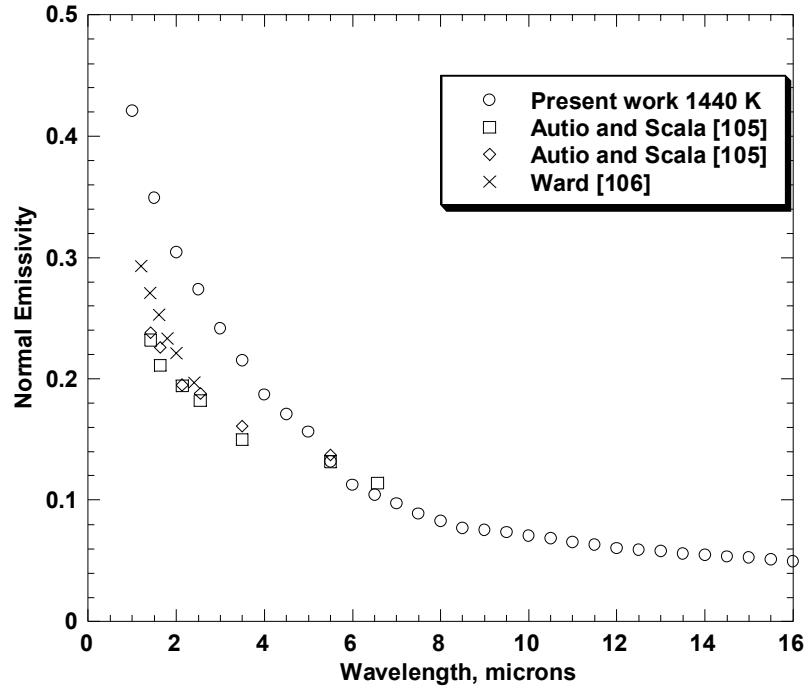


Figure 33 Spectral-normal emissivity of nickel comparison (b)

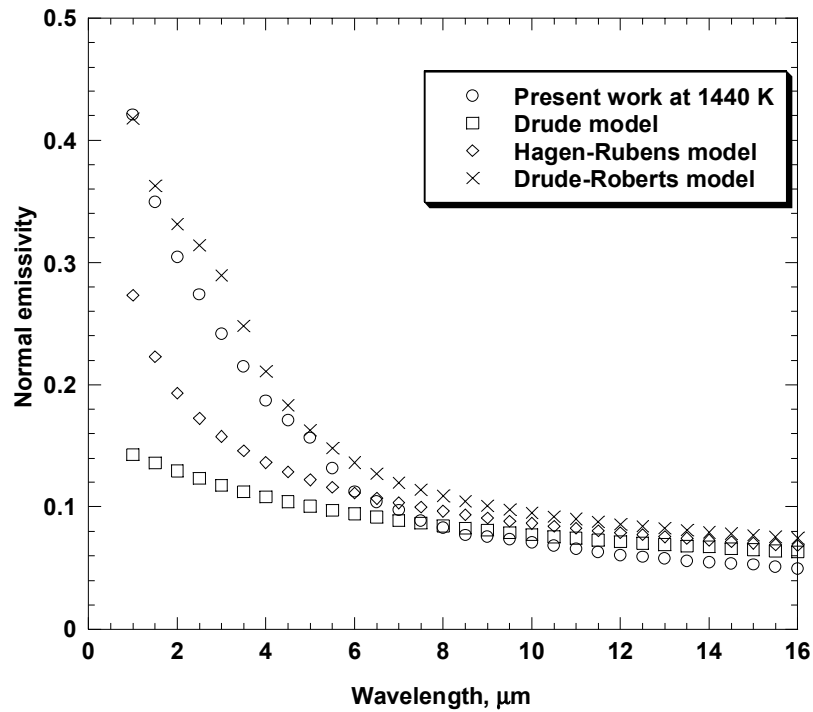


Figure 34 Normal emissivity of nickel prediction and present work

This might be explained by a difference in surface roughness, which in [105] seems to be lower as the sample was mechanically polished in a metallographic laboratory where the final polish was performed using alumina powder with a size of 0.05 μm . Furthermore, the sample used in [105] had a slightly different purity (99.95%) than the sample in the present work and the reported uncertainty of $\pm 9\%$ at 1.43 μm is significantly higher than that in the present work.

The spectral normal emissivity of nickel reported in [106] at 1373 K is higher than that reported in [105] at 1403 K and smaller than that of present work at 1440 K. Neither composition nor surface roughnesses were reported.

Figure 34 presents the normal emissivity of nickel from the present work at 1440 K as well as the theoretical predictions from several available models. The normal spectral emissivity of nickel according to the Drude model was derived according to Eqns. 23 and 24. At 1440 K the electrical resistivity of nickel was evaluated from compiled data [5], and its density is taken from [107]. The normal spectral emissivity of nickel derived according to the Drude-Roberts model gives a qualitative agreement with the present work. Agreement is also observed for the Drude and Hagen-Rubens models beyond 8 μm .

Roberts [11] postulated that the contribution of bound electrons at wavelengths long compared to their wavelengths of resonance, K_∞ , and attributed a value of 2.7 by fitting the reflectance data. In the present study we have considered K_∞ to be a variable parameter rather than a fixed value.

The normal spectral emissivity of high purity nickel from the present work is used to determine the parameters of Drude-Roberts model, and a dependence of K_∞ on

temperature was found. Regression analysis performed on K_{∞} and temperature from the reported emissivity data is shown on Fig. 35. A very strong linear association between K_{∞} and temperature is found, according a value of the coefficient of determination of 0.99. It needs to be pointed out that only data from the present work, together with data reported by Roberts at room temperature and [49] at 673 K, could be fitted. A strong linear association was also found for the relaxation wavelength parameter λ_2 as shown on Fig. 36. Consequently, the complex index of refraction was determined; both the refractive index and the extinction coefficient are shown on Figs. 37 and 38. The refractive index of nickel generally increases with increasing wavelength and temperature within spectral range considered. The extinction coefficient increases with increasing wavelength and decreases with increasing temperature. The effects of both free and bound electrons are seen on both the refractive index and the extinction coefficient. The maximum error between the complex index of refraction and normal spectral emissivity data was found to be less than 3%.

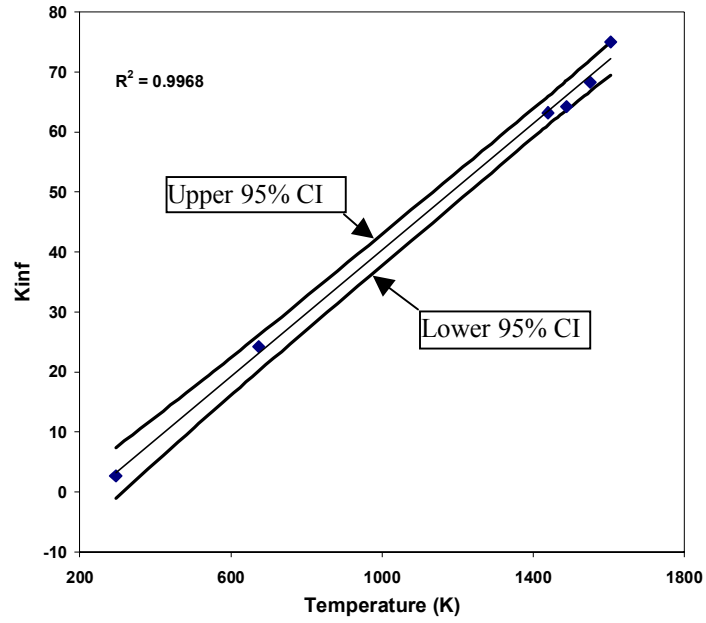


Figure 35 K_{∞} versus temperature for nickel

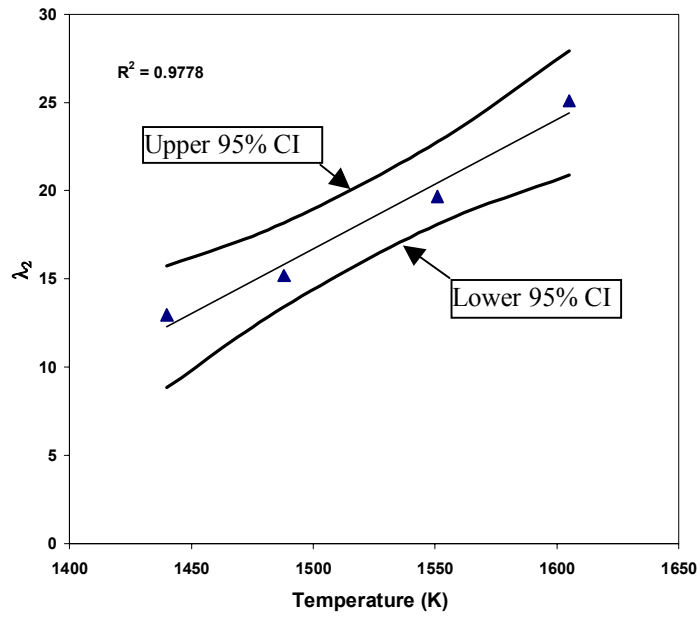


Figure 36 λ_2 versus temperature for nickel

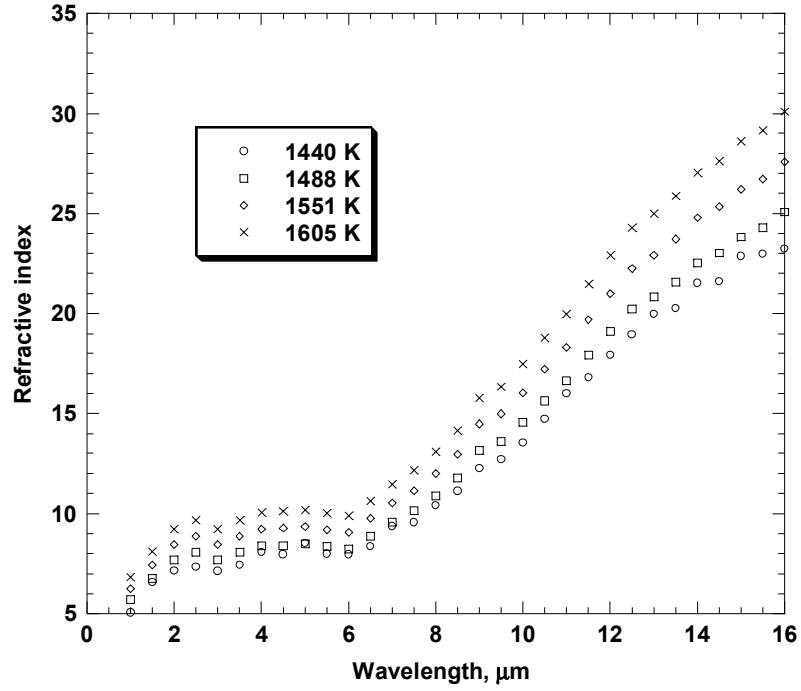


Figure 37 Refractive index of nickel

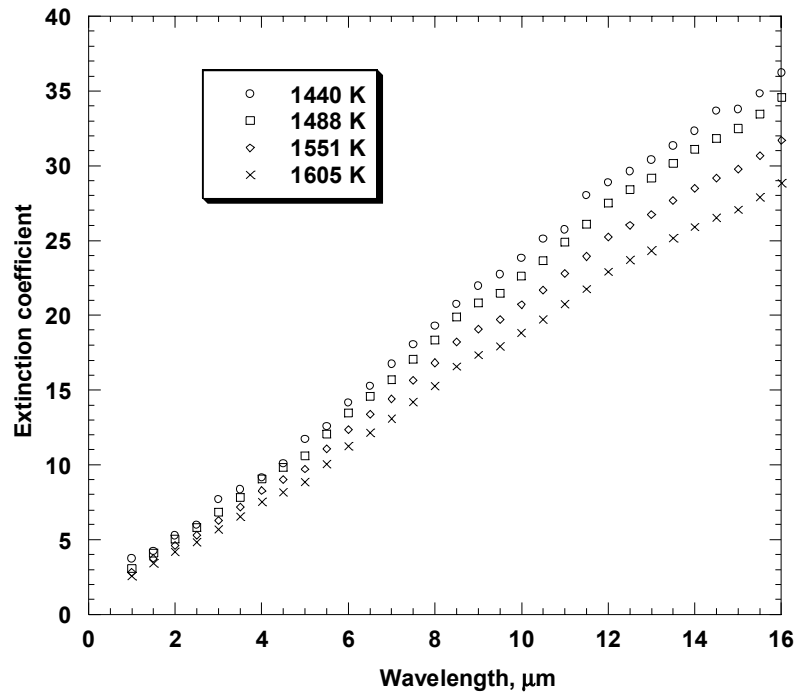


Figure 38 Extinction coefficient of nickel

5.5 Zirconium

Zirconium (99%) is readily available at low cost, and is used in industrial processes on metals such as casting, forming, and refining. However, its high temperature radiative emissivity is practically unavailable beyond 7 μm . This study will extend insight into the high temperature zirconium behavior up to wavelength of 16 μm and temperatures above 1173 K, and will compare it with available theoretical predictions. Zirconium possesses a risk of contamination at high temperature, making it difficult to measure its radiative emissivity using traditional methods [108]. Therefore, a non-contact heating method is more appropriate. Zirconium has a hexagonal structure at temperatures below 1173 K and can dissolve large amount of oxygen, but upon transformation to a body center cubic above 1173 K, the amount of oxygen dissolved decreases to a few atomic percent [109].

5.5.1 Specific Literature Review

Relatively few studies [110-113] have been reported on the normal spectral emissivity of zirconium, especially at elevated temperatures where metals are highly reactive and the tendency of oxides to form on their surfaces is great. The reported data are scattered and the spectral range is often very narrow. Bradshaw [110] determined the emissivity of zirconium in a vacuum at a mean temperature of 1581 K using a pyrometer by comparing the radiative heat flux emitted from the sample and a that of small cavity drilled into the sample itself. The emissivity was determined to be 0.426 at 0.652 μm . Autio and Scala [111] measured the spectral normal emissivity of single crystal zirconium at 1063 K. The average emissivity of the basal and prismatic faces was found to decrease with increasing wavelength, although peaks in emissivity were found between

2 and 3 μm and at 7 μm . Dmitriev et al. [112] determined the emissivity of zirconium at 1422 K and observed that emissivity decreased as wavelength increased for a spectral range between 1 and 5 μm . Coffman et al. [113] measured normal spectral emissivity of zirconium specimens in a vacuum for a spectral range from 0.4 to 4 μm at 1400 K, 1600 K, 1800 K and 2000 K. The emissivity was found to decrease with increasing wavelength and to decrease with temperature, although some contradictory data was reported.

5.5.2 Normal Spectral Emissivity of Zirconium Measurement

Zirconium samples (99% pure) of 6 mm diameter were used in this experiment. The samples were CNC machined from a zirconium rod, resulting in a very smooth sample surface. The sample was electromagnetically heated until it reached a steady state at four temperatures: 1359 K, 1478 K, 1622 K, and 1678 K.

The sample surface was visually inspected after all experiments, and no evidence of surface oxidation was observed. The sample surface was clear and mirror like. The X-ray diffraction pattern from the zirconium sample shown in Fig. 39, indicates no sample surface oxidization; zirconium (hexagonal) peaks were indexed.

The maximum uncertainty in emissivity was found to be less than 4% for the spectral and temperature ranges considered, as shown in Table 8, Appendix E.

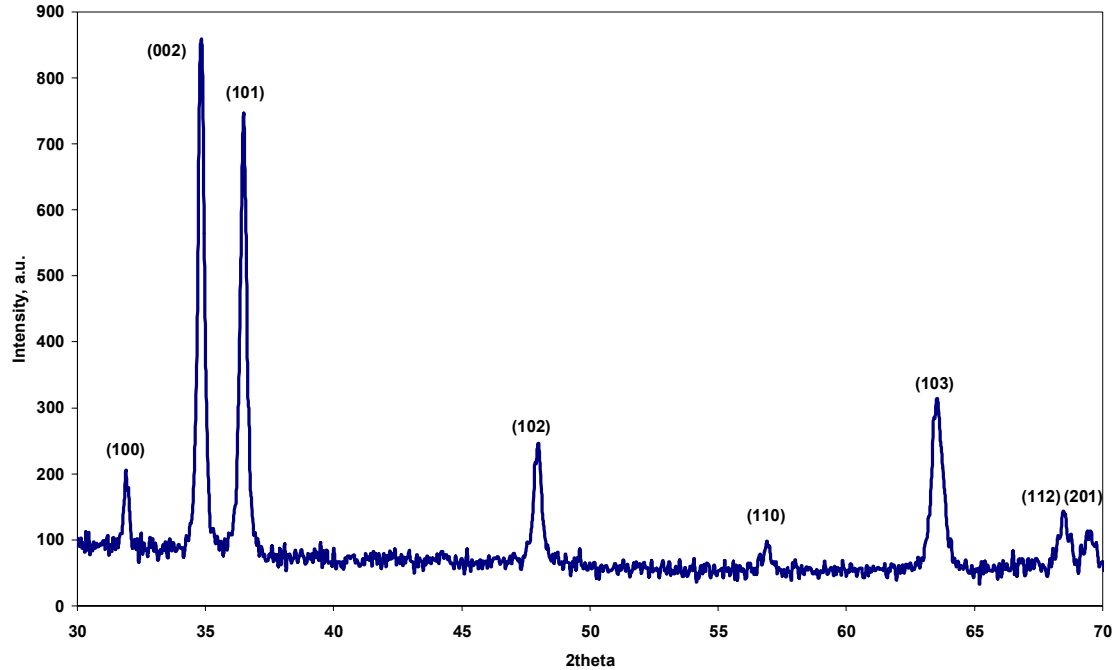


Figure 39 X-ray diffraction pattern of zirconium sample

5.5.3 Experimental Results & Discussion

Figure 40 shows the measured spectral-normal emissivity of zirconium at the four temperatures considered. The spectral-normal emissivity of zirconium is found to increase slightly with increasing temperature from 1359 K to 1678 K, and to decrease with increasing wavelength between 1 μm and 16 μm . The measured spectral-normal emissivity of high purity zirconium shows good agreement with characteristic metallic behavior reported by [4].

Spectral-normal emissivity data from [113] are shown together with the present work in Fig. 41. Data reported in [113] for specimen 2 at 1400 K, 1600 K and 2000 K are inconsistent with typical metallic behavior, show a decrease of emissivity with increasing temperature from 1400 K to 2000 K and an anomalous peak at 2000 K, around 1 μm .

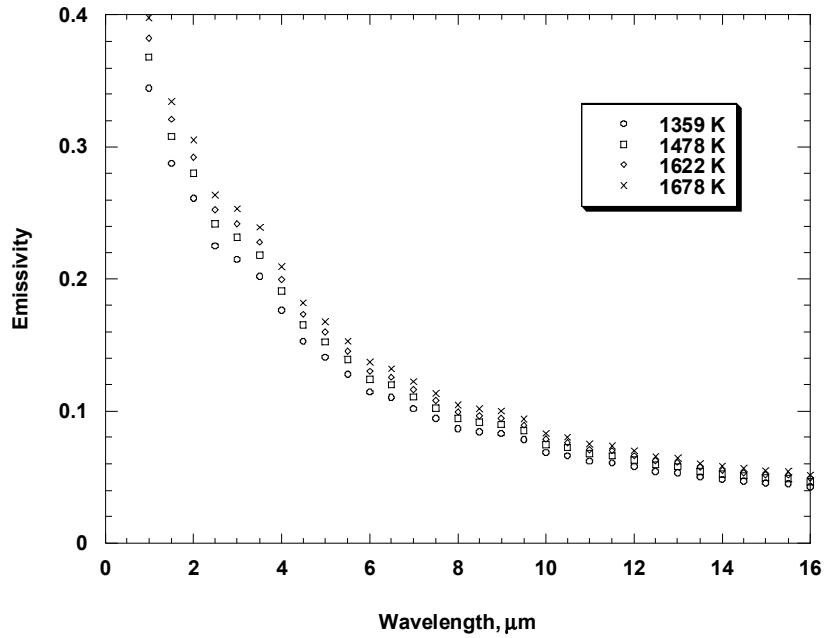


Figure 40 Normal spectral emissivity of zirconium

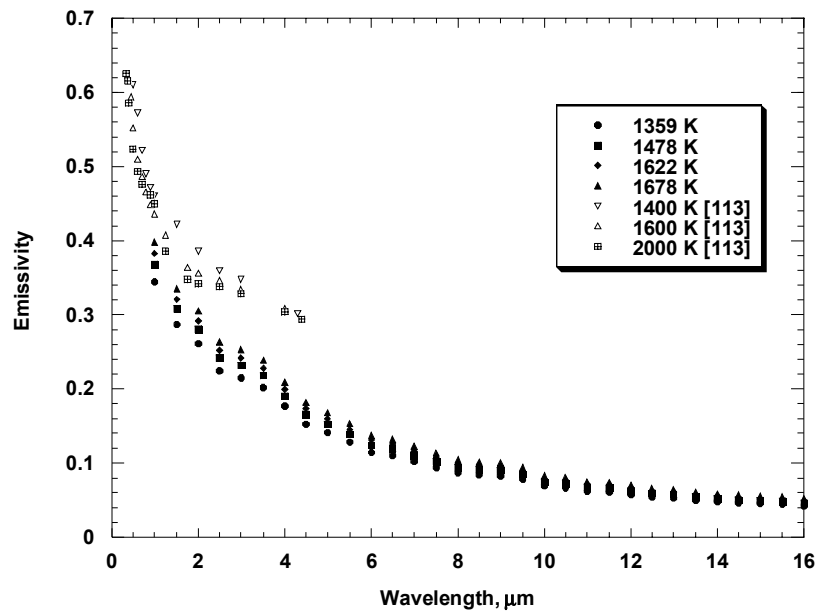


Figure 41 Normal spectral emissivity of zirconium comparison

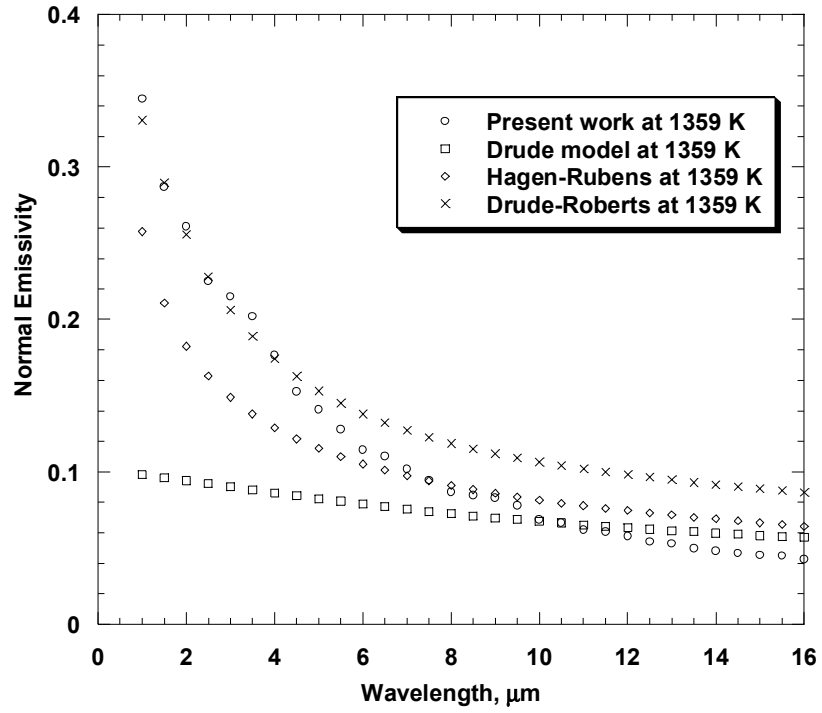


Figure 42 Normal emissivity of zirconium predictions and present work

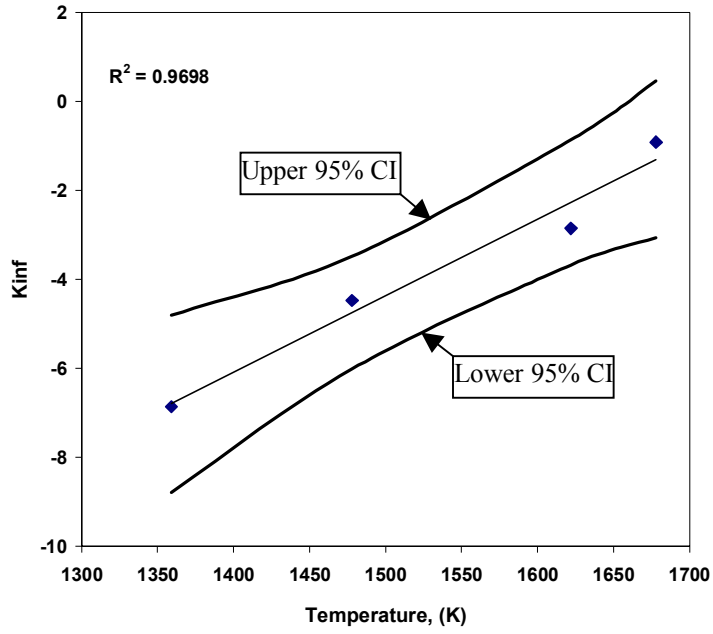


Figure 43 K_{∞} parameter versus temperature for zirconium

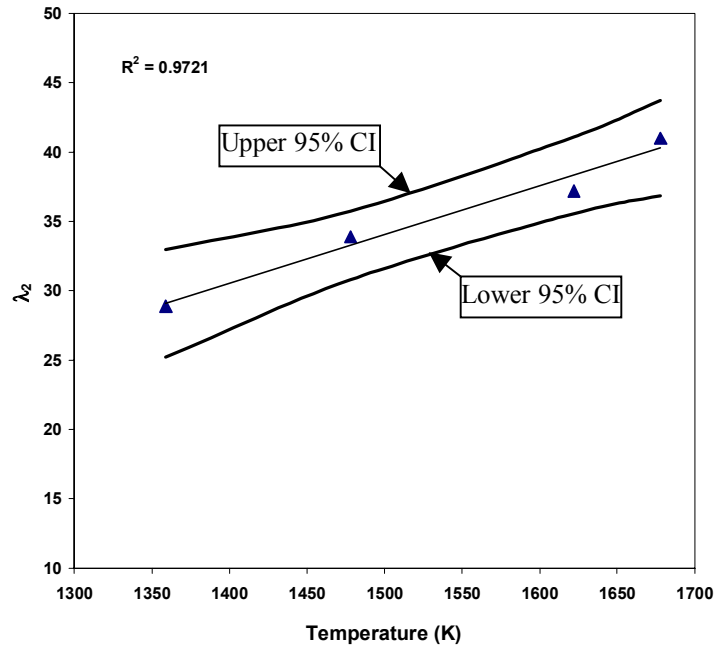


Figure 44 λ_2 parameter versus temperature for zirconium

Although the normal emissivity of zirconium from the present work was not determined for wavelengths shorter than 1 μm due to optical constraints, a qualitative agreement with data from [113] can be extrapolated at these shorter wavelengths. Furthermore, for wavelengths above 1 μm , the normal emissivity of zirconium reported in [113] is significantly higher than the normal emissivity of zirconium from the present work. This can be attributed to oxidization due to inadequate vacuum level (maximum of 10^{-5} Torr). This is also suggested by the peak in emissivity which appears around 0.9 μm at a temperature of 2000 K. However, the authors reported that the sample surface became blackened during heating and that the black deposit formed on the sample's surface was removed by further heating.

Figure 42 represents the normal emissivity of zirconium measured in the present work at 1359 K, as well as theoretical predictions from available models. The electrical resistivity of zirconium at 1359 K was evaluated from compiled data [5], and its density taken from [35]. Qualitative agreement is observed with the Drude and Hagen-Rubens models beyond 10 μm . The normal spectral emissivity of zirconium derived from the Drude-Roberts model gives a good agreement with the present work only at shorter wavelengths and over-predicts the emissivity at longer wavelengths.

The normal spectral emissivity of high purity zirconium from the present work is used to determine the parameters of the Drude-Roberts model by implementing a temperature dependent parameter K_{∞} rather than a fixed one, and a strong dependence of K_{∞} on temperature was found. Regression analysis performed on K_{∞} and temperature from reported emissivity data is shown in Fig. 43. A very strong linear association between K_{∞} and temperature is found yielding a value of the coefficient of determination

of 0.97. A very strong linear association was found between λ_2 and temperature as shown in Fig. 44. In fitting emissivity data, constant values of σ_2 were used over the temperature range studied, which suggests σ_2 does not depend on temperature.

The complex index of refraction was also determined, and both the refractive index and the extinction coefficient are shown on Figs. 45 and 46. The refractive index of zirconium generally increases with increasing wavelength and decreases with temperature in the spectral range considered. The extinction coefficient increases with increasing wavelength and decreases with increasing temperature. The maximum error between the complex index of refraction and normal spectral emissivity data was found to be less than 5%. A structure is seen on the refractive index plot at short wavelengths indicating bound electrons effects. The effects of free electrons are observed at long wavelengths as long as the refractive index pattern is similar to Drude model [122].

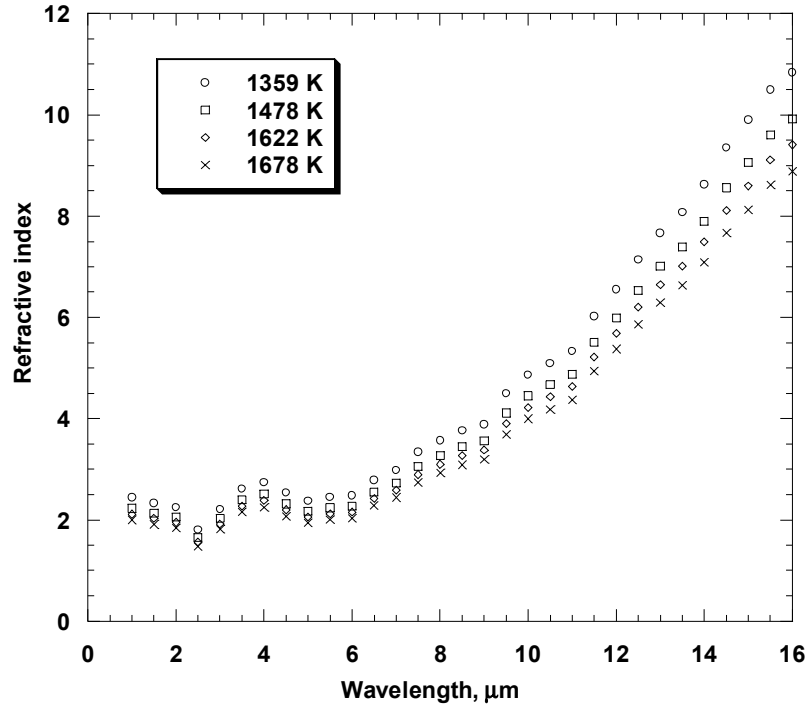


Figure 45 Refractive index of zirconium

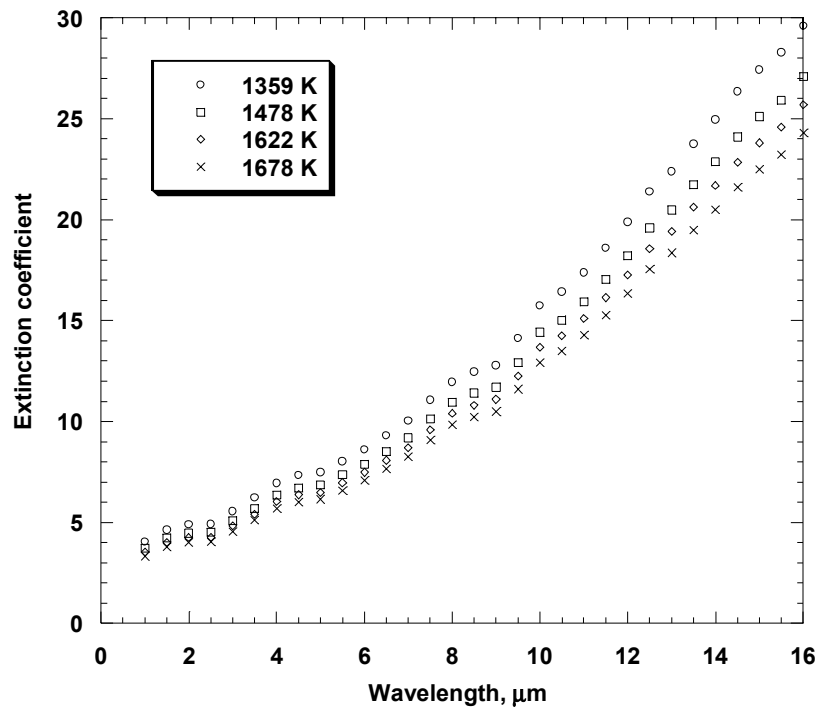


Figure 46 Extinction coefficient of zirconium

5.6 Titanium

Titanium is widely used in industrial processes because of its low density, good ductility and strength, and its resistance to corrosive environments. The available high temperature spectral emissivity data is rather contradictory, most probably due inadequate vacuum conditions. Titanium exhibits a high risk of contamination at high temperatures, so a non-contact heating method is more suitable than a traditional method [108] for spectral emissivity measurements. Titanium possesses a large oxygen solubility at temperatures below 1173 K in a hexagonal phase, but this is greatly reduced to a few atomic percent at higher temperatures in a body centered cubic phase [109]. This study will provide spectral emissivity data for a broad spectral range and at temperatures above 1173 K, which together with theoretical models can be further used to reduce the number of required measurements.

5.6.1 Specific Literature Review

Bradshaw [110] determined the normal emissivity of titanium at a pyrometer operating wavelength of 0.652 μm at temperatures between 1223 K and 1623 K, and found a very slight decrease in emissivity from 0.484 to 0.471, probably indicating an X-point at a wavelength greater than 0.652 μm . However, the uncertainty in measurement was not reported. Adams [114] determined the normal spectral emissivity of titanium with a reported error of $\pm 5\%$ for specimens under different heat treatments. The spectral range considered was from 1 μm to 15 μm and temperatures between 773 K and 1023 K. The emissivities measured in a vacuum were quite large indicating a possible contamination/oxidization. Seemueller and Stark [87] determined the spectral normal emissivity of 99.5% purity titanium in a high vacuum at 0.65 μm for temperatures from

1426 K up to the melting point, and the results show a decrease of emissivity with increasing temperature slightly higher than that reported in [110]. Michels and Wilford [115] measured the normal emissivity of commercial titanium at 0.665 μm between 1050 K and 1400 K and observed a decrease in emissivity with increasing temperature from a value of 0.72 at 1050 K to 0.69 at 1400 K. These authors also determined the total hemispherical emissivity which increased with increasing temperature. Although there is some qualitative agreement among reported data (in visible range of the spectrum) for titanium, there is a substantial difference between reports due to the different conditions and samples used in the experiments, and to outdated equipments.

5.6.2 Normal Spectral Emissivity of Titanium Measurement

Titanium samples (99% pure) of 6 mm diameter were used in this experiment. The samples were CNC machined from a rod, resulting in a very smooth sample surface. The sample was electromagnetically heated until it reached a steady state at four temperatures above 1273 K.

Visual sample inspection after all experiments, showed no evidence of surface oxidation. The sample surface was clear and mirror-like. The X-ray diffraction pattern shown in Fig. 47 indicates no surface oxidization and the strongest reflection peaks were indexed. The maximum uncertainty of emissivity was found to be less than 4% for the spectral and temperature ranges considered Table 9, Appendix F.

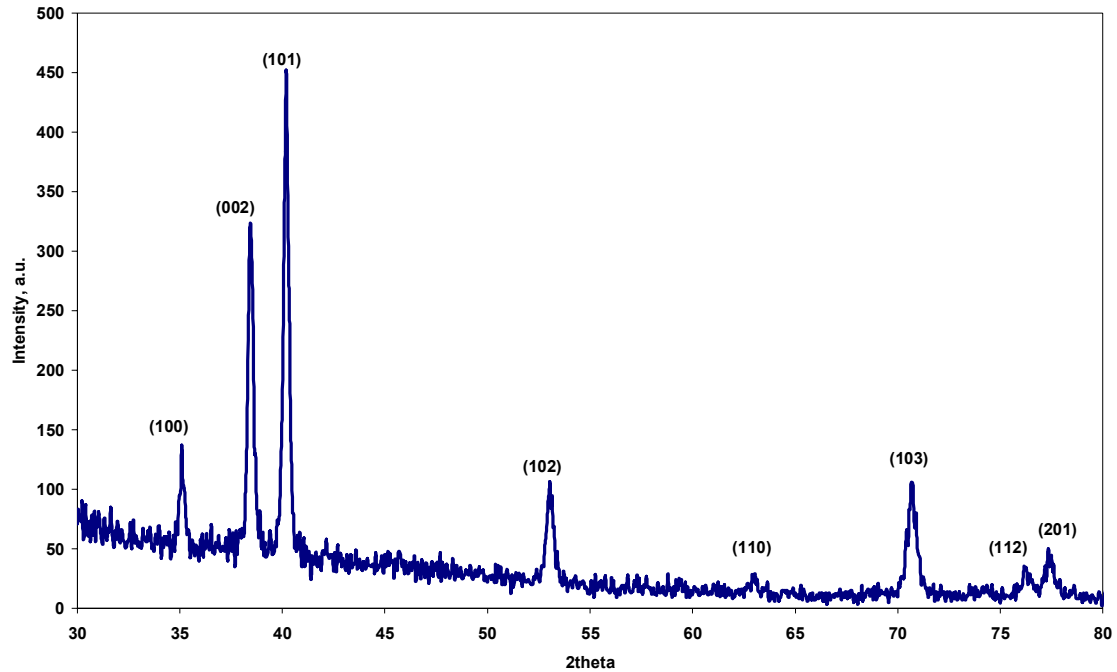


Figure 47 X-ray diffraction pattern of titanium sample

5.6.3 Experimental Results & Discussion

The spectral normal emissivity of titanium measured in the present work is shown in Fig. 48. The spectral normal emissivity of titanium was found to increase slightly with increasing temperature from 1361 K to 1614 K, and to decrease with increasing wavelength from 1 μm and 16 μm . It is important to note that the decrease in titanium normal emissivity is not consistently monotonic at shorter wavelengths between 1 μm and 3.5 μm , although the surface oxidization was not visually observed and neither confirmed by the X-ray diffraction performed on the sample shown on Fig. 47. For a spectral range between 6 μm and 16 μm , the normal emissivity of titanium decreases very slowly, indicating agreement with the Hagen-Rubens relation.

The spectral normal emissivity of titanium from the present work is shown in Fig. 49, together with data reported by [114]. The as-received specimen spectral normal emissivity reported in [114] shows a qualitative agreement with data from the present work, although the magnitude is higher and small peaks can be observed in [114]. This might suggest a sample surface oxidization or contamination.

The measurements on the titanium sample performed in air at 1023 K in [114] exhibit a broad peak around 7 μm , indicating sample oxidization. Measurements performed in a vacuum at 1023 K in [114] show a broad peak in emissivity around 4 μm . The specimen used in [114] was heated at 1073 K for 30 min. in a vacuum of 2.8×10^{-5} Torr before taking measurements. Both the broad peak developed around 4 μm , and the high emissivity magnitude, clearly indicate a departure from metallic behavior. This can possibly be explained as due to inadequate vacuum level and/or sample contamination.

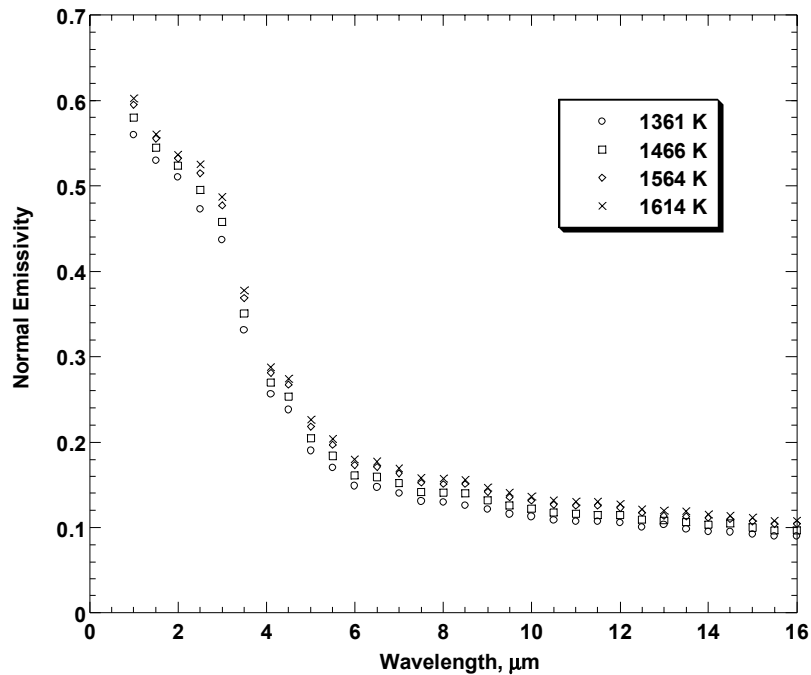


Figure 48 Normal spectral emissivity of titanium

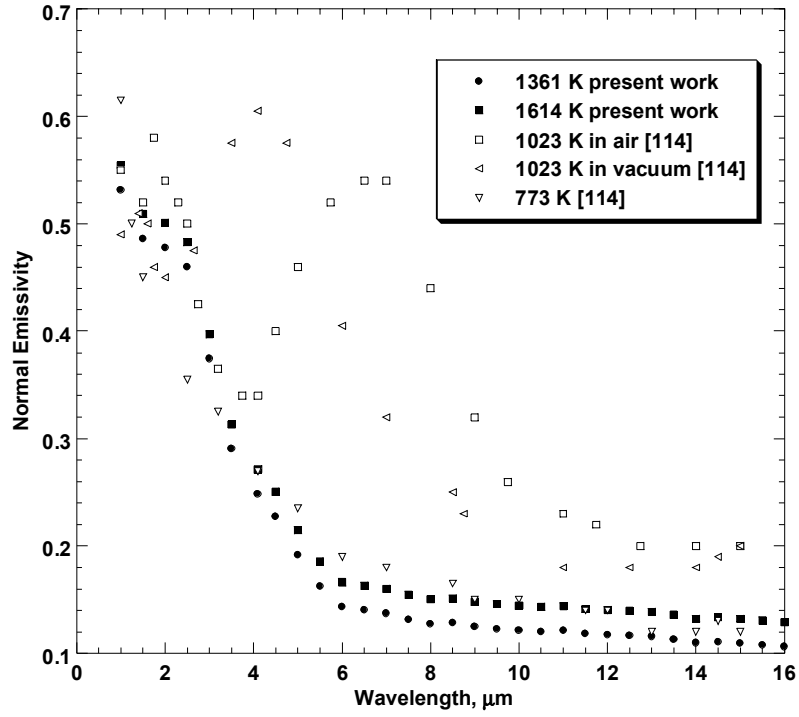


Figure 49 Spectral-normal emissivity of titanium comparison

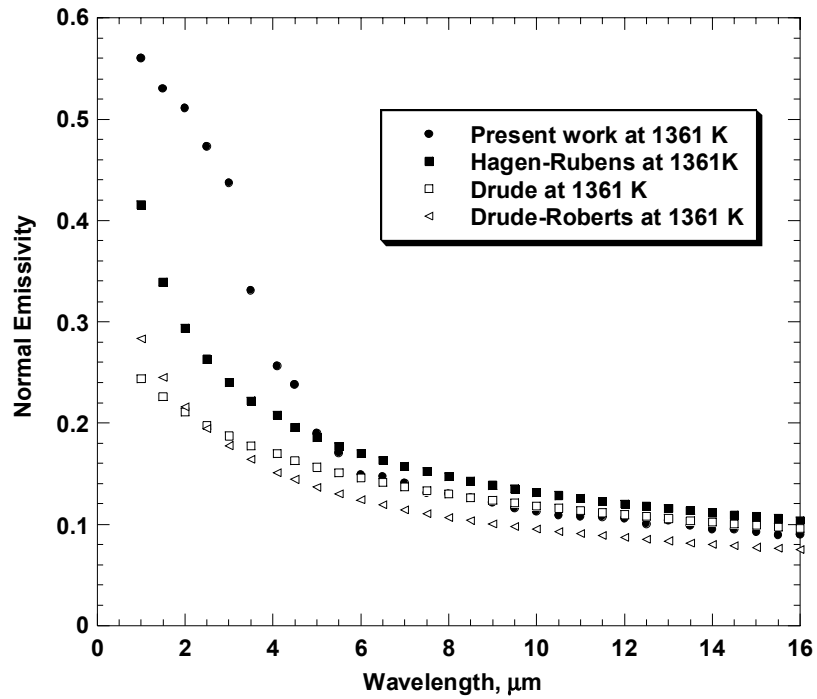


Figure 50 Normal emissivity of titanium prediction and present work

Figure 50 presents the normal-spectral emissivity of titanium from the present work at 1361K, as well as the theoretical predictions from available models. At 1361 K, the electrical resistivity of titanium was evaluated from compiled data [5] and its density taken from [108]. The spectral normal emissivity of titanium derived according to the Drude-Roberts model gives only a qualitative agreement with the present work. A better agreement is observed for the Drude model than for the Hagen-Rubens model beyond 6 μm .

The Drude-Roberts model was modified in order to find the best fit for normal emissivity data of titanium. A variable parameter K_∞ and a fixed σ_∞ proved to work reasonably well in fitting the two band model. Significant linear associations were found for both K_∞ and λ_2 according to Figs. 51 and 52.

The index of refraction determined together with the extinction coefficient based on a modified Drude-Roberts two parameter model are represented in Figs. 53 and 54. The maximum error found between the modified model and the normal emissivity of titanium was less than 8%. The complex index of refraction displays the effects of both bound and free electrons. Both n and k increase monotonically with wavelength beyond 6 μm due to free electrons. The structure of n and k at shorter wavelengths indicates bound electron effects.

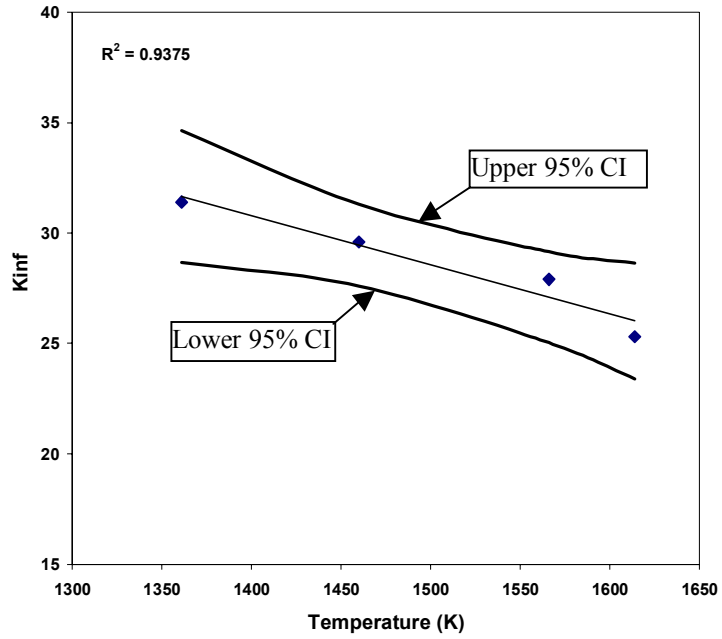


Figure 51 K_{∞} parameter versus temperature for titanium

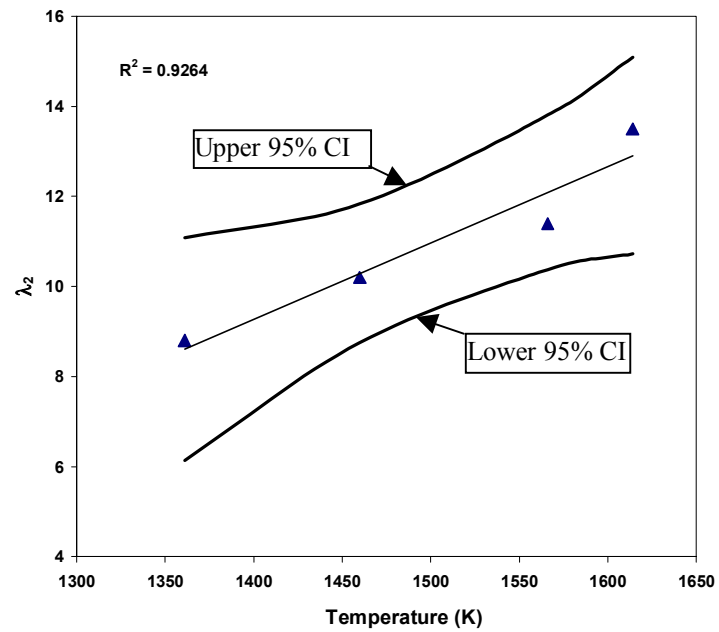


Figure 52 λ_2 parameter versus temperature for titanium

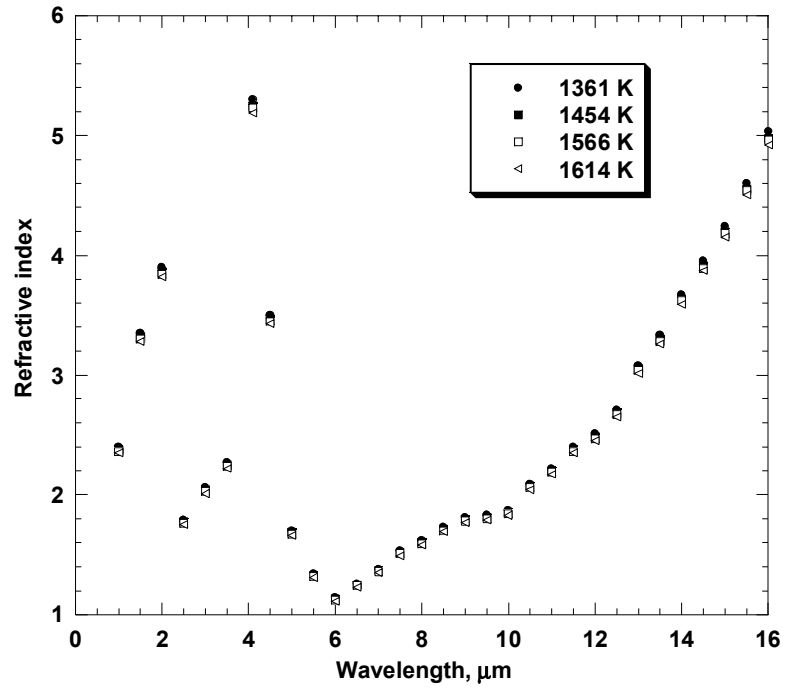


Figure 53 Refractive index of titanium

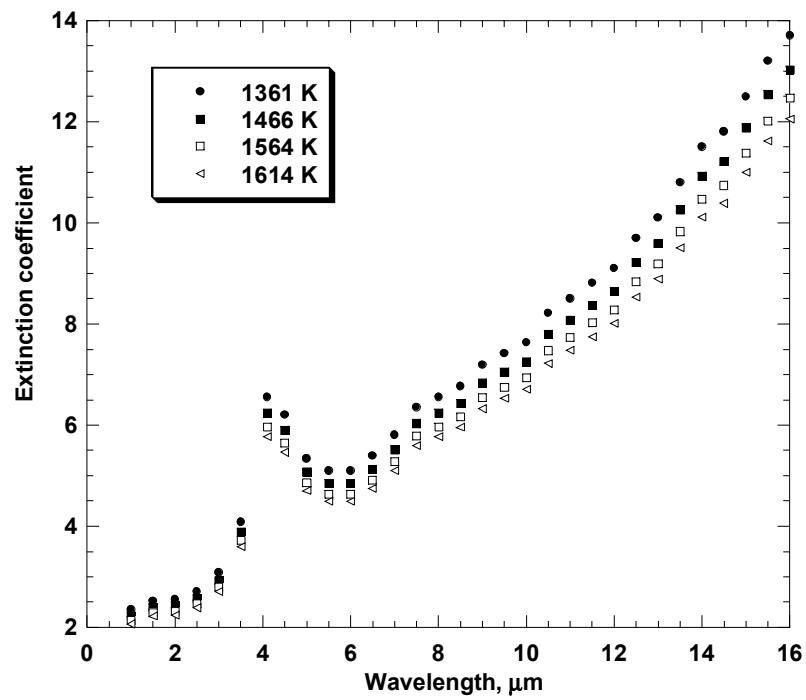


Figure 54 Extinction coefficient of titanium

6 GENERAL DISCUSSION OF RESULTS

Engineers and scientists are facing a serious challenge when emissivity of a given material is needed. The first thing is obviously identifying the material for which emissivity is required. Generally, most materials can be classified as nonconductors (insulators), semiconductors, and conductors based on their ability to conduct electrical current. The electrical conductivity of materials at room temperature spans more than 25 orders of magnitude, according to [10]. All materials may emit and absorb radiative energy at different frequencies. From ultraviolet to mid infrared electromagnetic waves are primarily absorbed by free and bound electrons or by change in energy level of lattice vibration [4].

In solids, a near continuum of possible energy states can be found due to a large number of electrons. The allowed energy states occur in bands. Between these bands of allowed energy, band gaps can be found. If there is a band gap between the completely filled (valence) and completely empty (conduction) bands, the material is a nonconductor. A wide or a narrow band gap divides nonconductors in insulators and semiconductors. A material which possesses an incompletely filled band or an overlapping of this band on an empty band is called conductor. For conductors, electrons can be excited into the next available state resulting in an electric current if electric field is applied. Both conductors and nonconductors are prone to interband transitions when electron moves into a different band, whereas conductors are likely to intraband

transitions, where electron changes its energy level within the same band. The above difference makes nonconductors to be transparent and weakly reflecting for photons with energies lower than the band gap and conductors to be highly absorbing and reflecting between visible and infrared spectrum [116].

After material identification and classification is performed, the type of emissivity data needed must be clarified. The required emissivity type might be normal, directional, or hemispherical, and might be spectral or total, as described in Chapter 2.1. Various conditions are known to be associated with emissivity measurements, such as: temperature, surface topology, contamination, composition, the surrounding atmosphere, etc.

Radiative properties of materials, such as emissivity and reflectivity, can be predicted from known theoretical models. Radiative properties of a surface can be evaluated from electromagnetic wave theory assuming that the complex index of refraction is known over the spectrum of interest. The complex index of refraction is useful in the treatment of wave propagation, and is related to the complex dielectric function (Chapter 2.2) which in turn is more appropriate for investigating microscopic mechanisms.

Specifically, there is a classical theory for evaluation of the dielectric function developed by Lorentz. This theory assumes that electrons and ions are harmonic oscillators (Chapter 2.3) and that they interact with electromagnetic waves. Drude simplified the Lorentz model to predict the radiative properties of conductors, and Hagen-Rubens developed an equation from Drude's model to obtain radiative properties

from electrical conductivity. Later, Roberts brought in the idea that two or even more types of charge carriers are responsible for radiative properties.

A significant number of radiative properties of materials can be found in the literature in compilations such as [5-7]. Overall, there is a significant lack of reported data, and uncertainty in the measurements can be as high as 20%. Among those reported, the vast majority is limited to normal emissivity rather than fully directional and measurements were performed only at a specific wavelength (typically a pyrometer wavelength) in the visible or near infrared part of the spectrum. The published data for a given material leads to a significant degree of scatter due to the many parameters that are involved. Often, the variation of emissivity data on a spectral basis is so large that it can take values anywhere between 0 and 1.

In order to accurately capture emissivity behavior, specific experimental setups have to be developed. Based on the information needed, an experimental setup can vary from a calorimetric technique for total hemispherical emissivity to a radiometric technique, which involves comparison with a blackbody radiator (Chapter 2.4). A radiometric technique can accommodate normal, spectral as well as directional measurements. Depending on the detector type, the spectral range can be limited to a single wavelength, multiple wavelengths, a narrow spectral region, or a very broad spectral region. As high temperatures are required, special precautions need to be taken in sample heating and preparation, uncertainty analysis, optics configuration, and specific designs to accommodate directional measurements. For measurements at temperatures close to melting point, high vacuum conditions are vital, and require more complex designs to accommodate sample heating in a closed system. Specific optics and viewports

with proprietary coatings are then necessary for the optical path between the sample and the detector. In order to characterize the sample surface, techniques as X-ray diffraction, scanning electron microscopy, and Auger spectroscopy can be applied.

Emissivity behavior of conductors (metals)

Emissivity behavior of metals can be predicted using theories such as Drude, Hagen-Rubens, and Drude-Roberts. Drude theory [16], developed to predict the dielectric function for metals, is related to the optical properties as described in Chapter 2.2.4. The optical properties are related with emissivity through Fresnel's equation (Chapter 2 Eqn. 12). Drude's theory implies that because free electrons propagate freely, they do not oscillate and therefore can be modeled as springs with vanishing spring constants, leading to a zero resonance frequency. Normal reflectivity and implicitly normal emissivity at room temperature of metals such aluminum [117], copper, and silver [118] show a very good agreement with Drude theory at wavelengths $\lambda > 1 \mu\text{m}$ for uncontaminated and highly polished samples.

Drude theory takes only free electrons into account. The bound electrons transition states, which are thought to affect emissivity of metals [11] are not considered. For example, aluminum shows a maximum emissivity of 0.2 at a wavelength $\lambda=0.8 \mu\text{m}$ which is thought to be due to bound electron transitions which are not considered by Drude theory [119]. Thus, for metals there is a frequency (wavelength) very close to the plasma frequency where $n \cong 1$ and $k \ll 1$, which implies that metals are highly transparent (neither absorb nor reflect) in the vicinity of this plasma frequency [4].

Drude's equation is generally applicable to metals, and satisfactory agreement with experimental data is reported only for certain spectral ranges. Qualitative agreement

was reported for molybdenum for $\lambda > 10 \mu\text{m}$ [120] and for tungsten for $\lambda > 5 \mu\text{m}$ [121]. It is also seen in the present work at temperatures greater than 1300 K for zirconium (Fig. 42, Chapter 5.5.1), titanium (Fig. 50, Chapter 5.6.3) for wavelength as short at $10 \mu\text{m}$ and for nickel beyond $7 \mu\text{m}$ [Fig. 34, Chapter 5.4.3]. Thus, Drude theory has a limited applicability to metals emissivity on spectral basis.

According to [121], for shorter wavelength regions, the classical free electron theory on which Drude's equation is based is inapplicable. The plot below shows a comparison between the Drude theory emissivity prediction for nickel and the present work measurements at two temperatures above 1300 K.

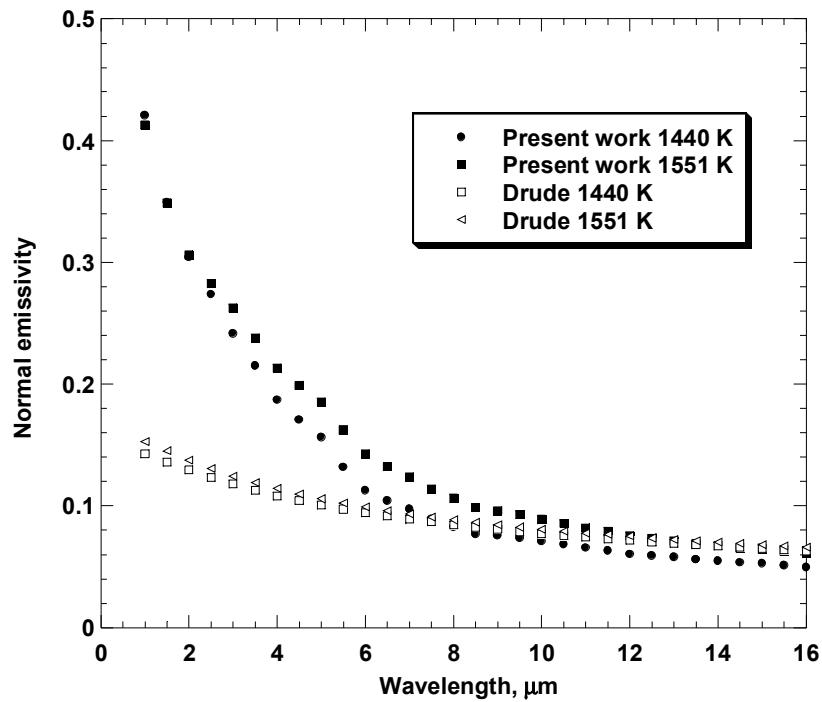


Figure 55 Nickel emissivity from Drude and present work

From the above plot, a qualitative agreement can be observed between Drude theory and the present work for wavelengths as short as 7 μm , considering the experimental error. For shorter wavelengths there is no agreement with Drude's theory. This is also illustrated by [4, 14, 122], as well as for both titanium and zirconium in the present work, as shown in Figs. 42 and 50. Drude's theory also predicts an increase in emissivity with increasing temperature, but this agrees only qualitatively with the experimental data. The shortcomings of Drude theory at shorter wavelengths may be explained through two parameters: the relaxation time (the time between two consecutive collisions) and the number of effective charge carriers. An explanation might be the dispersion of the relaxation time and the number of effective charge carriers, or in other words, wavelength dependency.

Another equation that describes the normal spectral emissivity of metals is the Hagen-Rubens equation, which was described in detail in Chapter 2.2.5. The Hagen-Rubens equation generally predicts that normal emissivity of a metal is proportional to $\sigma_{dc}^{-1/2}$. Therefore, since the electrical conductivity is inversely proportional to temperature, Hagen-Rubens equation at long wavelengths can be used to predict normal emissivity temperature dependence. The direction of the temperature dependence of the spectral normal emissivity of a metal in the infrared spectrum is determined by the change in the electrical resistance with temperature. Havstad [122] studied the prediction of the spectral normal emissivity of tungsten with temperature using the Hagen-Rubens equations and found only a qualitative agreement which applies at $\lambda > 10 \mu\text{m}$.

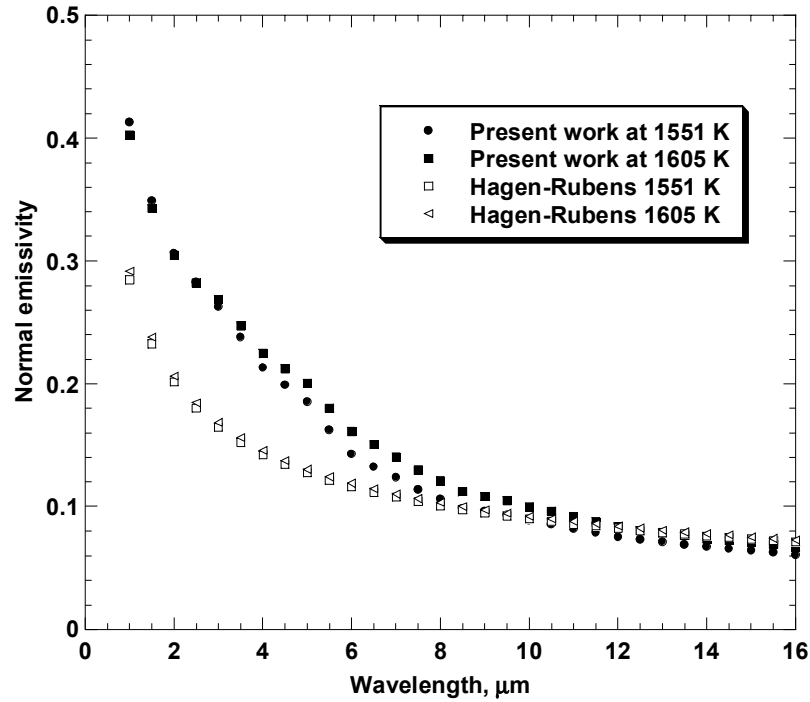


Figure 56 Normal emissivity of nickel from Hagen-Rubens and present work

It can be observed from the Fig. 56 that the normal emissivity of nickel from the present work at 1551 K and 1605 K agrees well with predictions from Hagen-Rubens for wavelengths as short as 8 μm . The same agreement can also be seen for zirconium for a limited spectrum range above 6 μm , and beyond 12 μm for titanium. At shorter wavelengths, the Hagen-Rubens equation generally underestimates the emissivity for highly smooth, pure surfaces [122], as is also observed from Fig. 56.

An obvious distinction between Drude's and Hagen-Rubens theories is clearly observed for all transition metals used in the present work. At shorter wavelengths the Hagen-Rubens equation gives a better prediction of emissivity than Drude's theory, but is still lower than the experimental data.

Roberts [11] tried to improve the Drude theory by picturing the electrons and holes, which are currently used to describe the electronic properties of metals as negative and positive ions. The Drude-Roberts equation, (Chapter 2.2.6, Eqn.28) is based on Drude theory, and assumes two types of charge carriers to be responsible for optical properties and have their own relaxation wavelengths. The model parameters need to be determined by fitting the model to reported data on optical properties, reflectivity, or emissivity data.

Drude-Roberts theory proved to bring some improvement to Drude's theory. It has been shown that Drude-Roberts predicted satisfactorily optical constants for metals such as nickel, copper, and tungsten [11] at room temperature for a limited spectral range from 0.25 μm to 2.5 μm . Roberts accounted for both interband and intraband transitions of electrons.

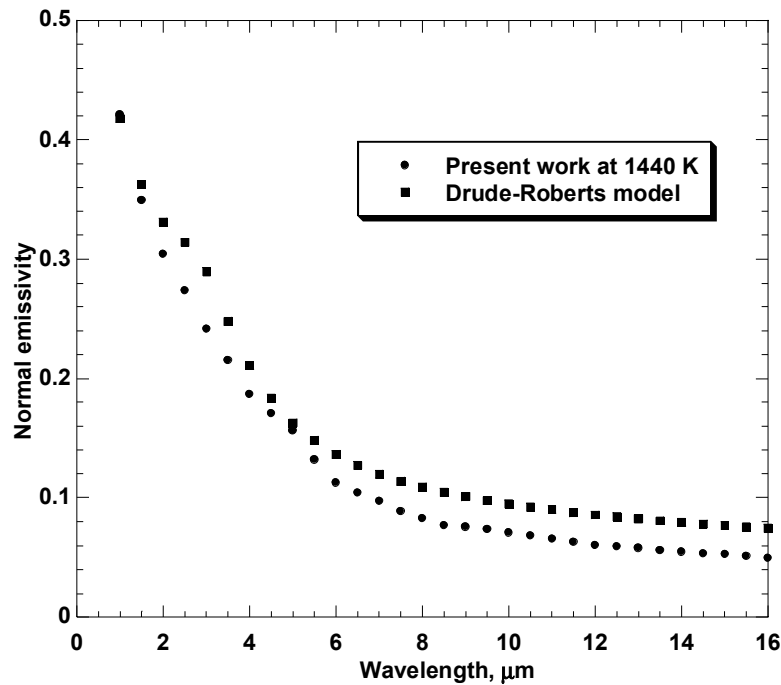


Figure 57 Normal emissivity of nickel present work and Drude-Roberts [11]

Reichman and Feldman [123] have used the Drude-Roberts model to fit optical properties of several transition metals beyond 6 μm at room temperature. The average deviations between the optical properties and the model were as high as 15%.

The spectral normal emissivity of nickel from the present work was satisfactorily fitted with the Drude-Roberts model (Fig. 57) using parameters reported by Roberts at room temperature. However, a better agreement with Drude-Roberts is observed in the present study by considering the contribution of bound electrons at wavelengths long compared to their wavelengths of resonance, K_∞ as temperature sensitive. Moreover, we have found strong temperature dependence for K_∞ , which is represented in Fig. 35 together with the 95% confidence interval. Regression analysis was performed on the K_∞ obtained from the present work on nickel as well as from [11] and [49]. The emissivity data presented in the literature review in Chapter 5.4.3 could not be fitted. The maximum difference between the present work on titanium and zirconium and the Drude-Roberts model fitted with reported parameters at room temperature [123] was about 18%.

Drude and Hagen-Rubens theories may be applied to a metal to qualitatively predict its spectral emissivity behavior at high temperatures at longer wavelengths (above 10 μm) using properties such density, electrical conductivity, and atomic mass. These theories imply that at those wavelengths the thermal radiation phenomena are contributed primarily by the intraband transition of electrons. The Drude-Roberts two parameter model shows a good agreement with measured optical properties at room temperature for some metals [11, 123] for limited spectral domains with differences as high as 15%. Extending the two parameter model to higher temperatures, significant differences between the model and experimental data were observed. However, strong temperature

dependence associated with parameters such relaxation wavelength and the contribution of bound electrons at wavelengths long compared to their wavelengths of resonance has been shown to provide a good agreement with the experimental data.

We have seen to this point that theories can only qualitatively predict the spectral emissivity of high purity metals at high temperature and for limited spectral range, generally beyond 10 μm . In addition, the prediction is limited to smooth, polished metallic surfaces, free of contaminations/oxidizations, defects, and heat treatments. The effect of temperature on spectral emissivity of a metal, which is also given by both Drude and Hagen-Rubens equations, predicts an increase of spectral emissivity with increasing temperature although the reported differences between experimental and theoretical predictions can be as high as 20% [4]. The majority of real surfaces generally exhibit higher emissivity, due to effects generally appearing during sample preparation [20]. Among these effects are: roughening, oxidation due to air exposure, and contaminations/interactions. An increased surface roughness can significantly increase the emissivity due to cavity effects (multiple reflections) [4] as well as oxidation as we will describe later in this chapter. Thus, in order to accurately determine the normal spectral emissivity of high purity metals at high temperatures at shorter wavelengths, measurements need to be performed.

Directional emissivity of a pure metal generally follows Lambert's law from a direction normal to the sample surface up to 40° , and then increases to reach a maximum at around 80° before diving to zero at grazing angles [124], according to Fresnel's equation. The Fig. 58 represents directional emissivity of a metal $n=1.5$, $k=7$ according to Fresnel's equation.

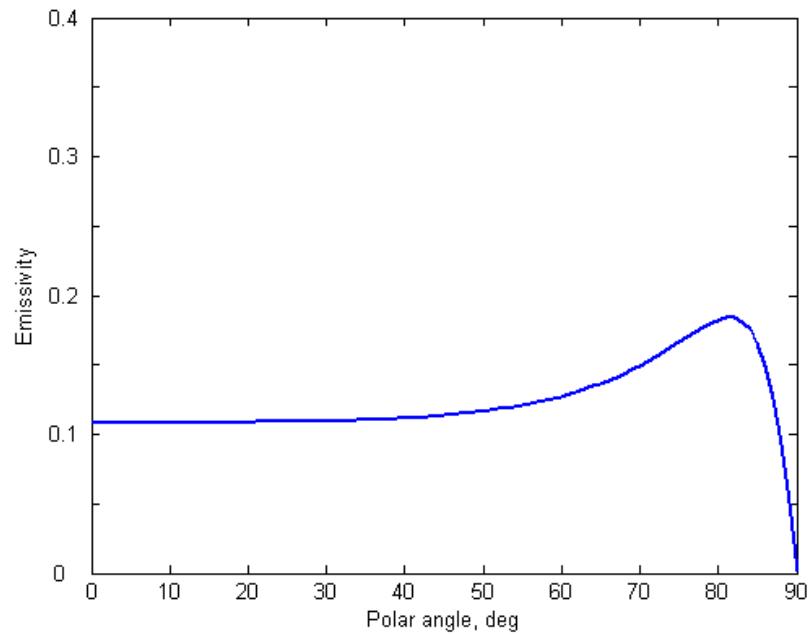


Figure 58 Directional emissivity of a metal [14]

The same trend of directional emissivity can also be seen in the present work on oxidized aluminum and nickel (optically thin films). From the Fig. 59, the directional emittance of aluminum at some representative wavelengths closely follows a metallic behavior according to Fresnel's equation from the surface normal up to 72° polar angle, although a thin film of metallic oxide covers the aluminum substrate. A good agreement with Fresnel's equation is also observed for oxidized nickel at 673 K in Fig. 60 below, although the Lambertian's behavior is only qualitative.

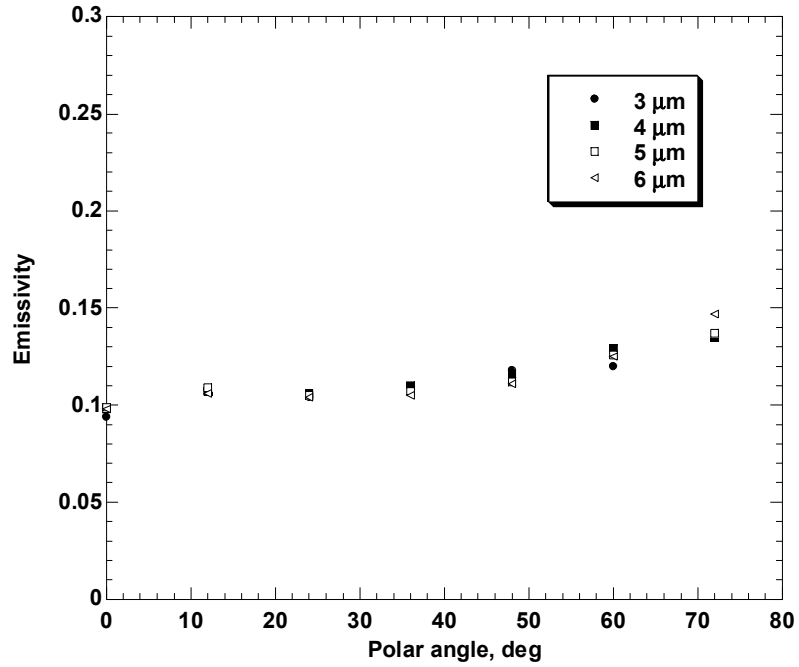


Figure 59 Directional emittance of oxidized aluminum at 673 K

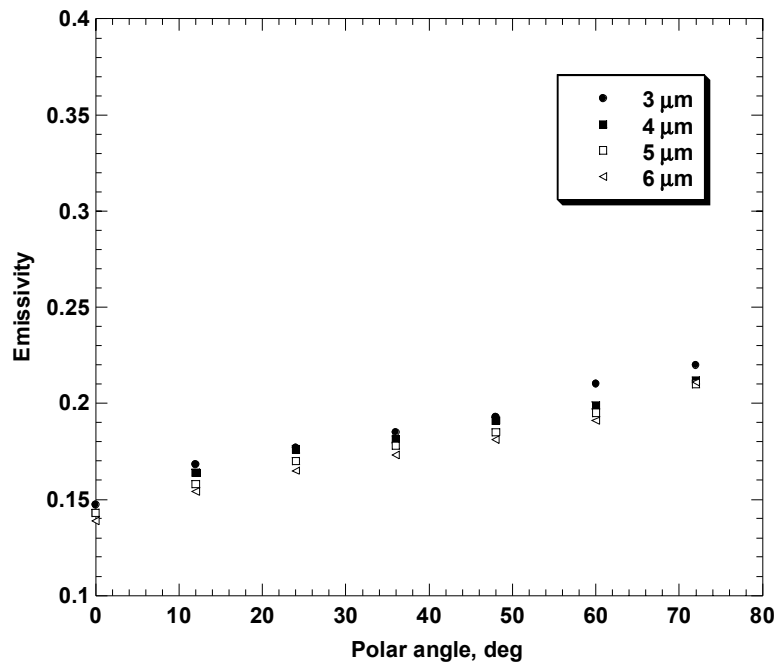


Figure 60 Directional emittance of oxidized nickel at 673 K

Generally, directional emissivity of a pure metal demonstrates the validity of Fresnel's equation [81, 36], and this also holds for optically thin films but only over certain spectral regions (Fig.59, 60). Inherently, changes in normal emissivity due to different parameters, discussed in the previous section, will affect directional emissivity as well.

Total hemispherical emissivity, defined in Chapter 2.1 is generally required in designing, modeling, and optimization of radiative heat transfer processes and for thermophysical properties measurement. Its measurement is generally accomplished using a calorimetric technique as described in Chapter 2.4. An approximate relation for total hemispherical emissivity was derived in [20], and is based on Hagen-Rubens theory. The relation uses temperature and electrical conductivity to calculate total hemispherical emissivity. Differences between the relation and the experiments for polished metals can be as high as 20% [20].

Total hemispherical emissivity is a spectral average of hemispherical emissivity with the spectral emissive power as a weighting factor. The broad spectrum of normal emissivity obtained in the present study allows us to determine total hemispherical emissivity by the use of Jakob ratio [56] of normal to hemispherical emissivity. Figures 61 and 62 represent the calculated total hemispherical emissivity of titanium and zirconium from the present work together with data reported in the literature data. The discrepancies may be attributed to differences in sample surface conditions.

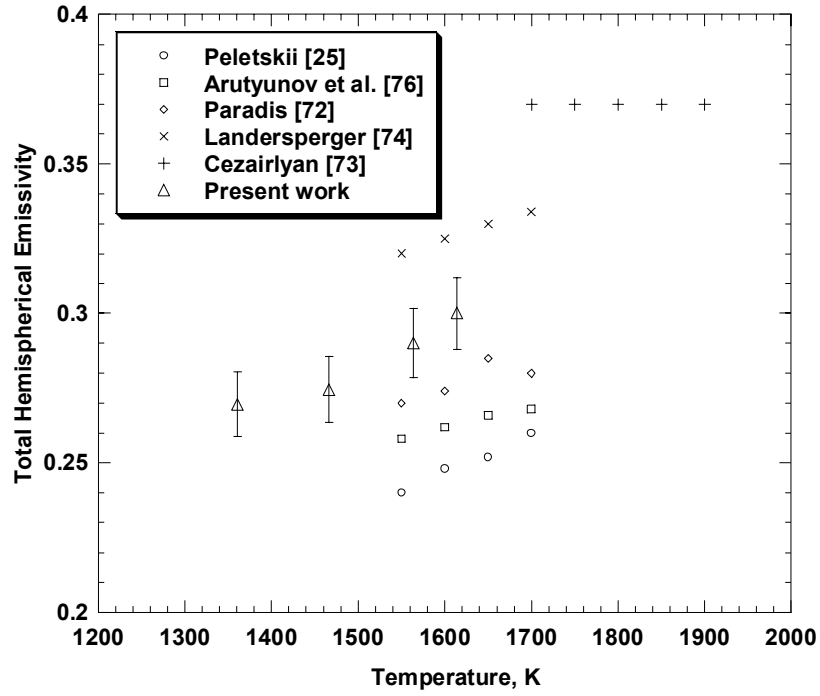


Figure 61 Total hemispherical emissivity of titanium

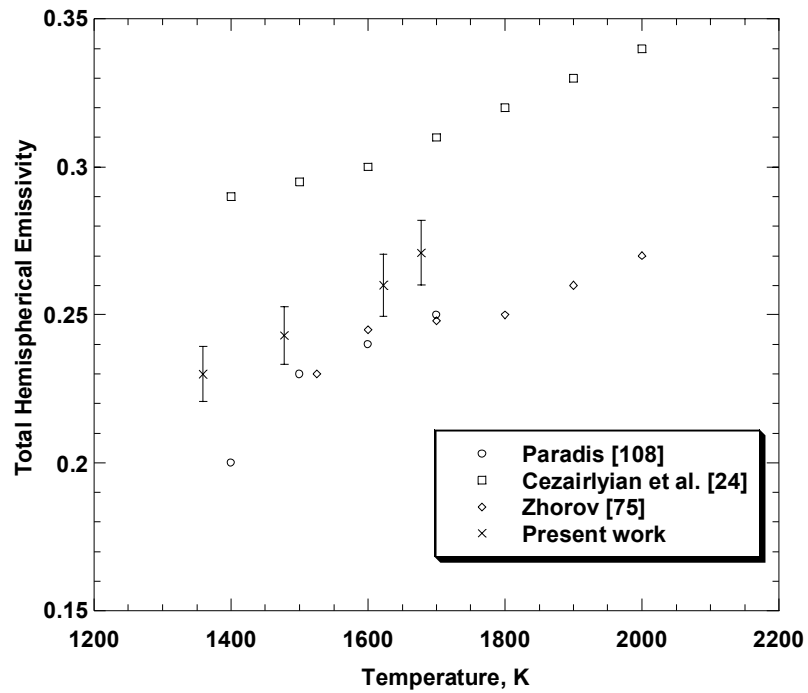


Figure 62 Total hemispherical emissivity of zirconium

The experimental procedure required to study the spectral emissivity of pure metals at high temperatures is highly complex, and its complexity arises not only from the elevated reactivity of metals and likelihood of contamination, but also from the difficulty of achieving a broad IR spectral range and a reasonable uncertainty. The experimental setup built in the present work for studying normal spectral emissivity of metals at high temperatures below the melting temperature in a vacuum practically ensures that the sample remains uncontaminated during the experiment due to the non-contact heating method, and avoids oxidation due to ultra high vacuum conditions (Chapter 4.3). In addition, the very broad spectral range from near to mid IR is achieved through proprietary optics and an FTIR detector with a maximum uncertainty of 4%.

Optically thin films

An optically thin film is a film with a characteristic optical thickness much less than 1, which is transparent to the radiative properties of the substrate. The optical thickness measures the ability of a path length to attenuate radiation of a given wavelength. Therefore a large optical thickness provides a large attenuation. Neglecting scattering, the optical thickness depends on the absorption coefficient and the path length. The normal spectral emittance of high purity aluminum with an optically thin layer of aluminum oxide grown on it is studied in the present work, together with the spectral normal emittance of aluminum oxide, previously reported in [40].

The influence of aluminum oxide higher emittance in mid infrared on artificially oxidized aluminum has been shown in Chapter 5.2.3 Fig. 20. This influence is seen through the development of two small peaks between 8.5 and 11 microns. This spectral region is in the proximity of the wavelength where aluminum oxide exhibits its highest

emittance, as shown in Fig. 63. Thus, the spectral normal emittance of a metal at high temperature in air (artificially oxidized) will be altered by the presence of heavy ions as Al^{3+} and O^{2-} with lower mobility [125]. Ngai [126] has found a characteristic low frequency (mid IR spectrum) associated with the relaxation time of these entities.

The generally monotonic decrease of emissivity with wavelength exhibited by a pure metal will gradually change with degree of oxidization, and this change will start in the spectral region where the metal oxide exhibits its greatest emittance. This suggests that the relaxation time and in the number of effective charge carriers (Drude model) become both wavelength dependent and this dispersion started around Christiansen point. The Christiansen point is the wavelength at which the emissivity has its highest value (as high as one) [125] and is a characteristic of most heteropolar dielectric materials.

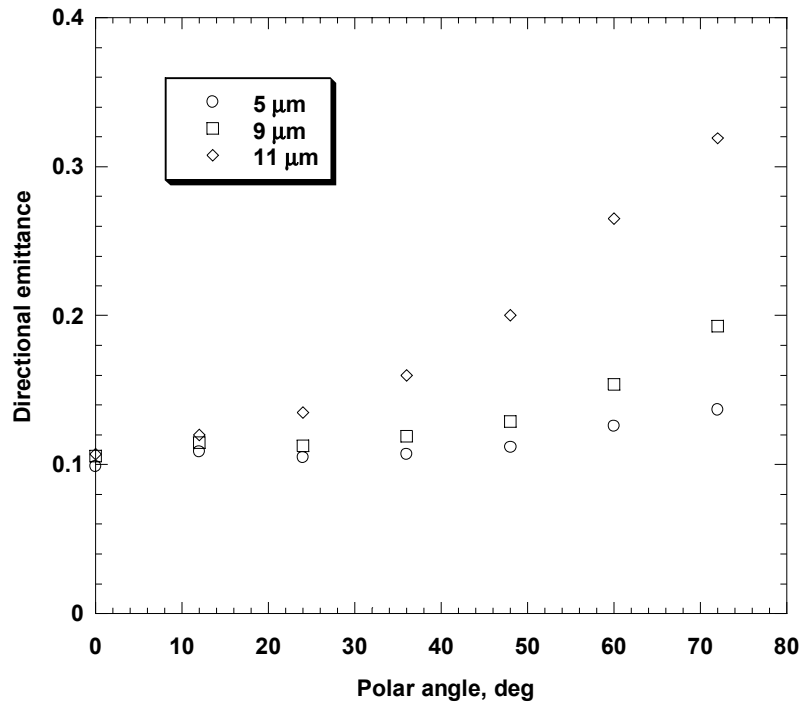


Figure 63 Directional emittance of oxidized aluminum

At wavelengths shorter than 8 μm , the directional emittance of oxidized aluminum from present work follows Lambert's law from a direction normal to the sample surface up to 40°, and then increases according to Fresnel's equation in order to reach a maximum, before decreasing rapidly to zero.

For wavelengths longer than 8 μm , which coincides with the wavelengths where peaks on normal emittance are evident, a departure from metallic behavior is observed (Fig. 63). Therefore, as long as the oxide thickness (290 nm) is neither sufficient enough nor consistent, the radiative emissivity of oxidized aluminum does not differ significantly from a pure metallic behavior at shorter wavelengths. The inconsistency of the aluminum oxide film is revealed in the present work by the AES spectrum which showed the presence of both Al^{3+} and Al. However, the directional emittance at peak wavelengths is significantly altered. It does not obey Lambert's law and continuously increases with increasing polar angle from normal until a maximum is reached around 70°, which is about three times higher than normal emittance as seen in Fig. 63.

The spectral normal emittance of oxidized nickel, also studied in this work, exhibits two peaks between 8 and 16 microns (Chapter 5.3.3., Fig. 26). These, can be attributed to the spectral region where nickel oxide exhibits the highest emissivity. These peaks are more evident than those developed on aluminum due to higher degree of oxidization. Directional emittance of oxidized nickel is also altered, and a deviation from Lambert's law is seen. The deviation is highest at peak wavelengths.

The emittance behavior of optically thin metal oxide films on a metal substrate is more complex than metallic or dielectric behaviors. As the optical thickness of the metal oxide changes from thin to thick the emittance behavior changes accordingly from a close

to a metallic to a close to a dielectric behavior. The emittance behavior of an optically thin metal oxide film generally follows a metallic behavior from near IR to mid IR but can have a higher magnitude due to increased surface roughness (present work). The metallic oxide film starts to affect both the relaxation time and the effective number of charge carriers at characteristic frequencies (wavelengths). These are low frequencies (mid IR) and were found close to Christensen's wavelength. Therefore, normal as well as directional emittance of the metal substrate is affected.

Emissivity behavior of nonconductors

Nonconductors (dielectrics) have completely filled valence bands and empty conduction bands, and therefore no intraband transitions such as classical infrared absorption can be seen. Because of the high band gap energy, the interband transitions cannot occur in the infrared or visible part of the spectrum. Therefore, the insulators are expected to be transparent from the far IR to the visible region of the spectrum. Nevertheless, a new absorption mechanism may take place in the IR by the excitation of phonons (light) by photons. A lattice vibration quantum called a phonon can absorb light under an interband transition type [10]. Therefore, the atoms which are thought to be oscillators by the Lorentz model can possess one or several resonance frequencies which depend on the atom mass, on the vibrational modes, and on the restoring force according to Eqn.16.

Typically the spectral normal emittance of a dielectric metallic oxide has three different regions according to [125]: the transparency region from the visible part of the spectrum to around 3 μm , the multiphonon or semitransparent region typically from 3 μm up to around 10 μm , where a maximum emittance is exhibited, and the phonon or opaque

region beyond the maximum value in emittance. Both the semitransparent and the opaque regions of aluminum oxide are shown in [40] and in the present work as shown in Fig.

64.

The semitransparent region lies between 3 and 10 μm and contains the maximum value of emissivity, and the opaque region is observed beyond 10 μm . All three regions were also seen in MgO [127], SiO₂ [121, 128], Al₂O₃ [45].

The single oscillator Lorentz model presented in Chapter 2.2.3 often gives good agreement with the experimental data. Spitzer et al. [129] report the normal reflectivity at room temperature for α -SiC from which normal emissivity was calculated, and is shown in Fig. 65. For wavelengths shorter than 10 μm and larger than 13 μm α -SiC is generally transparent due to k much smaller than 1 and weak reflectance.

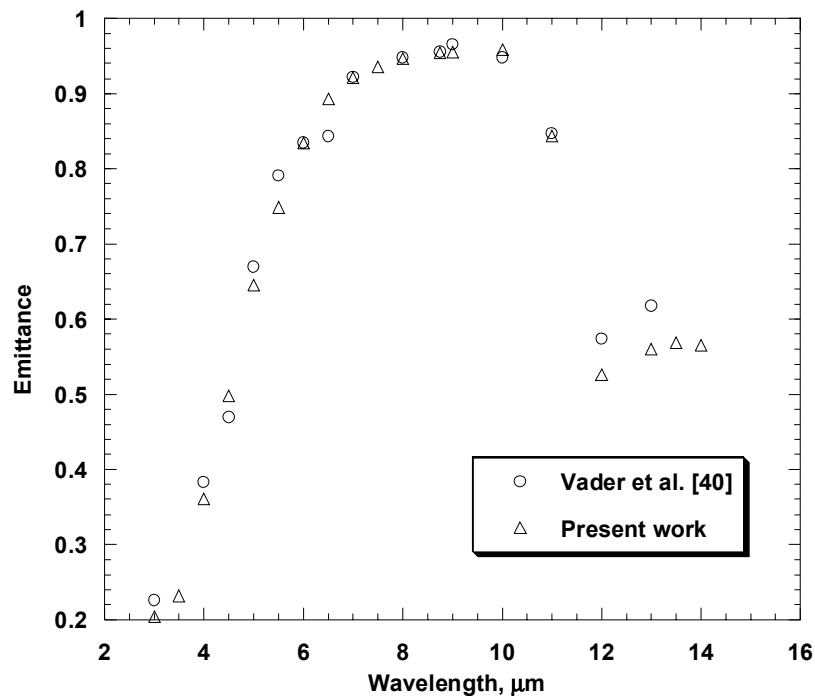


Figure 64 Normal emittance of aluminum oxide

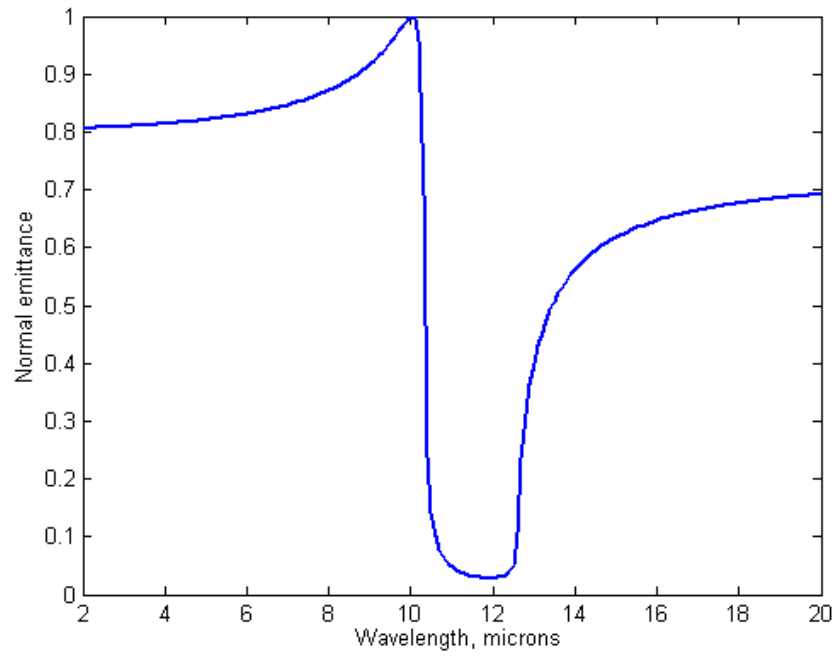


Figure 65 Normal emittance of SiC [129]

Between 10 μm and 13 μm SiC is highly reflecting (low emittance) and opaque since k is larger than 1. Although the Lorentz model can be used to describe certain crystals by a single oscillator model, its applicability is limited and more complex models containing two or more vibrational transitions and the resulting overlapping bands may be required [4, 14].

The effect of temperature on radiative properties of dielectrics is more complex and difficult to quantify than for metals [4, 124]. The absorption bands observed from mid to far infrared in ionic solids due to lattice vibration excitations are seen to decrease with increasing temperature [127, 130] for MgO and SiC, although the dielectric behavior is similar to that of metals from near to low infrared as observed by [131, 132] for aluminum oxide and also for cupric oxide in the present work.

Directional emittance of an optically smooth dielectric is described by Fresnel's equation, and also follows Lambert's law from angles normal to the sample surface to typically 50-60° before a sudden decrease to zero [4, 124]. A characteristic dielectric directional behavior is represented in Fig. 66 for $n=5.5$ and $k=0$.

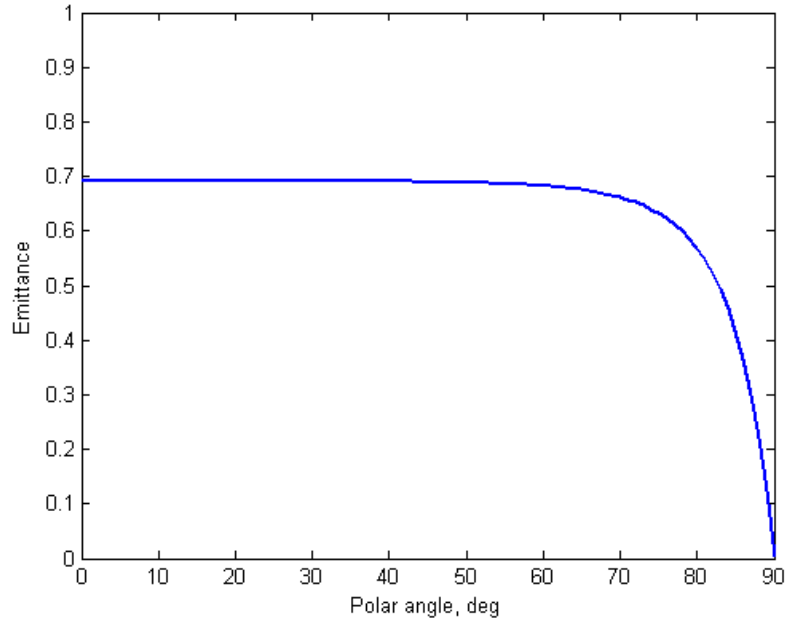


Figure 66 Directional emittance of a dielectric

This is supported by results for cupric oxide from the present work, which closely agree with Fresnel's equation as seen in Fig. 9 Chapter 5.1.3 from normal up to 72° , and a Lambertian behavior is observed up to 48° polar angle.

Optically thick films

Thermal radiative properties of oxidized metals can swing from close to pure metallic behavior to a practically dielectric behavior depending on optical thickness of the metal oxide layer formed on the surface. Accordingly, the metal oxide layer can be transparent so the radiative properties are mainly those of the metal substrate, or opaque where the radiative properties are given only by the metal oxide. An intermediate case is also common where the metal oxide is both transparent and opaque in different spectral regions, based on the magnitude of the absorption coefficient.

Optical thicknesses calculated after the complex index of refraction was determined proved that the cupric oxide is optically thick (Ch. 5.1.3, Fig. 8) for all reported wavelengths and temperatures. Hence, its radiative properties are not affected by the substrate radiative properties; in other words, cupric oxide is not transparent. Normal emittance of cupric oxide at high temperature increases with increasing wavelength and temperature for the spectral range and temperature domain considered here (Fig. 12). A higher emissivity value is to be expected somewhere beyond 8 μm to define an emission band and a reflection band in near infrared is also to be expected according to [124].

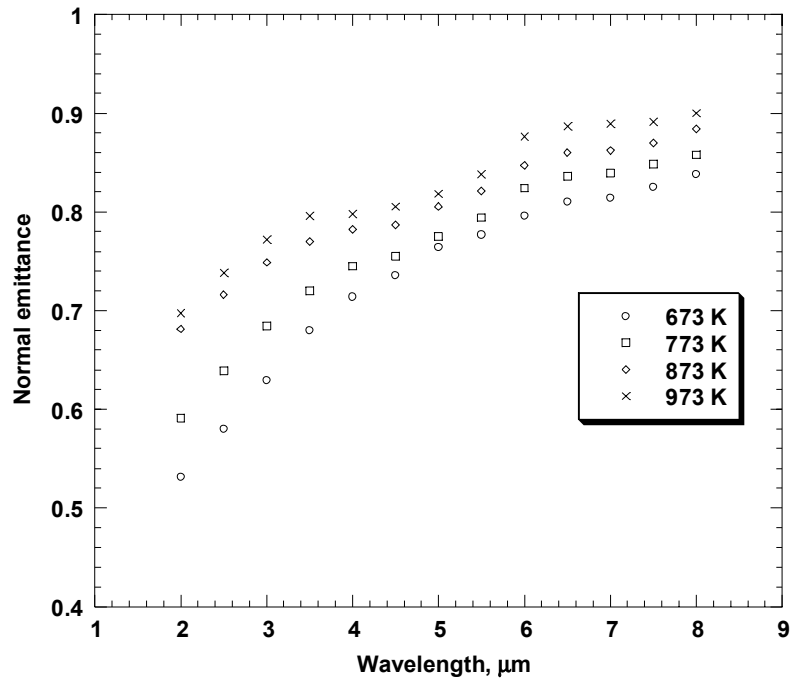


Figure 67 Normal emittance of cupric oxide

The emission band of cupric oxide was not totally captured in the present work due to spectral range limitations of the experimental setup. Figure 67 represents the normal emittance of cupric oxide from the present work at four temperatures, which is within the semitransparent region according to [125]. From Fig. 67 it can also be

observed that a maximum (Christiansen's point) in emittance of cupric oxide is expected somewhere beyond $8\ \mu\text{m}$ as described by [124, 125].

Directional emittance of cupric oxide at wavelengths of 3, 4, 5, 6 μm , shown on Fig. 68, follows Lambert's law from angles normal to the sample surface up to 48° before diving to zero at grazing angles according to Fresnel's equation [4, 124]. Based on both normal spectral and directional emittance determined, optically thick metal oxide closely follows a dielectric behavior.

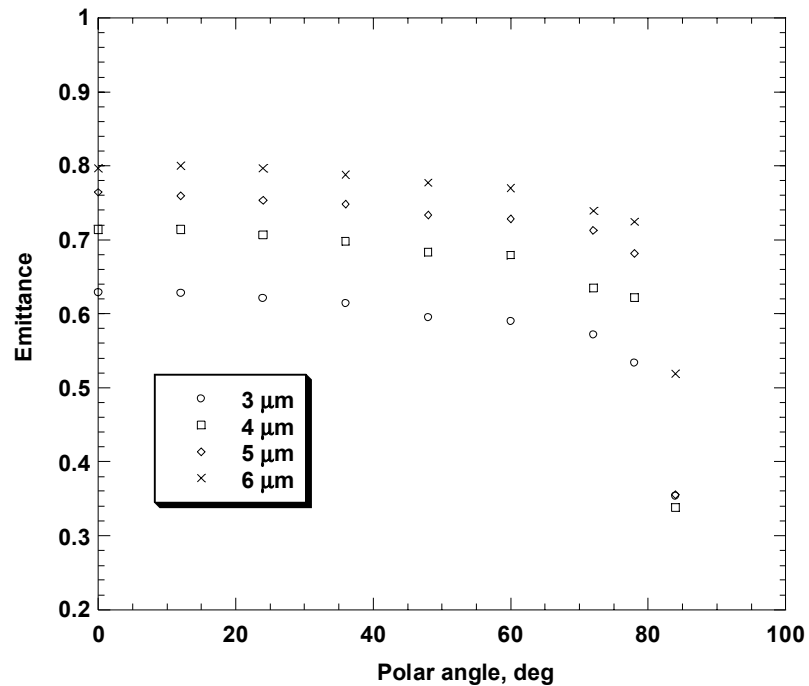


Figure 68 Directional emittance of CuO

The experimental setup required to study the spectral and directional emissivity of oxidized metals in atmospheric conditions at high temperature is complex, and needs to ensure not only a broad spectral range but also a reasonable uncertainty. The experimental setup for measurements in air, built in the present work (Chapter 4.2),

allows the sample surface to be viewed from different directions rather than only normal to the sample surface [40, 48, 49, 121, 122]. Thus, such an experimental setup which allows comprehensive directional measurements, not only provide knowledge of emission versus direction but also can be used together with theory to derive complex index of refraction of materials at high temperature.

7 SUMMARY

Careful study of the emissive behavior of high purity metals can minimize the errors due to surface contamination or any other detrimental surface effects usually encountered at high temperature. These types of errors are widespread in published work for thermal radiative properties. In addition, a broad infrared spectral range from 1 to 16 μm has been achieved.

The experimental device uses an high vacuum chamber and optics with proprietary coatings for very high infrared transmission to direct the radiation which leaves the sample to the FTIR detector. The sample is heated inside the high vacuum chamber by a non-contact method to greatly minimize sample surface contaminations or interactions. A high temperature blackbody with platinum heating elements and wall controlled temperature is used as reference. The system's calculated uncertainty is found to be less than $\pm 4\%$ for the temperature range and spectral ranges considered.

The spectral normal emissivity of high purity nickel at temperatures above 1440K is found to slightly increase with increasing temperature. Nickel spectral normal emissivity was found to follow a metallic behavior and displays the effects of both bound and free electrons. An X-point of nickel at wavelength of 2 μm was found as noted in an earlier work [70].

As expected from the indication of bound electron effects, neither the Hagen-Rubens nor the Drude relations could be fitted for the entire spectrum. The Drude-Roberts two parameter model was modified in order to obtain good agreement, and temperature dependence of the model parameter was found. Based on modified Drude-Roberts model, n and k increase monotonically beyond 6 μm due to free electrons. At shorter wavelengths the structure of n and k indicates bound electron effects.

The spectral normal emissivities of zirconium and titanium at temperatures above 1300 K slightly increase with increasing temperature and monotonically decrease with increasing wavelength from 1 to 16 μm , indicating no departure from metallic behavior. Comparison with Drude and Hagen-Rubens relations exhibit bound electron effects at shorter wavelengths.

The Drude-Roberts model was modified in order to obtain the complex index of refraction, which shows stronger bound electron effects at shorter wavelengths and free electron effects at larger wavelengths. The samples were inspected using X-ray diffraction and no sample oxidization was found.

Study of the emittance behavior of oxidized metals is achieved by considering both optically thick and thin metal oxide layers.

An optically thick metal oxide layer such as cupric oxide was grown on high purity copper due to a rapid oxidation process at the maximum operating temperature of the experimental setup. The uncontaminated cupric oxide orthorhombic structure was identified using X-ray diffraction.

The optically thick cupric oxide was obtained by heating, in air, high purity copper with a known surface roughness. Optical thickness calculated after the complex

index of refraction was determined proved that the cupric oxide is optically thick for all reported wavelengths and temperatures. Hence, its radiative properties are not affected by the substrate radiative properties; in other words, cupric oxide is not transparent. Normal emittance of cupric oxide at high temperature increases with increasing wavelength and temperature for the spectral range and temperature domain considered here, and a maximum (Christiansen's point) in emittance of cupric oxide is expected somewhere beyond 8 μm . The emission band of cupric oxide was not totally captured in the present work due to spectral range limitation of the experimental setup using a pyroelectric detector.

Directional emittance of cupric oxide follows Lambert's law from angles normal to the sample surface up to 48° before diving to zero at grazing angles according to Fresnel's equation. Based on the determination of both normal spectral and directional emittance, optically thick metal oxide closely follows a dielectric behavior. The calculated complex index of refraction follows a dielectric behavior with $k \approx 0$ and $n > 0$.

Throughout the course of study, the disadvantages of the experimental setup with a pyroelectric detector (used for oxidized copper study) were overcome when the spectral discrimination system was replaced by a FTIR spectrometer. Such an experimental setup, with a fast response time, very broad IR spectrum, and the capability of collecting data over comprehensive directional properties, proved to be a unique and accurate device in studying high temperature radiative emittance in air. Its uncertainty was less than $\pm 3.5\%$ for the temperature and spectral range considered.

The spectral normal and directional emittance of an optically thin layer of aluminum oxide grown on high purity aluminum is studied in the present work. The

thermally grown oxide layer composition consisted of Al_2O_3 and Al, shown by the binding energies. The AES depth profile showed an increasing concentration of elemental Al from the surface to the bottom of the oxide layer, and consequently a decrease in oxygen content from the surface to the bottom of the oxide layer.

Normal emittance of oxidized aluminum increases with increasing temperature from 673K to 873K. The influence of aluminum oxide higher emittance in mid infrared on artificially oxidized aluminum is seen through two small peaks between 8.5 and 11 microns. This spectral region is in the proximity of the wavelength where aluminum oxide exhibits the highest emittance - the Christiansen wavelength. Thus, the spectral normal emittance of aluminum at high temperature in air will be altered by the presence of heavy ions as Al^{3+} and O^{2-} with lower mobility than free electrons.

At wavelengths shorter than 8 μm , directional emittance of oxidized aluminum from the present work follows Lambert's law from a direction normal to the sample surface up to 40° , and then increases according to Fresnel's equation to reach a maximum near 80° , before decreasing rapidly to zero. For wavelengths longer than 8 μm , which coincides with the wavelengths where peaks on normal emittance appeared, a departure from metallic behavior is observed. At these wavelengths, emissivity does not obey Lambert's law or Fresnel's equation, and continuously increases with increasing polar angle from normal until a maximum is reached around 70° , which is about three times higher than normal emittance.

The normal spectral and directional emittance of oxidized nickel in air is studied for an extended spectral range from 2 to 20 μm . Nickel oxide grown by heating high

purity nickel in air was identified using X-ray diffraction. Sample surface modifications due to nickel oxide grain formation were revealed using SEM.

Spectral normal emittance of oxidized nickel slightly increases with increasing temperature between 673K and 873K. The spectral normal emittance of oxidized nickel exhibits two peaks between 8 and 16 microns. We can attribute those peaks to the spectral region (Christiansen wavelength) where nickel oxide exhibits its highest emissivity. Thus, the spectral normal emittance of nickel at high temperature in air will be altered by the presence of heavy ions as Ni^{2+} and O^{2-} with lower mobility than free electrons.

Directional emittance of nickel is also affected at these wavelengths, and a deviation from Lambert's law is seen. The deviation is highest at peaks wavelengths.

A generally monotonic decrease in emittance with wavelength for both aluminum and nickel, due to both bound and free electrons, will change gradually with the degree of oxidization, and this change will start in the spectral region where the metal oxide exhibits the greatest emittance. This might indicate that the relaxation time and the number of effective charge carriers become both wavelength dependent, and the dispersion of the relaxation time and the number of effective carrier charges starts around the metal oxide's Christiansen wavelength.

8 CONCLUSIONS

Generally, the emissive behavior of high purity metals studied in the present work at high temperature can only be qualitatively described by classical free electron models. Specifically, this qualitative agreement holds only at longer wavelengths or within limited spectral domains. At shorter wavelengths, where bound electron effects are prevalent, more complex models are needed. New models based on two or more parameters were introduced by fitting the literature data, although their applicability is limited. Thus, for high purity metals, measurement of emissivity continues to be necessary.

The emissive behavior of oxidized metals is studied in the present work through optically thin and thick films formed by oxidation of metals in air at elevated temperatures. Optically thin metallic oxide film effects on both spectral normal as well as directional emittance were found. The effects were associated with heavier metal and oxygen ions which altered the relaxation time and the number of charge carriers of the substrate. The emittance prediction of an oxidized metal is also a complex matter due to the numerous parameters that need to be included. Thus, for oxidized metals, measurement of emissivity also continues to be necessary.

The optically thick metal oxide layer studied within the transparent region of the spectrum displays no departure from dielectric behavior for normal and directional emissivities, and for the complex index of refraction. The emittance theory prediction for dielectrics is more limited than for metals, and generally complex dielectric functions are needed.

Experimental setups for emissivity measurement (emissometers) are not commercially available; thus, they need to be developed. The experimental setup developed for oxidized metal study in air at high temperatures permits measurement of emittance values near grazing angles over a broad infrared spectrum. The experimental setup built for high purity metals in ultra-high vacuum conditions allows a sample to be heated by a non-contact method (electromagnetically) to avoid oxidization and other interactions.

9 FUTURE WORK

The directions of the future work can be addressed through studying several aspects. Firstly, let's consider radiative properties of materials in air. As metals at high temperatures in air rapidly oxidize, and their emissivity is altered, further studies should include developing predictive models of emissivity. Such models must include besides temperature and wavelength, parameters such as surface roughness, oxidation rate, composition, alloying components, etc.

The problems encountered in understanding the emission/absorption mechanisms and dispersion in non conductors are immense. Future work on non conductors in air such as metal oxides will bring an insight on those mechanisms through developing dielectric function models which can fit the measured emissivity data. These dielectric function models accommodate the temperature dependence and help predict and understand the optical properties. Such developed dielectric functions will help explain and understand the electronic band structures at high temperatures though the knowledge of parameters such as the relaxation time, the number of effective charge carriers and their dispersion. In addition, these dielectric functions can be successfully used to study melting and premelting effects of materials with a high melting temperature as recently reported [125].

Secondly, let's consider radiative properties of materials in high vacuum conditions.

Additional work on high purity metals and alloys is highly needed. Most metals have not been studied at elevated temperatures below and above melting and in spectral ranges of interest for both scientists and engineers. Measurements of radiative emissivity will help determine appropriate dielectric function models which hold for a broadband IR spectrum over a large high temperature domain. These models will bring an insight on electronic transitions at high temperature which will help understand the absorption mechanisms.

Thirdly, an extended emission spectrum in visible and near IR will greatly improve the capability of the experimental setup which incorporates the EML and the FTIR. This involves modifications of its optics to extend the spectrum into visible and near IR. This may also require the second FTIR detector with detection ranges from visible to mid IR. Directional measurements would greatly improve the capability but would require changes to the vacuum chamber. Additional work with the present apparatus may also be performed on levitated metallic samples, which again will require a change in design of the vacuum chamber.

REFERENCES

1. Guo B Teodorescu G Wang D Overfelt RA (2005) Numerical model for specific heat measurement modulation power of electromagnetically levitated samples by modulation power method, Materials Science & Technology Conference and Exhibition, Pittsburgh, PA, Sept. 25-28, (2005)
2. Guo B (2006) MS Thesis, Auburn University, Auburn, AL
3. Lide D (2006) Handbook of Chemistry and Physics, 87th Ed., CRC Press LLC, New York, (2006)
4. Modest MF (2003) Radiative Heat Transfer, 2nd edition, Academic, (2003)
5. Touloukian YS DeWitt DP (1970) Thermal Radiative Properties, vol. 7, Thermophysical Properties of Matter, IFI/Plenum, New York, (1970)
6. Chaney JF Ramdas V Rodriguez CR (1982) Thermophysical Properties Research Literature Retrieval Guide, 1900-1980, Plenum Press, New York
7. Sala A (1986) Radiant Properties of Materials, Tables of Radiant Values for Blackbody and Real Materials, Physical Sciences data 21, Elsevier, Warszawa, 91986)
8. Roebuck B Edwards G Gee MG (2005) Mater Sci Tech 21(7): 831
9. Furukawa T Iuchi T (2000) Rev Sci Instrum 71(7): 2843
10. Hummel RE (2004) Electronic properties of materials, Springer, 3rd Ed., (2004)
11. Roberts S (1955) Phys Rev 100: 1667
12. Wieder H Czanderna AW (1966) J Appl Phys 37(1):184

13. Cagran C Wiltham B Pottlacher G (2004) *Int J Thermoph* 25(5): 1551
14. Siegel R Howell J (2002) *Thermal Radiation Heat Transfer*, 4th edition, Taylor & Francis, New York, (2002)
15. Phillips HR (1973) *J Electrochem Soc* 120: 295
16. Drude P (1902) *The Theory of Optics*, Longmans, Green and Co., New York, (1902)
17. Schultz LG (1954) *J Opt Soc Am* 44: 540
18. Slater JC (1967) *Insulators, Semiconductors and Metals*, McGraw-Hill Book, Co., New York, (1967)
19. Mott NF Jones H (1936) *The Theory of the Properties of Metals and Alloys*, Dover, New York, (1936)
20. Parker WJ Abbott GL (1965) *Theoretical and Experimental Studies of the Total Emittance of Metals*, Symposium on Thermal radiation of Solids (Katzoff, S.-editor), NASA SP-55, 11, (1965)
21. Richmond JC Harrison WN (1960) *Am Ceram Soc Bull* 39(11): 668
22. Petrov VA Chekhovskoi VY Sheinblin (1963) *High Temp* 1:19
23. Rudkin RL Parker WL Jenkins RJ (1964) *Measurements of The Thermal Properties of Metals at Elevated Temperature, Measurement of the Thermal Radiation Properties of Solids* (J.C. Richmond, Editor), NASA SP-31, 523 (1964)
24. Cezairliyan A Morse MS Berman HA Beckett CW (1971) *J Res NBS* 75A (1) pp 1-13
25. Peletskii VE (1989) *High Temp High Pres* 21:377
26. Cheng SX (1984) *High Temp High Pres* 16:459

27. Gier JT Dunkle RV Bevens JT (1954) J Opt Soc Am 44:558
28. Edwards DK Catton I (1965) Radiation characteristic of rough and oxidized metals, Advances in Thermophysical Properties at Extreme Temperatures and Pressures, Symposium on Thermophysical Properties pp189-99 (1965)
29. Dunkle RV (1960) Spectral Reflectance Measurements, Surface Effects on Spacecraft Materials, F.J. Clauss, Editor, Wiley and Sons, (1960)
30. Gates DM Shaw CC Beaumont D (1958) J Opt Soc Am 48 (2): 88
31. Hsia JJ Richmond JC (1976) J Res Natl Bureau Stand 80A: 189
32. Branderberg WM (1962) The Reflectivity of Solids at Grazing Angles, NASA SP-3(75) (1962)
33. Dunn ST Richmond JC Wiebelt JA (1966) J Res Natl Bureau Stand 70C(2): 75
34. Seifter A Boboridis K Obst AW (2003) Emissivity Measurements on Metallic Surfaces with Various Degrees of Roughness: A Comparison of Laser Polarimetry and Integrating Sphere Reflectometry, 15th Symposium of Thermophysical Properties, June, Boulder, Colorado, (2003)
35. Latyev LN Chekhovskoi VY Shestakov EN (1969) High Temp High Pres 7:610
36. Branderberg WM Clausen OW (1964) Int Aeros Abstr 4(19): 313
37. De Vos JC (1954) Physica XX: 690
38. Larabee RD (1959) J Opt Soc Am 49: 619
39. Hylton JO (1976) J AIAA 14(9): 1303
40. Vader DT Viskanta R Incropera FP (1985) Rev Sci Instrum 57(1): 87
41. Postlethwait MA Sikka KK Modest M (1994) J Thermoph Heat Trans 8(3):412
42. Reynolds PM (1961) Brit J Appl Phys 12:111

43. Richmond JC Harrison WN Shorten FJ (1963) An approach to Thermal Emittance Standards, Measurement of Thermal Radiation Properties of Solids (J.C. Richmond, Editor) NASA SP-31, 403 (1963)
44. Conroy CM Guthrie JG Sharkins AJ Sparr BJ Crocombe RA Curbelo R (1987) Appl Spectrosc 41(4): 688
45. Markham JR Solomon PR Best PE (1990) Rev Sci Instr 61(12): 3700
46. Ballico MJ Jones TP (1995) Appl Spectrosc 49(3): 335
47. Ishii J Ono A (2001) Meas Sci Technol 12: 2103
48. Clausen S Morgenstjerne A Rathmann O (1996) Appl Opt 35(28):5683
49. Bauer W Oertel H Rink M (2003) Spectral Emissivities of Bright and Oxidized Metals at High Temperatures 15th Symposium of Thermophysical Properties, June, Boulder, Colorado, (2003)
50. Jones PD Nisipeanu E (1995) Int J Thermoph 17(4): 967
51. Jones PD Dorai-Raj DE McLeod DG (1996) J Thermoph Heat Trans 10(2): 343
52. Jones PD Teodorescu G Overfelt RA (2004) Spectral-Directional Emittance of CuO at High Temperatures, Proceedings of ASME Summer Conference, July, Charlotte, North Carolina, (2004)
53. Jones PD Teodorescu G Overfelt RA (2006) J Heat Transfer 128:382
54. Teodorescu G Jones PD RA Overfelt Guo B (2006) J Mater Sci 41:7240
55. Teodorescu G Jones PD RA Overfelt Guo B (2006) Int J Thermophys 27(2):554
56. Jakob M (1949) Heat Transfer, John Wiley & Sons Inc., (1949)
57. Burgess GK Waltenberg RG (1915) Natl Bureau Stand Bulletin 11:591
58. Bidwell CC (1914) Phys Rev B, 3 (6): 439

59. Worthening AG (1926) Phys Rev 28:174
60. Whitney LV (1935) Phys Rev 48: 458
61. Petrov VA Checkovskoi VY Sheindlin AE (1963) High Temp 1(3): 416
62. Milosevic ND Vukovic GS Pavicic DZ Maglic KD (1999) Int J Thermoph 20(4): 1129
63. Sennet RS Scott GD (1950) J. Opt Soc Am 4: 203
64. Marple DTP (1956) J Opt Soc Am 7: 490
65. Blickensderfer R Deardorf DK Lincoln RL (1971) J Less Common Met 51:13
66. Tien CL (1960) J Heat Trans 3:252
67. Forsythe WE Adams EG (1945) J Opt Soc Am 2: 108
68. Barnes TB (1966) J Opt Soc Am 56 (11): 1546
69. Hurst C (1933) P Roy Soc London A 142: 466
70. Price DJ (1947) Proc Phys Soc London 59: 118
71. Riethof TR De Santis VJ (1963) Report NASA-SP-31, pp 565-584, (1963)
72. Paradis PF Rhim WK (1999) J Mater Res 14(9): 3713
73. Cezairliyan A Miiler AP (1977) High Temp High Press 9:319
74. Landersperger W Stark DZ (1964) Phys 180:178
75. Zhorov GA (1967) High Temp (USSR) 5:881
76. Arutynov AV Druzhinin VP, (1973) High Temp. (USSR) 9:487
77. Peletskii VE Druzhinin VP (1973) High Temp (USSR) 11: 188
78. Bruckner M Schafer JH Uhlenbusch J (1989) J Appl Phys 66(3):1326
79. Otter M (1961) Z. Phys 161:539
80. Schley U (1960) Naturwiss 47: 222

81. Price DJ (1946) *Nature* 157: 765
82. Lund H Ward L (1952) *Proc Phys Soc London B* 65: 535
83. Cennamo F (1939) *Nuovo Cim* 16:253
84. Seban RA (1963) WADD-TR-60-370 (Pt 3), pp 1-68, (1963)
85. Furman SC McManus PA (1960) USAEC, GEAP-3338, pp 1-46, (1960).
86. Riethof TR (1961) *Gen. Elec. Co., Space Sci. Lab.*, pp 1-34, (1961)
87. Seemueller H Stark D (1967) *Zeitschrift fuer Physik* 198(2):201
88. Coblenz WW (1912) *Natl Bureau Stand Sci Paper* 196
89. Randolf CF Overholzer MJ (1913) *Phys Rev* 1(2nd Ed.):144
90. Schmidt E Eckert E (1935) *Forschung auf dem Gebiete des Ingenieurwes*, 6: 175
91. Cammerer JS (1938) *Holz als Rohund Wenkstoff* 1(6): 206
92. Wade WR (1958) *Measurement of Total Hemispherical Emissivity of Oxidized Metals at High Temperatures*, NACA TN 4206, March, (1958)
93. Brannon RR Goldstein RJ (1970) *J Heat Transfer* 92C: 257
94. Drobny VF Pulfrey DL (1979) *Thin Solid Films* 61:89
95. Karlsson B Ribbing CG Roos A Valkonen E Karlsson T (1982) *Phys Scripta* 25(6): 111
96. Jian L Vizkelethy G Revesz P Mayer JW (1991) *J Appl Phys* 69(2): 1020
97. Paidassi J (1958) *Acta Metall* 6:216
98. Lahiri SK Waalib Singh NK Heng KW Ang L Goh LC (1998) *Microelectr J* 29:335
99. Yongfu Z Mimura K Ishikawa Y Isshiki M (2001) *J JCBRA* 40:96
100. Incropera FP DeWitt DP (2002) *Fundamentals of Heat and Mass Transfer*, 5th edition, Wiley, New York, (2002)

101. Moffat RJ (1998) *Exp Therm Fluid Sci* 1: 3
102. Newman R Chrenko RM (1959) *Phys Rev* 114(6): 1507
103. Atkinson A (1985) *Rev. Modern Phys.* 57(2): 437
104. Riethof TR (1961) *High-Temperature Spectral Emissivity Studies*, Report AD 250-274. General Electric Space Sciences Laboratory, pp 85-105 (1961)
105. Autio GW Scala E (1965) *AIAA J.* 3(4): 738
106. Ward L (1956) *Proc Phys Soc London B* 69: 339
107. Ishikawa T Paradis PF Saita Y (2004) *Nippon Kinzoku Gakkaishi* 68(9): 781
108. Paradis PF Rhim WK (2000) *J Chem Thermodyn* 32(1): 123
109. Lawless KR (1974) *Rep Prog Phys* 37: 231
110. Bradshaw FJ (1950) *Proc Phys Soc B* 63:573
111. Autio GW Scala E (1968) *Anisotropy Single-Crystal, Refractory Compounds*, Proceedings International Symposium, Dayton, Ohio, Meeting Date 1967, 1, pp 357-381, (1968)
112. Dmitriev VD Kholopov GK (1968) *Teplofizika Vysokikh Temperatur* (1968) 6(3):550
113. Coffman JA Kibler GM Lyon TF Acchione BD (1963) *Carbonization of Plastics and Refractory Materials Research*, Technical Report, Gen. Elec. Co., WADD-TR-60-646, II, pp 100-147 (1963)
114. Adams JG (1962) *Northrop Corporation Report*, Novair Div. pp 1-259
115. Michels WC Wilford S (1949) *J Appl Phys* 20: 1223
116. Gubareff GG Janssen JE Torborg RH (1960) *Thermal radiation properties survey*, Honeywell Research Center, MI, (1960)

117. Ehrenreich H Phillip HR Segall B (1963) Phys Rev 132(5): 1918
118. Ehrenreich H Phillip HR (1962) Phys Rev 128(1): 1622
119. Shiles E Sasaki T Inokuti M Smith DY (1980) Phys Rev B 22:1612
120. Ribault G. (1934) Optical Pyrometry, Landsberg, (1934)
121. Svet DY (1965) Thermal Radiation, New York, (1965)
122. Havstad MA McLean W (1993) Rev Sci Instrum 64(7): 1971
123. Reichman J Feldman C (1969) J Opt Soc Am 59(11):1404
124. Maldague X (2001) Theory and Practice of Infrared Technology and Nondestructive Testing, Wiley& Sons, New York, (2001)
125. Brun JF De Sousa Menesses D Echegut P (2003) Spectral Emissivity of Dielectric Oxides Below and Above the Melting Point, Fifteenth Symposim of Thermophysical Properties, Boulder, CO, USA, (2003)
126. Ngai KL (1979) Comment Sol State Phys 9:127
127. Jasperse JR Kahan A Plendl JN Mitra SS (1966) Phys Rev 140(2): 526
128. Neuer G Jaroma-Weiland G (1998) Int J Thermoph 19(3): 917
129. Spitzer WG Kleinman DA Frosch CJ Walsh DJ (1960) Optical Properties of Silicon Carbide, Proceedings of the Conference of Silicon Carbide, Boston, Massachussets, Pergamon Press, pp 347-365, (1960)
130. Roy S Bang SY Modest MF Stubican VF (1993) Appl Opt 32(19):3550
131. Tiernan RJ Saunders JE (1988) J Appl Phys 64(2):459
132. Bigio L (1999) Normal Spectral Emittance Measurements of Polycrystalline Alumina at High Temperatures, GE Research & Development Center, 99 CRD 128, Technical Report, 1999.

APPENDICES

Appendix A - Cupric Oxide

$\lambda, \mu\text{m}$	Polar angle .deg								
	0°	12°	24°	36°	48°	60°	72°	78°	84°
1.5	-	-	-	-	-	-	-	-	-
	0.520	0.515	0.519	0.515	0.506	0.515	0.524	0.381	0.242
	0.654	0.648	0.641	0.620	0.600	0.600	0.587	0.419	0.248
	0.658	0.650	0.642	0.636	0.626	0.601	0.582	0.413	0.267
2.0	0.532	0.525	0.521	0.510	0.515	0.525	0.538	0.413	0.368
	0.591	0.587	0.585	0.584	0.577	0.562	0.556	0.473	0.299
	0.681	0.677	0.667	0.658	0.636	0.628	0.595	0.471	0.280
	0.697	0.694	0.685	0.675	0.656	0.632	0.606	0.467	0.289
2.5	0.580	0.584	0.569	0.565	0.549	0.548	0.550	0.480	0.317
	0.639	0.637	0.633	0.629	0.621	0.609	0.583	0.529	0.342
	0.716	0.707	0.698	0.711	0.688	0.648	0.613	0.543	0.317
	0.738	0.733	0.734	0.727	0.719	0.682	0.628	0.542	0.389
3.0	0.629	0.628	0.621	0.614	0.595	0.590	0.572	0.534	0.354
	0.684	0.680	0.672	0.668	0.664	0.652	0.593	0.575	0.371
	0.749	0.742	0.729	0.745	0.722	0.687	0.632	0.592	0.347
	0.772	0.768	0.768	0.759	0.749	0.719	0.664	0.589	0.412
3.5	0.680	0.679	0.673	0.666	0.649	0.644	0.622	0.581	0.320
	0.720	0.719	0.714	0.708	0.705	0.691	0.631	0.614	0.324
	0.770	0.763	0.753	0.748	0.740	0.725	0.666	0.624	0.280
	0.796	0.790	0.787	0.784	0.771	0.743	0.702	0.617	0.324
4.0	0.714	0.714	0.707	0.698	0.683	0.679	0.635	0.622	0.338
	0.745	0.742	0.738	0.735	0.729	0.715	0.660	0.645	0.335
	0.782	0.773	0.765	0.761	0.760	0.738	0.684	0.642	0.289
	0.798	0.791	0.791	0.789	0.775	0.749	0.716	0.626	0.348
4.5	0.736	0.733	0.728	0.720	0.706	0.701	0.683	0.648	0.344
	0.755	0.753	0.749	0.746	0.741	0.727	0.675	0.663	0.333
	0.787	0.777	0.769	0.773	0.772	0.744	0.690	0.653	0.278
	0.805	0.805	0.797	0.791	0.787	0.755	0.721	0.631	0.347
5.0	0.764	0.759	0.753	0.748	0.733	0.728	0.713	0.682	0.355
	0.775	0.773	0.769	0.765	0.760	0.747	0.701	0.675	0.341
	0.805	0.794	0.786	0.780	0.789	0.765	0.717	0.685	0.276
	0.818	0.813	0.811	0.808	0.797	0.767	0.728	0.668	0.353
5.5	0.777	0.774	0.767	0.764	0.747	0.743	0.726	0.705	0.355
	0.794	0.790	0.787	0.785	0.783	0.768	0.726	0.710	0.345
	0.821	0.811	0.806	0.809	0.808	0.789	0.744	0.716	0.275
	0.838	0.834	0.832	0.828	0.822	0.788	0.753	0.701	0.299
6.0	0.796	0.800	0.797	0.788	0.777	0.770	0.739	0.724	0.519
	0.824	0.821	0.812	0.811	0.808	0.804	0.767	0.765	0.517
	0.847	0.845	0.833	0.838	0.839	0.818	0.768	0.741	0.480
	0.876	0.870	0.873	0.864	0.863	0.835	0.777	0.762	0.479
6.5	0.810	0.806	0.803	0.798	0.787	0.776	0.746	0.738	0.511
	0.836	0.834	0.827	0.824	0.820	0.818	0.770	0.742	0.499
	0.860	0.850	0.844	0.846	0.841	0.821	0.775	0.756	0.491
	0.887	0.884	0.885	0.876	0.875	0.843	0.788	0.780	0.516
7.0	0.814	0.810	0.806	0.806	0.794	0.785	0.752	0.740	0.508
	0.839	0.835	0.827	0.825	0.824	0.819	0.775	0.750	0.510
	0.862	0.850	0.847	0.844	0.846	0.827	0.775	0.772	0.501
	0.889	0.885	0.887	0.881	0.875	0.847	0.792	0.790	0.518
7.5	0.825	0.820	0.815	0.816	0.805	0.796	0.755	0.748	0.516
	0.848	0.845	0.837	0.832	0.829	0.826	0.771	0.755	0.501
	0.870	0.855	0.854	0.852	0.852	0.835	0.780	0.770	0.518
	0.891	0.890	0.891	0.889	0.881	0.853	0.797	0.790	0.516
8.0	0.838	0.832	0.824	0.830	0.819	0.808	0.761	0.760	0.506
	0.858	0.856	0.853	0.846	0.840	0.839	0.775	0.758	0.508
	0.884	0.868	0.867	0.868	0.855	0.843	0.783	0.784	0.516
	0.900	0.898	0.899	0.898	0.892	0.860	0.804	0.795	0.526

Table 1 Measured Spectral Directional Emittance of CuO at 673 K (1st row), 773 K (2nd row), 873 (3rd row), and 973 K (4th row)

$\lambda, \mu\text{m}$	673 K			773 K			873 K			973 K		
	ϵ_λ	n_λ	k_λ	ϵ_λ	n_λ	k_λ	ϵ_λ	n_λ	k_λ	ϵ_λ	n_λ	k_λ
1.5	-	-	-	0.417	5.625	0.099	0.557	3.988	0.099	0.564	3.977	0.099
2.0	0.494	5.705	0.099	0.535	4.649	0.099	0.588	3.726	0.099	0.600	3.555	0.099
2.5	0.527	4.896	0.099	0.577	4.072	0.099	0.627	3.357	0.099	0.655	3.135	0.099
3.0	0.571	4.203	0.099	0.617	3.677	0.099	0.661	3.061	0.099	0.689	2.854	0.099
3.5	0.613	3.668	0.099	0.647	3.294	0.099	0.674	2.970	0.099	0.702	2.710	0.007
4.0	0.643	3.356	0.099	0.672	3.091	0.099	0.688	2.857	0.040	0.709	2.681	0.007
4.5	0.667	3.175	0.091	0.682	3.002	0.099	0.694	2.789	0.009	0.720	2.636	0.003
5.0	0.693	2.973	0.006	0.701	2.819	0.012	0.711	2.635	0.006	0.729	2.534	0.002
5.5	0.706	2.849	0.006	0.721	2.670	0.007	0.731	2.475	0.001	0.744	2.375	0.001
6.0	0.746	2.636	0.001	0.764	2.466	0.001	0.779	2.285	0.001	0.800	2.087	0.001
6.5	0.753	2.574	0.001	0.773	2.375	0.001	0.787	2.229	0.001	0.815	2.013	0.001
7.0	0.757	2.545	0.001	0.777	2.354	0.001	0.792	2.192	0.001	0.821	1.999	0.001
7.5	0.766	2.474	0.001	0.783	2.290	0.001	0.798	2.149	0.001	0.822	1.971	0.001
8.0	0.775	2.379	0.001	0.793	2.223	0.001	0.808	2.114	0.001	0.830	1.910	0.001

Table 2 Spectral-hemispherical emittance and complex refractive index of CuO.

Appendix B - Oxidized Aluminum

Parameter	Estimated $\pm 2\sigma$ confidence limits(%)
Sample surface temperature	0.4
Blackbody temperature	0.4
Stability of the BB temperature	0.05
Stability of sample temperature	0.05
Total uncertainty in emissivity $[\Sigma(\delta\mu_i)^2]^{1/2}$	0.0026
Total % uncertainty in emissivity ($\epsilon=0.0944$, at $T=400^\circ\text{C}$)	2.8%

Table 3 Uncertainty estimates of oxidized aluminum

Polar angle, deg							
λ , μm	0°	12°	24°	36°	48°	60°	72°
3	0.094	0.108	0.104	0.109	0.118	0.120	0.135
	0.121	0.137	0.137	0.142	0.150	0.168	0.161
	0.152	0.163	0.166	0.173	0.184	0.211	0.206
4	0.098	0.113	0.106	0.110	0.116	0.129	0.135
	0.117	0.132	0.131	0.136	0.144	0.162	0.162
	0.141	0.151	0.153	0.159	0.169	0.196	0.199
5	0.099	0.109	0.105	0.107	0.112	0.126	0.137
	0.112	0.126	0.124	0.128	0.137	0.155	0.163
	0.132	0.141	0.142	0.147	0.158	0.184	0.198
6	0.098	0.106	0.104	0.105	0.111	0.125	0.147
	0.107	0.120	0.118	0.123	0.131	0.150	0.169
	0.125	0.132	0.132	0.138	0.148	0.175	0.204
7	0.097	0.105	0.101	0.103	0.108	0.125	0.158
	0.105	0.116	0.114	0.118	0.127	0.146	0.181
	0.122	0.126	0.126	0.131	0.142	0.169	0.218
8	0.096	0.103	0.100	0.102	0.107	0.124	0.160
	0.103	0.112	0.110	0.115	0.123	0.144	0.183
	0.118	0.121	0.121	0.126	0.137	0.166	0.220
9	0.106	0.115	0.113	0.119	0.129	0.154	0.193
	0.111	0.121	0.122	0.130	0.145	0.173	0.212
	0.125	0.129	0.131	0.140	0.157	0.193	0.244
10	0.101	0.109	0.109	0.116	0.128	0.157	0.205
	0.107	0.116	0.117	0.126	0.143	0.177	0.224
	0.120	0.122	0.125	0.135	0.154	0.195	0.255
11	0.107	0.120	0.135	0.160	0.200	0.265	0.319
	0.114	0.127	0.143	0.175	0.225	0.296	0.344
	0.126	0.135	0.155	0.191	0.247	0.326	0.376
12	0.099	0.108	0.110	0.119	0.139	0.181	0.237
	0.101	0.109	0.113	0.128	0.153	0.197	0.253
	0.114	0.114	0.122	0.137	0.166	0.217	0.285
13	0.095	0.104	0.106	0.110	0.128	0.162	0.219
	0.100	0.105	0.108	0.119	0.139	0.174	0.233
	0.111	0.110	0.115	0.126	0.149	0.191	0.265
14	0.097	0.102	0.106	0.106	0.124	0.154	0.213
	0.098	0.103	0.104	0.114	0.130	0.163	0.225
	0.109	0.106	0.110	0.119	0.138	0.179	0.255

Table 4 Measured Spectral-Directional Emittance of Thermally Oxidized Aluminum at 673 K (1st row), 773 K (2nd row), and 873 K (3rd row)

Appendix C - Oxidized Nickel

Parameter	Estimated $\pm 2\sigma$ confidence limits(%)
Sample surface temperature	0.4
Blackbody temperature	0.4
Stability of the BB temperature	0.05
Stability of sample temperature	0.05
Total uncertainty in emissivity $[\Sigma(\delta\mu_i)^2]^{1/2}$	0.0051
Total % uncertainty in emissivity ($\epsilon=0.151$, at $T=400^\circ\text{C}$)	3.4%

Table 5 Uncertainty Estimates of Oxidized Nickel Emittance Measurement

$\lambda, \mu\text{m}$	Polar angle, deg						
	0°	12°	24°	36°	48°	60°	72°
2	0.151	0.174	0.169	0.172	0.200	0.202	0.242
	0.169	0.184	0.190	0.203	0.201	0.216	0.184
	0.213	0.228	0.235	0.248	0.254	0.258	0.242
3	0.147	0.168	0.177	0.185	0.193	0.210	0.220
	0.164	0.179	0.184	0.193	0.202	0.213	0.219
	0.189	0.209	0.218	0.231	0.242	0.251	0.253
4	0.143	0.164	0.176	0.181	0.191	0.199	0.212
	0.156	0.171	0.176	0.184	0.195	0.208	0.218
	0.175	0.192	0.200	0.214	0.226	0.237	0.246
5	0.143	0.158	0.170	0.178	0.185	0.195	0.210
	0.150	0.162	0.168	0.175	0.186	0.199	0.212
	0.163	0.178	0.185	0.200	0.211	0.223	0.237
6	0.139	0.154	0.165	0.173	0.181	0.191	0.211
	0.142	0.155	0.159	0.167	0.178	0.192	0.211
	0.154	0.167	0.173	0.187	0.199	0.212	0.231
7	0.139	0.152	0.165	0.170	0.179	0.188	0.214
	0.140	0.150	0.155	0.162	0.172	0.188	0.210
	0.148	0.158	0.164	0.179	0.191	0.205	0.228
8	0.131	0.143	0.155	0.162	0.170	0.184	0.209
	0.135	0.143	0.146	0.154	0.165	0.183	0.212
	0.142	0.151	0.157	0.175	0.187	0.202	0.230
9	0.143	0.156	0.171	0.186	0.203	0.227	0.260
	0.150	0.160	0.166	0.177	0.194	0.218	0.261
	0.155	0.166	0.174	0.196	0.219	0.242	0.278
10	0.143	0.153	0.170	0.185	0.202	0.222	0.255
	0.152	0.159	0.166	0.176	0.191	0.215	0.257
	0.156	0.166	0.174	0.195	0.220	0.243	0.280
11	0.129	0.136	0.150	0.161	0.175	0.195	0.233
	0.136	0.142	0.145	0.154	0.170	0.195	0.240
	0.144	0.150	0.157	0.178	0.201	0.225	0.268
12	0.122	0.129	0.140	0.150	0.163	0.181	0.218
	0.129	0.132	0.132	0.143	0.156	0.178	0.225
	0.134	0.139	0.143	0.164	0.183	0.204	0.245
13	0.120	0.127	0.137	0.148	0.161	0.180	0.215
	0.125	0.130	0.129	0.139	0.153	0.174	0.221
	0.131	0.134	0.138	0.160	0.179	0.200	0.242
14	0.120	0.127	0.137	0.148	0.161	0.180	0.215
	0.126	0.126	0.128	0.139	0.154	0.178	0.227
	0.130	0.132	0.137	0.158	0.180	0.204	0.251
15	0.137	0.141	0.149	0.170	0.181	0.194	0.237
	0.140	0.140	0.140	0.156	0.169	0.198	0.248
	0.143	0.142	0.148	0.172	0.198	0.225	0.277
16	0.115	0.121	0.131	0.148	0.162	0.188	0.232
	0.123	0.123	0.124	0.138	0.160	0.192	0.247
	0.131	0.131	0.140	0.167	0.197	0.232	0.295
17	0.113	0.117	0.127	0.143	0.160	0.184	0.234
	0.117	0.122	0.124	0.138	0.164	0.200	0.262
	0.130	0.130	0.139	0.169	0.206	0.249	0.323
18	0.117	0.113	0.126	0.140	0.158	0.187	0.235
	0.121	0.120	0.123	0.136	0.158	0.197	0.258
	0.128	0.130	0.137	0.166	0.205	0.242	0.310
19	0.106	0.111	0.112	0.136	0.149	0.172	0.227
	0.114	0.113	0.118	0.129	0.149	0.189	0.250
	0.125	0.121	0.129	0.158	0.195	0.230	0.298
20	0.100	0.106	0.110	0.137	0.146	0.174	0.227
	0.113	0.111	0.113	0.123	0.145	0.188	0.245
	0.123	0.120	0.127	0.155	0.192	0.231	0.293

Table 6 Measured spectral-directional emittance of at 673 K (1st row), 773 K (2nd row), 873 K (3rd row)

Appendix D - Nickel

Parameter	Estimated $\pm 2\sigma$ confidence limits(%)
Sample surface temperature	0.5
Blackbody temperature	0.3
Stability of the temperature control	0.04
Total uncertainty in emissivity $[\Sigma(\delta\mu_i)^2]^{1/2}$	0.0168
Total % uncertainty in emissivity ($\lambda=1 \mu\text{m}$, at $T=1167^\circ\text{C}$)	4.1%

Table 7 Uncertainty Estimates of Nickel Emissivity Measurement

Appendix E - Zirconium

Parameter	Estimated $\pm 2\sigma$ confidence limits(%)
Sample surface temperature	0.5
Blackbody temperature	0.3
Stability of the temperature control	0.04
Total uncertainty in emissivity $[\Sigma(\delta\mu_i)^2]^{1/2}$	0.0132
Total % uncertainty in emissivity ($\lambda=1 \mu\text{m}$, at $T=1086^\circ\text{C}$)	4%

Table 8 Uncertainty Estimates of Zirconium Emissivity Measurement

Appendix F - Titanium

Parameter	Estimated $\pm 2\sigma$ confidence limits(%)
Sample surface temperature	0.5
Blackbody temperature	0.3
Stability of the temperature control	0.04
Total uncertainty in emissivity $[\Sigma(\delta\mu_i)^2]^{1/2}$	0.0222
Total % uncertainty in emissivity ($\lambda=1 \mu\text{m}$, at $T=1088^\circ\text{C}$)	3.97%

Table 9 Uncertainty Estimates of Titanium Emissivity Measurement